DEVELOPMENT OF TARGETED siRNA THERAPEUTICS FOR TRIPLE NEGATIVE BREAST CANCER AND LIVER FIBROSIS

A DISSERTATION IN
Pharmaceutical Sciences
and
Chemistry

Presented to the Faculty of the University
of Missouri-Kansas City in partial fulfillment of
the requirements for the degree

DOCTOR OF PHILOSOPHY

by

ZHEN ZHAO

B. S., China Pharmaceutical University, 2011

Kansas City, Missouri

2018

DEVELOPMENT OF TARGETED siRNA THERAPEUTICS FOR TRIPLE NEGATIVE BREAST CANCER AND LIVER FIBROSIS THERAPY

Zhen Zhao, Candidate for the Doctor of Philosophy Degree

University of Missouri-Kansas City, 2018

ABSTRACT

The objective of this dissertation is to develop various systems to deliver small interfering RNA (siRNA) for the treatment of triple negative breast cancer (TNBC) and liver fibrosis. siRNAs targeting vascular endothelial growth factor (VEGF) and IκB kinase ε (IKBKE) were used for treating TNBC, while siRNA targeting poly(rC) binding protein 2 (PCBP2) was used for treating liver fibrosis.

In Chapter 1, we briefly introduced the background about TNBC and liver fibrosis. We also presented the Statement of the Problems and Objectives.

In Chapter 2, we reviewed the molecular mechanisms and potential treatments for TNBC and liver fibrosis.

In Chapter 3, we developed a poly(ethyleneimine) (PEI) conjugated biodegradable multiblock polymer to form nanocomplexes with VEGF siRNA for TNBC treatment. The nanocomplex is able to deliver the VEGF siRNA into TNBC cells with a high transfection efficiency and low cytotoxicity. *In vitro* activity studies showed that the siRNA nanocomplexes significantly inhibit migration and invasion of TNBC cells. More importantly, the VEGF siRNA nanocomplex efficiently inhibit tumor growth *in vivo* and successfully downregulate VEGF expression in the tumor. These results suggested that

VEGF siRNA is a promising anti-tumor agent for TNBC therapy, and the PEI 1800 conjugated bio-degradable multiblock polymer is a promising system to deliver siRNAs to TNBC cells.

In Chapter 4, we developed a CD44-targeting, cholesterol modified cationic peptide nanocomplex to co-deliver IKBKE siRNA and cabazitaxel (CTX) for TNBC therapy. IKBKE siRNA significantly inhibits the proliferation, migration, and invasion of TNBC cells but has no apoptosis-inducing effect. *In vivo* studies also indicated that IKBKE siRNA can inhibit TNBC tumor growth. CD44-targeting CHA/CP/siRNA/CTX nanocomplex showed the synergistic effect of IKBKE siRNA and cabazitaxel on the inhibition of invasiveness and growth of TNBC tumors with an enhanced CD44 specific targeting effect. CHA/CP/siRNA/CTX nanocomplexes also exhibited a significant anti-tumor effect through IKBKE siRNA and cabazitaxel *in vivo*. Thus, IKBKE siRNA may be a promising anti-tumor agent for TNBC therapy, and co-delivery of IKBKE siRNA and cabazitaxel through a CD44-targeting nanocomplex is a potential strategy for TNBC treatment. Moreover, this multifunctional delivery system can also provide a good option for combined gene therapy and chemotherapy.

In Chapter 5, we prepared three neutravidin-based siRNA nanocomplexes with different targeting ligands to deliver PCBP2 siRNA to hepatic stellate cells (HSCs). Insulin-like growth factor 2 receptor (IGF2R) is overexpressed in activated HSCs and therefore can be utilized for HSC-specific drug delivery. Compared to vitamin A and cholesterol, the IGF2R-specific peptide exhibited the highest targeting effect to human LX-2, rat HSC-T6 cell line, and activated primary rat HSCs. Accordingly, the IGF2R-specific peptide coupled nanocomplex demonstrated higher silencing activity of PCBP2

and better inhibition on the migration of activated HSCs. The IGF2R-specific peptide coupled nanocomplex also showed the highest uptake in the liver and lowest uptake in the lung and kidney of the rats with CCl_4-induced liver fibrosis.

APPROVAL PAGE

The faculty listed below, appointed by the Dean of the School of Graduate Studies, have examined the dissertation titled "Development of Targeted siRNA Therapeutics for Triple Negative Breast Cancer and Liver Fibrosis", presented by Zhen Zhao, candidate for the Doctor of Philosophy Degree, and certify that in their opinion it is worthy of acceptance.

Supervisory Committee

Kun Cheng, Ph.D., Committee Chair
Division of Pharmacology & Pharmaceutical Sciences

Zhonghua Peng, Ph.D.
Department of Chemistry

Mridul Mukherji, Ph.D.
Division of Pharmacology & Pharmaceutical Sciences

Nathan A. Oyler, Ph.D.
Department of Chemistry

Xiangping Chu, Ph.D.
Department of Biomedical Sciences

TABLE OF CONTENTS

LIST OF ILLUSTRATIONS

Figure Page

LIST OF TABLES

ACKNOWLEDGEMENTS

I would first like to express my greatest gratitude and deep appreciation to my advisor, Dr. Kun Cheng for his excellent, patient guidance and mentorship, persistent encouragement and motivation, and continuous support throughout all the time of my Ph.D. study.

I would like to thank Dr. Mridul Mukherji of the Division of Pharmacology & Pharmaceutical Sciences, Dr. Zhonghua Peng and Dr. Nathan A. Oyler of the Department of Chemistry, Dr. Xiangping Chu of the Department of Biomedical Sciences, for their valuable guidance and thought insightful suggestions for my research and the dissertation, and kindly serving in my supervisory committee.

I would like to express my special thanks to my colleagues, Dr. Rubi Mahato, Dr. Ravi Shukla, Dr. Zhijin Chen, Dr. Wei Jin, Ashutosh Barve, Akshay Jain, Hao Liu, Yuanke Li, Bahaa Mustafa, Pratik Ahikary, John Fetse and Maryam Nakkjiri for their time, support and friendship during my research and study in UMKC.

In addition, I am grateful to other professors, staff members, and fellow students in the Division of Pharmacology & Pharmaceutical Sciences for their help and friendship.

Finally, I would like to express my deepest thanks to my wife, Yuanke Li, for her encouragement, support, and love for both my research study and life. I also thank my parents for their understanding and sacrifices during my graduate study.

CHAPTER 1

INTRODUCTION

1.1 Overview

Triple-negative breast cancer (TNBC) is one subtype of breast cancer that lacks expression of estrogen receptor (ER), progesterone receptor (PR) and human epidermal growth factor receptor 2 (HER2). TNBC accounts for 12 to 17% of breast cancers. Compared to other breast cancers, TNBC grows more rapidly and is more likely to metastasize. As a result, there is a great need to develop novel therapeutics for the treatment of TNBC[2]. RNA interference, which uses small 19-23 nucleotides RNAs (siRNA) to knock down target genes by binding to their complementary mRNA and triggering mRNA degradation, has been showing considerable promise for cancer therapy.

Liver fibrosis is a wound healing process characterized by the accumulation of excess extracellular matrix (ECM) in the liver. It is induced by chronic liver injuries caused by nonalcoholic steatohepatitis, hepatitis, alcohol abuse, and metal poisoning[3, 4]. The expression of ECM increases dramatically when quiescent hepatic stellate cells (HSCs) are activated to become myofibroblast-like cells[3, 5-7]. Using siRNA to silence the poly(rC) binding protein 2 (PCBP2) gene can reduce the expression of type I collagen in activated HSCs[8]. However, targeted delivery of antifibrotic siRNA to HSCs is a major challenge in liver fibrosis therapy because of the excessive accumulation of ECM, closure of the endothelial fenestrae, and the reduced flow exchange between sinusoid blood and liver cells[9].

1.2 Statement of the problems

Current treatments in clinics for TNBC are limited to chemotherapy, including taxanes and anthracyclines, rather than targeted therapies such as trastuzumab, pertuzumab and palbociclib[10-14]. Small interfering RNA (siRNA), which specifically down-regulates a target gene with high potency, has been a promising strategy for the treatment of a variety of diseases, many of which are being evaluated in clinical trials[15-18]. The first siRNA drug was recently approved by the U.S. Food and Drug Administration (FDA) in August 2018.

Vascular endothelial growth factor (VEGF) plays important roles in the angiogenesis process and is correlated with high metastasis of breast cancer. Particularly, VEGF is highly expressed in TNBC[19-22]. Based on the results obtained in clinic trials, patients with TNBC display significantly higher VEGF expression than other breast cancer subtypes[20]. Thus, silencing VEGF expression in TNBC cells can be a promising strategy for the treatment of TNBC.

The aberrant activation of nuclear factor-kappa B (NF-κB) was reported to be regulated as a key factor in TNBC[23]. IκB kinase ε (IKBKE, also known as IKKε), an important mediator in the activation of the NF-κB pathway, has been identified as an oncogene in breast cancer[24]. IKBKE was shown to be aberrantly amplified in TNBC cells associated with STAT3 activation and cytokine production[25]. *Thanh et al.,* discovered that IKBKE is related to proliferation, migration and survival in TNBC cells by driving CCL5 and IL-6 production, indicating that deactivation of the NF-κB pathway using IKBKE siRNA may be a promising strategy for TNBC treatment[25].

However, negative charge and large molecular weight (~14 kDa) of siRNAs limit their delivery, cellular uptake and endosome release[15]. Poly(ethyleneimine) (PEI) is a promising polymer for siRNAs delivery, but cytotoxicity of the PEI/siRNA compomex is highly correlated with the molecular weight of PEI[26]. Modification of PEI with a biodegradable polymer can significantly reduce cytotoxicity, and PEI with a molecular weight of less than 2kDa was showed to be nontoxic even at high concentrations. However, transfection efficiency of a low-molecular-weight PEI is also reduced as compared to a high-molecular-weight PEI[27, 28]. Therefore, there has been growing interest in developing biodegradable polymer-modified PEIs for siRNA delivery. Another strategy for siRNA delivery is the use of cationic micelles to simultaneously deliver siRNA and small molecules[29, 30]. In this dissertation, we aimed to develop a low toxic and biodegradable polymer modified PEI delivery system for VEGF siRNA. Moreover, we also aimed to develop a multifunctional cationic nanocomplex for dual delivery of IKBKE siRNA and cabazitaxel for the treatment of TNBC.

Targeted delivery of antifibrotic agents to HSCs is a major challenge in liver fibrosis therapy. Therapeutic agents cannot easily reach HSCs because of the excessive accumulation of ECM, the closure of the endothelial fenestrae, and the reduced flow exchange between sinusoid blood and liver cells[9]. The delivery of antifibrotic agents to HSCs is also limited by the reduced perisinusoidal space (or space of Disse)[31]. One promising strategy to improve the delivery of antifibrotic agents to HSCs is to modify drug carriers with a specific ligand that binds to a moiety on activated HSCs[32-34]. In this dissertation, we aimed to develop a peptide ligand-modified siRNA nanocomplex and to specifically deliver the PCBP2 siRNA to HSCs.

1.3 Objectives

The objectives of the dissertation are as follows:

1. To conjugate low-molecular-weight branched PEIs with different molecular weights (600 Da, 1800 Da, and 10k Da) to a linear multiblock polymer to form a positively charged carrier for the targeted delivery of VEGF siRNA. We will also evaluate siRNA condensation efficiency, cytotoxicity and serum stability of pPEI/siRNA nanocomplexes. Transfection efficacy, cellular uptake and silencing activity of pPEI/VEGF siRNA nanocomplexes at the protein level in MDA-MB-231 cells will be measured. We will also determine the biodistribution of $pPEI_{1800}$/VEGF siRNA nanocomplex *in vivo*.

2. To investigate the migration, invasion and proliferation of $pPEI_{1800}$/VEGF siRNA nanocomplexes in MDA-MB-231 cells and anti-tumor activity in an MDA-MB-231 orthotopic xenograft model. We will determine the expression of VEGF in tumor tissue by ELISA and the density of CD31 in tumors tissue by immunohistochemistry.

3. To investigate whether $pPEI_{1800}$/VEGF siRNA nanocomplex-treated MDA-MB-231 cells inhibit proliferation and tube formulation of HUVEC cells.

4. To investigate the anti-tumor activities of IKBKE siRNA in MDA-MB-231 cells. mRNA and protein levels of IKBKE will be measured. We will also investigate the proliferation, migration, invasion, apoptosis and anti-tumor efficacy of IKBKE siRNA in MDA-MB-231 cells.

5. To develop a CD44-targeting, cabazitaxel- and IKBKE siRNA-loaded nanocomplex for TNBC therapy. We will synthesize cholesterol-modified peptides, which contains a cathepsin B-specific linker (Val-Cit), and cholesterol-modified

hyaluronic acid to encapsulate IKBKE siRNA and cabazitaxel into micelles. We will also investigate siRNA condensation efficiency, serum stability and silencing efficacy at the mRNA and protein levels in MDA-MB-231 cells.

6. To evaluate the cellular uptake, apoptosis and anti-tumor activity of the CHA/CP/siRNA/CTX hybrid nanocomplex. We will also determine the expression of IKBKE in tumor specimens.

7. To prepare PCBP2 siRNA nanocomplexes with different targeting ligands, including cholesterol, vitamin A and IGF2R-specific peptide. These ligands will be conjugated to biotin via a PEG linker and then mixed with neutraviding, PCBP2 siRNA and protamine to form siRNA nanocomplexes. We will characterize the nanocomplexes and evaluate their serum stability.

8. To investigate the cellular uptake and silencing activity of these siRNA nanocomplexes in HSC-T6 cells and rat primary HSCs. We will also evaluate the migration of alcohol-induced HSC-T6 cells and their biodistribution in rats with CCl_4-induced liver fibrosis.

CHAPTER 2

LITERATURE REVIEW

2.1 Therapy options for triple negative breast cancer

2.1.1 Biological characteristics of triple negative breast cancer

Triple-negative breast cancer (TNBC), defined as lacking the expression of estrogen receptor (ER), progesterone receptor (PR) and human epidermal growth factor receptor 2 (HER2), accounts for approximately 12-17% of all breast cancers. TNBC is more aggressive, proliferative and has poorer prognoses and survival rates than non-TNBC[35, 36]. In general, breast cancer is classified into five molecular subtypes based on DNA microassays: Luminal A (ER+ or PR+, HER2-) and Luminal B (ER+ or PR+, HER2+), Basal-like (ER-, PR- & HER2-), HER2 overexpressing (ER-, PR- & HER2+) and normal breast-like[2, 37]. Basal-like breast cancer is also defined by high expression of the basal markers myoepithelial cytokeratin14 (CK14), CK5/6, and epidermal growth factor receptor (EGFR)[2]. Approximately 80% of basal-like breast cancers are TNBC, but TNBCs are heterogeneous compared to basal-like breast cancers at the genetic level[2]. Seventy-one percent of TNBCs were reported to be positive for one or more of these basal markers, but some cases of TNBC are all basal marker-negative[2, 38, 39]. TNBCs are frequently prevalent in African-American women at a 2.4-fold higher rate relative to other races and are also more prevalent in younger women under age 40, unlike the median age of breast cancer diagnosis at 62 years old[40]. Even though the total breast cancer death rate was reduced by 39% from 1985 to 2015, the first 5-year survival rate of TNBC is still lower than those of other breast cancer subtypes[14, 40].

Patients with TNBC tend to have larger tumor size, poorer overall survival, shorter locoregional recurrence, and short time to distant metastasis[41].

2.1.2 Diagnosis of triple negative breast cancer

Currently, no biomarkers can be used to positively define TNBC, and the clinical definition of TNBC involves the use of fluorescence *in suit* hybridization (FISH) analysis and immunohistochemistry (IHC) to determine the lack of expressions of ER, PR, and HER2[42]. The guidelines for ER, PR and HER2 status determination using IHC were recently published by ASCO (American Society of Clinical Oncology) and CAP (College of American Pathologists)[43-46]. Less than 1% of tumor cells with immunoreactivity in clinical trials will be considered ER/PR-negative, and using normal breast tissues such as stromal cells and myoepithelial cells as ER/PR-negative controls can efficiently avoid false-negatives[43, 44]. The ASCO/CAP updated guideline defined HER2-negative status by IHC as exhibiting no stating or 1+ in two situations: weak incomplete staining in any proportion of tumor cells or less than 10% of cells with weak complete staining at the protein level. In addition, a FISH assay with gene copy number ratio of HER2/chromosome 17(CEP17) less than 1.8 or average HER2 less than 4[46].

In addition to the detection of ER, PR and HER2 expression, several other biomarkers, such as EGFR and CK5/6, can be measured to identify TNBC or basal-like breast cancer [43]. Approximately 90% of patients with BRCA1 (breast cancer 1 gene)-mutated tumors were estimated to be basal-like or TNBC, indicating that the BRCA1 gene can also be a diagnosis-guiding biomarker[47]. Because TNBC patients have a

higher chance of locoregional recurrence and distant metastasis, clear and correct diagnosis and identification of the optimal treatment have become more important.

2.1.3 Treatments of triple negative breast cancer

2.1.3.1 Surgery

Unlike ER, PR or HER2-positive breast cancer patients can be treated with receptors-specific targeted therapy, surgery and chemotherapy are still the few options for TNBC patients in clinical practices[48]. To date, there is still no targeted therapy drug approved by the FDA for TNBC treatment[42]. With the development of surgery technology in recent decades, breast conservation therapy (BCT) nowadays has been more considered than simple mastectomy because of the improved locoregional outcomes in early-stage TNBC[48, 49]. Some reports have suggested that BCT with routine radiation is more appropriate for TNBC patients than mastectomy[50, 51]. BCT, especially for locoregional surgery, is limited to early TNBC and other breast cancer subtypes[48]. Meanwhile, it was reported that the locoregional recurrence rate in TNBC patients receiving BCT was greater than that for other breast subtypes[52, 53]. A 15-year outcome meta-analysis involving approximately twenty thousand breast cancer patients showed a higher risk for local relapse and overall recurrence in TNBC groups relative to other non-TNBC groups treated with BCT[54]. Due to the high risk of relapse and highly metastatic ability of TNBC, primary system therapy is a better option than surgery for patients with TNBC[48].

2.1.3.2 Radiotherapy

Currently, there is no difference with radiotherapy for TNBC relative to other breast cancer subtypes[37]. Generally, it is suggested that breast cancer patients with invasive carcinoma receive combination treatment with radiation therapy followed by BCT or mastectomy if the tumor size is over 5 cm or has positive axillary nodes[41]. Whole breast radiation therapy (WBRT) is normally combined with lumpectomy as a BCT for early, invasive breast cancer, including TNBC[49]. Survival benefits have been found in breast cancer patients treated with lumpectomy combined with WBRT or mastectomy with postmastectomy radiation therapy (PMRT) relative to simple surgery[55, 56]. Current guidelines for PMRT treatment do not consider breast cancer subtypes. ASCO suggested that patients with positive nodes, positive margins and stage III or T3 tumors should be treated with PMRT[57]. Although a phase III trial for early-stage TNBC patients has shown significant improvement with additional PMRT treatment, the relationship between PMRT outcome and TNBC is still unclear[49, 58]. Another radiation therapy refers to faster radiation delivery methods, includes accelerated partial breast irradiation (APBI) and hypofractionated WBRT, which have much shorter delivery times and improved patient convenience. Due to the higher risk of residual invasive and residual tumor burden for TNBC after lumpectomy, APBI, defined as delivering a high dose of radiation to a small area around the lumpectomy cavity, is more frequently considered for the TNBC subtype[49]. A study analyzing the outcomes for different breast cancer subtypes treated with single-entry catheter APBI for nearby 1500 patients showed that TNBC patients have a related higher 5-year breast tumor recurrence

rate of approximately 5.4% relative to 2.6% overall, 2.1% for luminal A, 1.5% for luminal B and 4.9% for HER2, which has a higher regional nodal recurrence rate[59].

2.1.3.3 Chemotherapy

A meta-analysis of over 6000 women patients in two decades in 46 clinical trials for ER-negative breast cancer showed a significant recurrence rate with combined polychemotherapy relative to local therapy alone[60]. It was reported that TNBC is sensitive to chemotherapy drugs, particularly to taxanes (paclitaxel, docetaxel and cabazitaxel) targeting the DNA repair complex and anthracyclines (doxorubicin, epirubicin) targeting cell proliferation, with a better initial therapeutic response relative to other subtypes of breast cancer[47, 61]. Adjuvant chemotherapy and neoadjuvant chemotherapy are used instead of chemotherapy for TNBC patients when the preferred chemotherapy is unavailable, and cytotoxic chemotherapy is still the mainstay treatment for early and advanced breast cancer[61, 62].

2.1.3.3.1 Taxanes based adjuvant & neoadjuvant chemotherapy

Taxanes, including paclitaxel, docetaxel, and cabazitaxel, are a group of tubulin polymerizers known as microtubule stabilizers that induce cellular apoptosis and were reported to be more effective in TNBC patients than non-TNBCs patients[63, 64]. Generally, taxanes are been utilized as an adjuvant or neoadjuvant chemotherapy with doxorubicin or epirubicin plus an alkylating agent such as cyclophosphamide[61, 62, 65]. Currently, there are no differences in adjuvant and neoadjuvant chemotherapy between TNBC and non-TNBC. The efficacy of taxane-based neoadjuvant chemotherapy has been

suggested by several clinical trials, and taxane-anthracycline combination treatment is utilized as the standard of care for moderate-advanced TNBC[60]. A long-term follow-up phase III study with 4,954 enrolled patients (The Eastern Cooperative Oncology Group E1199) was performed to evaluate the efficacy of taxanes in operable breast cancer. In this study, women patients with advanced breast cancer were treated with taxanes (paclitaxel or docetaxel) combined with doxorubicin plus cyclophosphamide, and the results suggested that weekly paclitaxel plus doxorubicin and cyclophosphamide significantly improved disease-free survival (DFS) and 5-year overall survival in TNBC groups[66]. The National Surgical Adjuvant Breast and Bowel Project (NASBP) also performed a B-30 study for 5351 patients that suggested a 69% DFS rate for a concurrent docetaxel-treated group and a small improvement in DFS with the combination of cyclophosphamide and doxorubicin followed by docetaxel (74% for 8-year DFS) compared to a doxorubicin/docetaxel-treated group (69% for 8-year DFS, P=0.001)[67]. In another phase II study, the addition of cisplatin to paclitaxel and epirubicin significantly improved the pathologic complete response (pCR) rate, DFS and OS values in early-stage TNBC. However, platinum salts agent-based neoadjuvant chemotherapy showed no difference between TNBC and non-TNBC patients with advanced or metastatic breast cancer[61]. Meanwhile, the combination of platinum salts with taxane-anthracycline showed no improvement in the pCR rates for TNBC groups in a phase II study[68].

Cabazitaxel (XRP-6258, CTX), is a novel second-generation semi-synthetic taxane developed by Sanofi-Aventis to overcome drug resistance and was approved by the FDA for the treatment of hormone-refractory prostate cancer[69]. As a microtubule

stabilizer, cabazitaxel has an equivalent potency and similar anti-proliferation activity to docetaxel but is more potent in chemo- or taxane-resistant tumors[69, 70]. The poor affinity of cabazitaxel for P-glycoprotein, which is involved in taxane resistance in cancer cells, improves the treatment efficacy of cabazitaxel in metastatic prostate cancer and indicates the promising potential of this drug for the treatment of metastatic breast cancer, especially metastatic TNBC[71, 72]. However, cabazitaxel was found to have a high systemic toxicity, which may limit its applications for TNBC treatment. As a result, a novel delivery strategy to alleviate its toxicity is highly needed for its clinical application [73]. Several reports have suggested that chemical modification or encapsulation of cabazitaxel into micelles or nanoparticles may significantly improve its anti-tumor efficacy with alleviated toxicity in metastatic TNBC[72-74].

2.1.3.4 Targeted therapy

The goals of adjuvant and neoadjuvant chemotherapy are to increase the OS time, pCR rate and improve BCT for TNBC patients. In addition to the chemotherapy agents mentioned above, novel targeted therapies have also received attention in recent decades.

2.1.3.4.1 Angiogenesis inhibitors in TNBC

The vascular endothelial growth factor family comprises VEGF-A, VEGF-B, VEGF-C, VEGF-D, and placenta growth factor (PIGF). VEGF plays important roles in the angiogenesis process and is correlated with high metastasis of breast cancer, particularly TNBC with high expression[19-22]. Based on the results of clinical trials, patients with TNBC display significantly higher VEGF expression than patients with

other subtypes of breast cancer[20]. Currently, anti-VEGF agents, including bevacizumab and ramucirumab, have failed in several phase III trials due to a lack of significant improvement in TNBC patients[75, 76]. Meanwhile, VEGFR blockade does not exert a biological effect on MDA-MB-231 cells (a TNBC cell line) because VEGFR-1 expression is only detected on the plasma membrane, and the lack of VEGFR-2 expression indicates that another route to target the VEGF/VEGFR axis in the plasma membrane must be identified to treat TNBC[77].

2.1.3.4.2 IκB kinase ε (IKBKE) in TNBC

Regulation of the aberrant activation of nuclear factor-kappa B (NF-κB) was reported to be a key factor in TNBC[23]. The NF-κB family contains five transcription factors, RelA (p65, NFκB3), c-Rel, RelB, NFκB1 (p50) and NFκB2 (p52), which are protein complexes that regulate genes to control DNA transcription, cytokine production, cell survival, proliferation, invasion, and metastasis and are also associated with tumor's chemo-resistance[78]. In general, NF-κB is present in an inactive form with different hetero- or homodimeric combinations, such as the p65/p50 complex bound to IκB (inhibitor of κB) proteins[79]. High constitutive NF-κB activation was found in several cancers, including breast cancer, and was associated with increased metastasis and faster tumor growth with larger size[78]. The regulation of NF-κB signaling includes two pathways: the canonical pathway and the noncanonical pathway. In cancer cells, inhibitory κB kinases (IKKs) phosphorylate IκBs and induce their degradation. The released NF-κB hetero- or homodimers then are translocated into the nucleus and regulate targeted gene expression[80]. In contrast to the canonical pathway, the noncanonical

pathway is present in cancer cells for NF-κB signaling regulation. NF-κB inducing kinase (NIK) and IKK1 are selectively activated to phosphorylate p100, leading to the release of the RelB/p52 homodimer to regulate gene and cytokine production[78, 80]. These activating NF-κB signaling pathways were found to enhance cellular proliferation, invasion, and metastasis and decrease cellular apoptosis in breast cancer, especially in ER-negative breast cancers such as TNBC[78].

IKKε, an important mediator in the activation of the NF-κB pathway, is identified as an oncogene in breast cancer[24]. The IKK family contains five members: IKKα, IKKβ, IKKγ, TBK-1 (TANK-binding kinase 1) and IKKε[16]. It was reported that IKKε has 65% similarity with TBK-1, including an N-terminal kinase domain, a C-terminal leucine zipper, a helix-loop-helix motif and a ubiquitin-like domain[81]. Both IKBKE and TBK-1 are related to the noncanonical NF-κB signaling pathway, but their function and regulation of targeting proteins are different[81]. Unrelated to its regulatory roles in the interferon response, IKBKE phosphorylates serine-536 to activate the NF-κB signaling pathway in breast cancer[82]. IKBKE can also induce NF-κB activation by phosphorylating TRAF2 and CYLD, and is overexpressed in approximately 30% of breast carcinomas and aberrantly overexpressed in TNBC[24, 25, 83-85]. A report also demonstrated that IKBKE protected cells against DNA damage-induced death through IKKε SUMOylation[86]. Using an IKBKE siRNA, *Qin et al.* found that silencing of IKKε expression in breast cancer cells (MCF7 and SK-BR-3) significantly suppressed proliferation and invasion of the cells[16]. As an oncogene in breast cancer, IKBKE is aberrantly amplified in TNBC cells and is associated with STAT3 activation and cytokine production[25]. By using IKBKE shRNAs and a TBK1/IKBKE, JAK signaling inhibitor

(CYT387), *Thanh et al.,* found that IKBKE mediates the proliferation, migration, and survival of TNBC cells by driving CCL5 and IL-6 production[25].

2.1.3.4.3 Other potential targeted therapies in TNBC

The BCRA1-mutated breast cancer appears into basal-like subtype gene expression profiles, which share features with TNBC. Seventy percent of BCRA1-mutated breast cancer patients show the ER-, PR- and HER2- peculiarity, which is defined as TNBC. However, less than 42% of TNBC patients have BCRA1 mutations[61]. BCRA1 plays an important role in repairing damaged DNA, and BCRA1-mutated breast cancer patients share histological peculiarities with TNBC, including DNA repair defects and p53 gene mutations[87, 88]. Poly ADP-ribose polymerase (PARP) enzymes are responsible for the DNA double-strand break repair involved in nucleotide excision repair (NER), and tumors with BCRA1 mutations are sensitive to PARP inhibitors[89]. PARP inhibitors can either inhibit NER to generate synthetic lethality or make TNBC/BCRA1-mutated cancer cells become sensitive to cyclophosphamide-based DNA alkylating agents[90].

The epithelial growth factor receptor (EGFR) contains 4 related receptor tyrosine kinases, EGFR (ErbB-1), HER2 (ErbB-2), HER3 (ErbB-3) and HER4 (ErbB-4), which all belong to the ErbB family. There are two kinds of EGFR inhibitors: small molecular EGF tyrosine kinase inhibitors and anti-EGFR antibodies. Sunitinib, dasatinib, and neratinib are EGF tyrosine kinase inhibitors and have been widely used as anti-tumor drugs in patients receiving chemotherapy. Cetuximab is an anti-EGFR monoclonal antibody that is available on the market for head and neck cancer, metastatic colorectal

cancer and metastatic non-small cell lung cancer. Three studies uing cetuximab for TNBC are now being evaluated in clinical trials.

2.1.4 Gene therapy for TNBC

Gene silencing has been a promising strategy for the treatment of a variety of diseases, and many of them are being evaluated in clinical trials[15-18]. Among the different gene silencing platforms, small interfering RNAs (siRNAs) with 19-23 nucleotides has the ability to specifically down-regulate a target gene with high potency[91]. Several siRNAs targeting different genes were developed for TNBC treatment. *Yang et al.,* treated TNBC by silencing Cyclin-dependent kinase 1 gene with siRNA significant suppress tumor growth *in vivo*[92]. A report also suggested that the metastasis of TNBC can be inhibited treated with a β3 integrin siRNA[93]. Co-delivery of anti-tumor drug (Doxorubicin) with multidrug resistance protein 1 (MRP1) targeting siRNA to overcome the chemo-resistance in TNBC was also developed[94].

However, the highly negative charge and large molecular weight (~14 kDa) of siRNAs limit their delivery, cellular uptake and endosome release[15]. Non-viral vectors with low immunogenicities, such as polymers, micelles, liposomes and nanoparticles, have been developed to overcome these obstacles of siRNA delivery[32, 95-97].

Poly(ethyleneimine) (PEI) is one of the promising polymer for siRNAs delivery. It is known that PEI efficiently neutralizes the negative charge of siRNA, forms a nanocomplex with the siRNA through electrostatic interactions and releases the siRNA from the endosome to cytosol via the “proton sponge effect”[98, 99]. However, the transfection efficiency and cytotoxicity of siRNA/PEI complexes are highly correlated

with the molecular weight of PEI[26]. High-molecular-weight (HMW) PEI has a high gene transfection efficiency but considerable cytotoxicity. On the contrary, low-molecular-weight (LMW) PEI has low cytotoxicity but exhibits low gene transfection efficiency due to its low condensation capacity[26, 100]. The low polymerization degree of LMW PEI is correlated with its small size and limits its ability to form strong electrostatic associations with DNA or RNA in nanoscale structures[26]. Another limitation of PEI is its non-degradable backbone[101, 102]. Poly (ethylene glycol) (PEG) has been widely used to improve the pharmacokinetics and stability of nanoscale drug delivery systems, including siRNA nanocomplexes, through the "stealth effect"[103].

Another strategy for siRNA delivery is the use of cationic lipid-nanoparticles or micelles. In August 2018, the lipid nanoparticle-formulated siRNA (Patisiran) treating hereditary transthyretin-mediated amyloidosis was approved by the FDA as the first siRNA drug in the world. A cholesterol-modified cationic peptide containing lysine and histidine was recently developed by our laboratory to deliver siRNA for cancer therapy[97]. The cholesterol-peptide/siRNA nanocomplex protects siRNA from serum degradation and delivers siRNA into various types of cancer cells with high silencing efficacy without inducing toxicity. The cholesterol-peptide forms micelles before complexation with the siRNA. As a result, hydrophobic chemotherapy drug can be encapsulated in the micelle and then complexed with siRNAs for combinational therapy.

siRNAs can also be delivered with cationic cell-penetrating peptides (CPPs) by conjugation or through the formation of CPP/siRNA polyplexes[91]. Protamines are low-molecular-weight cationic proteins approved by the FDA as the antidote for heparin. For example, *Song et al.,* conjugated protamine to a single-chain antibody to deliver siRNAs

to HIV-infected or envelop-transfected cells[104]. Our laboratory recently developed a streptavidin-based nanocomplex to deliver siRNA for liver fibrosis. Biotin was conjugated to siRNA with a disulfide linker and assembled a nanocomplex with a biotin-conjugated cholesterol ligand via a streptavidin-biotin interaction, then condensed with protamine to form an siRNA delivery nanocomplex[32].

Due to the lack of ER, PR, and HER2 in TNBC for targeted therapy, despite surgery, radio- and chemo-therapy, the use of siRNA to silence oncogenes may be a promising strategy for TNBC treatment. In this dissertation, we aim to develop polymer-PEI conjugated delivery systems to deliver VEGF siRNA to inhibit the proliferation and invasion of TNBC cells. We also combine cabazitaxel with an siRNA targeting IKKε oncogene into a modified cholesterol peptide-based micelle structure nanocomplex with a targeting ligand (hyaluronic acid) to specifically deliver siRNA and cabazitaxel into TNBC cells.

2.2 Targeting therapy for liver fibrosis

2.2.1 Biological characteristics of liver fibrosis

Liver fibrosis is a wound healing process characterized by the accumulation of excess extracellular matrix (ECM) in the liver. It is induced by chronic liver injuries caused by nonalcoholic steatohepatitis, hepatitis, alcohol abuse, and metal poisoning[3, 4]. If left untreated, liver fibrosis will develop into liver cirrhosis, which is irreversible and affects nearly 633,233 adults in the United States[105]. Up to now, with the exception of liver transplantation or the removal of lesion, there is still no effective treatment available for liver fibrosis[106]. Several antifibrotic agents, such as

simtuzumab, which targets lysyl oxidase homolog 2 (LOXL2), candesartan, and losartan, are currently in clinical trials[107, 108]. Recent reports indicated that liver fibrosis can be reversible, which suggests a potential novel treatment therapy[8, 106].

2.2.2 Hepatic stellate cells and ECM for liver fibrosis

In the process of liver fibrosis, hepatic stellate cells are playing an important role. Although HSCs only constitute approximately 5-8% of total liver cells[109], they are the major contributors for liver fibrosis and are able to cover the entire microcirculatory network of hepatic sinusoidal[110]. The HSCs can be activated by several factors like alcohol and the activation process including two parts: initiation and perpetuation starting from gene expression mutation to the profile changes in proliferation and fibrogenesis[111]. The expression of ECM increases dramatically more than 50 folds when quiescent HSCs are activated to myofibroblast-like cells[3, 5-7]. Type I collagen is the most abundant protein in ECM, and its abnormal accumulation is primarily due to the increased half-life of its collagen α1(I) mRNA[112, 113]. *Shukla et al.* recently discovered a siRNA to silence the poly(rC) binding protein 2 (PCBP2) gene in HSCs to inhibit the expression of αCP2 protein, which is responsible for stabilization of the collagen α1(I) mRNA. Silencing of the PCBP2 gene reduced the expression of type I collagen in activated HSCs[8].

2.2.3 Targeting options for liver fibrosis treatment

Targeted delivery of antifibrotic agents to HSCs is a major challenge in liver fibrosis therapy. Therapeutic agents cannot easily reach HSCs because of the excessive

accumulation of ECM, the closure of endothelial fenestrae, and the reduced flow exchange between sinusoid blood and liver cells[9]. The delivery of antifibrotic agents to HSCs is also limited by the reduced perisinusoidal space (or space of Disse)[31]. Due to such reduced space in liver vasculature nanomedicines with 100-200 nm diameter are more likely to accumulate in the fibrotic liver[114]. These nano delivery vehicles can be substantially improved by modification with specific molecules targeting the highly expressed proteins on the surface of HSCs[32-34]. Therefore, by targeting such unique receptor proteins can be an effective way to delivery antifibrotic agents to treat liver fibrosis. One promising strategy to improve the delivery of agents to HSCs is to modify drug carriers with a specific ligand that binds to a moiety on activated HSCs[32-34]. Various receptors including low-density lipoprotein receptor (LDLR), cellular-binding protein type I (CRBP-1), and insulin-like growth factor 2 receptor (IGF2R) have been exploited to enhance drug delivery to HSCs.

2.2.3.1 Cellular Retinol-binding protein type I (CRBP-1)

CRBP-1 belongs to the retinol-binding protein (RBP) family, which consists of the receptors for vitamin A and retinyl analogs on the surface of HSCs and hepatocytes, but the expression of CRBP is significantly downregulated in advanced human fibrotic liver[115-117]. Approximately 50-80% of vitamin A in the body is stored as retinyl palmitate in lipid droplets in HSCs, which are taken up through CRBP-1[116, 118]. Vitamin A has therefore been utilized to deliver agents to HSCs. For example, *Sato et al.,* developed a vitamin A coupled liposome to deliver gp46 siRNA to fibrotic liver[34]. In addition to CBRP-1, other RBP family members can also bind with vitamin A, such as

the plasma retinol-binding protein in the serum, which acts as a retinol transport vehicle, and RBPs overexpressed on the surface of hepatocytes receive and metabolize retinoids, limiting the targeting effects of vitamin A as the ligand for a delivery system[116, 119].

2.2.3.2 Low-density lipoprotein receptor (LDLR)

The expression of LDLR and high-density lipoprotein receptor-scavenger receptor class B type1 (SR-B1) was reported highly expressed in the liver[120, 121], and these proteins can be targeted by cholesterol[32, 122, 123]. A triplex-forming oligonucleotide (TFO) conjugated with cholesterol was discovered to target the Type I collagen promoter in fibrotic liver with a 4-fold increase in cellular uptake[123]. In another study, cholesterol was used as a targeting ligand and modified into a streptavidin-based siRNA delivery nanocomplex. When compared in two different cell lines, HSC-T6 (LDLR+) and Caco-2 (LDLR-), the cholesterol-modified nanocomplex showed a higher uptake in HSC-T6 cells. Meanwhile, after adding puromycin(an LDLR inhibitor), the reduced cellular uptake in HSC-T6 cells also indicated the function of cholesterol in the nanocomplex by specifically targeting LDLR[32]. However, the lipophilic effects of cholesterol also limit the targeting of HSCs *in vivo*[124].

2.2.3.3 Insulin-like growth factor 2 receptor (IGF2R)

The insulin-like growth factor 2 receptor (IGF2R), also known as the mannose-6-phosphate receptor (M6PR), is a 300 kDa glycoprotein that plays a critical role in the insulin-like growth signaling system. IGF2R contains 3 domains: an extracellular domain, a transmembrane domain and a cytoplasmic domain[125]. Due to its upregulated

expression during the process of liver fibrogenesis[126, 127], IGF2R can be utilized as a targeting receptor for HSC-specific drug delivery. Studies have shown that the expression of IGF2R can be increased by ~20 folds in activated HSCs relative to quiescent HSCs [128]. Moreover, approximately 16% of IGF2Rs are located on the cell membrane surface, and IGF2R-mediated endocytosis is 3 times faster in activated HSCs relative to quiescent HSCs[128]. Because its expression is upregulated during liver fibrogenesis, IGF2R has been utilized as a targeting moiety for HSC-specific drug delivery. For example, *Ye et al.,* delivered triplex-forming oligonucleotides to fibrotic rat liver using M6P as a ligand targeting IGF2R/M6PR[33]. Our laboratory recently discovered an IGF2R-specific peptide, peptide 431 (VHWDFRQWWQPS), using a novel combinatorial biopanning strategy. Peptide-431 and its dimeric form showed high and specific affinity to activated human and rat HSCs, suggesting this peptide may be a promising targeting ligand for HSC delivery[127].

2.2.3.4 Other potential targeting receptors

In addition to CRBP-1, LDLR and IGF2R, many receptors that are highly expressed during liver fibrosis can be actively targeted. Platelet-derived growth factor receptor (PDGFR), which has two isoforms, PDGFRα and PDGFRβ, are upregulated in a liver fibrosis model, and a peptide specifically recognized by PDGFβR was discovered to carry INFγ and improve anti-fibrotic effects[129]. Integrins are also involved in liver fibrogenesis by mediating the interaction between ECM and HSCs, and an RGD peptide ligand was utilized to modify nanoparticles for liver fibrosis treatment[130].

In summary, liver fibrosis is a wound healing process characterized by the accumulation of ECM in the liver and can be reversed by specifically reducing Type I collagen expression. Targeted delivery of antifibrotic agents to HSCs is a major challenge in liver fibrosis therapy because of the excessive accumulation of ECM, the closure of the endothelial fenestrae, and the reduced flow exchange and reduced perisinusoidal space. In this dissertation, we aim to prepare siRNA nanocomplexes modified with three different ligands (cholesterol, vitamin A and IGF2R-specific peptide) and evaluate their cellular uptake, biodistritubion and anti-fibrotic effects for liver fibrosis.

CHAPTER 3

DEVELOPMENT OF A POLYETHYLENIMINE CONJUGATED LINER MULTIBLOCK POLYMER TO DELIVER VEGF siRNA FOR TRIPLE NEGATIVE BREAST CANCER

3.1 Rationale

Triple negative-breast cancer is an aggressive type of breast cancer that lacks the expression of estrogen receptor, progesterone receptor and human epidermal growth factor receptor 2. Although TNBC only accounts for 12-17% of all breast cancers, it represents the most difficult breast cancer subtypes to treat because of its aggressiveness, high proliferation, poor prognosis, and low survival rates[35, 36]. Current treatments in clinics for TNBC are limited to chemotherapy, including taxanes and anthracyclines, or biological inhibition agents, instead of receptors targeted therapies, such as trastuzumab, pertuzumab for HER2 and tamoxifen targeting ER[10-14]. The vascular endothelial growth factor family comprises VEGF-A, VEGF-B, VEGF-C, VEGF-D and placenta growth factor (PIGF). VEGF plays important roles in the angiogenesis process and is correlated with high metastasis of breast cancer, particularly TNBC with high expression[19-22]. Based on the results of clinical trials, patients with TNBC display significantly higher VEGF expression than patients with other breast cancer subtypes[20]. Currently, anti-VEGF agents, including bevacizumab and ramucirumab, have failed in several phase III trials due to a lack of significant improvement in TNBC patients[75, 76]. Meanwhile, VEGFR blockade does not exert a biological effect on MDA-MB-231 cells (a TNBC cell line) because VEGFR-1 expression is only detected on the plasma membrane, and the lack of VEGFR-2 expression indicates that another route

to target the VEGF/VEGFR axis in the plasma membrane must be identified to treat TNBC[77]. In our previous study, we developed a VEGF siRNA and reported its inhibitory effect on breast cancers by knocking down VEGF expression[131].

Gene silencing has been a promising strategy for the treatment of a variety of diseases, and many of them are being evaluated in clinical trials[15-18]. Among the different gene silencing platforms, small interfering RNAs (siRNAs) with 19-23 nucleotides has the ability to specifically down-regulates a target gene with high potency[91]. However, the highly negative charge and large molecular weight (~14 kDa) of siRNAs limit their delivery, cellular uptake and endosome release[15]. Non-viral vectors with low immunogenicities, such as polymers, micelles, liposomes and nanoparticles, have been developed to overcome these obstacles of siRNA delivery[32, 95-97]. In August 2018, the lipid nanoparticle-formulated siRNA (Patisiran) treating hereditary transthyretin-mediated amyloidosis was approved by the FDA as the first siRNA drug in the world.

Poly(ethyleneimine) is one of the promising polymer for siRNAs delivery. It is known that PEI efficiently neutralizes the negative charge of siRNA, forms a nanocomplex with the siRNA through electrostatic interactions and releases the siRNA from endosome to cytosol via the "proton sponge effect"[98, 99]. However, the transfection efficiency and cytotoxicity of siRNA/PEI complexes are highly correlated with its molecular weight[26]. High-molecular-weight (HMW) PEI has a high gene transfection efficiency but considerable cytotoxicity. On the contrary, low-molecular-weight (LMW) PEI has low cytotoxicity but exhibits low gene transfection efficiency due to its low condensation capacity[26, 100]. The low polymerization degree of LMW PEI is

correlated with its small size and limits its ability to form strong electrostatic associations with DNA or RNA in nanoscale structures[26]. Another limitation of PEI is its non-degradable backbone[101, 102]. Poly (ethylene glycol) (PEG) has been widely used to improve the pharmacokinetics and stability of nanoscale drug delivery systems, including siRNA nanocomplexes, through the "stealth effect"[103]. In our previous study, a PEG-based linear multiblock polymer was synthesized with degradable lysine-glutaric acid backbone to generate a polymer-drug conjugate[132]. In this present study, low-molecular-weight branched PEIs with different molecular weights (600 Da, 1800 Da, and 10k Da) were conjugated to the linear multiblock polymer to form a highly positively charged carrier for targeted delivery of the VEGF siRNA to TNBC with low cytotoxicity, high transfection efficiency and enhanced permeability and retention (EPR) effect *in vitro & in vivo*[133].

3.2 Materials and methods

3.2.1 Materials

Poly(ethyleneimine) (MW 600, 1800, 10k), BD Matrigel, Annexin V-FITC apoptosis kit, GelRed™ and chimerical regents were purchased from Fisher Scientific (Pittsburg, PA). Lipofectamine® 2000, VEGF siRNA, Cy5-labeled siRNA were obtained from Invitrogen (Carlsbad, CA). VEGF ELISA kit was ordered from R&D system (Minneapolis, MN)**.** The CellTiter-Glo luminescent cell viability assay kit was purchased from Progema (Madison, WI).

3.2.2 Cell culture

MDA-MB-231 and HeLa cells were purchased from American Type Culture Collection and cultured with DMEM with 10% fetal bovine serum(FBS), 100 μg/mL streptomycin and 100 units/mL penicillin. Human Umbilical Vein Endothelial Cells (HUVEC) were purchased from Fisher Scientific and cultured with endothelial cell growth medium containing supplement reagents (R&D Syetems Inc, Minneapolis, MN). Cells were incubated in a humidified atmosphere at 37° with 5% CO_2 and performed experiments in the growth logarithmic phase.

3.2.3 Synthesis of polymer-PEI conjugate

The synthetic reaction scheme is presented in Figure 1A. Poly[*bis*(ε-Lys-OBn)Glut-PEG] was synthesized using methods described in our previous report[132], and then formed a multiblock linear polymer (Poly[bis(ε-Lys)Glut-PEG]) by reduction with Pd/C in the presence of H_2 to release two activated carboxyl groups in each unit. After purification, 50 mg of Poly[bis(ε-Lys)Glut-PEG polymer was dissolved in dimethylformamide (DMF) with 75 mg of 1-ethyl-3-(3-dimethylaminopropyl) carbodiimide (EDC) and 75 μl of Triethylamine (TEA). Different amounts of PEI 600, 1800 and 10k were added to the solution at different molar ratios (1:1, 1:10 and 1: 20, respectively). The mixture was stirred at room temperature for 24 h with N_2 protection, and the polymer-PEIs ($pPEI_{600}$, $pPEI_{1800}$ and $pPEI_{10k}$) were precipitated by adding cold diethyl ether and dialyzed for 24 h (MWCO: 14kDa). The conjugates were confirmed by ^{1}H-NMR.

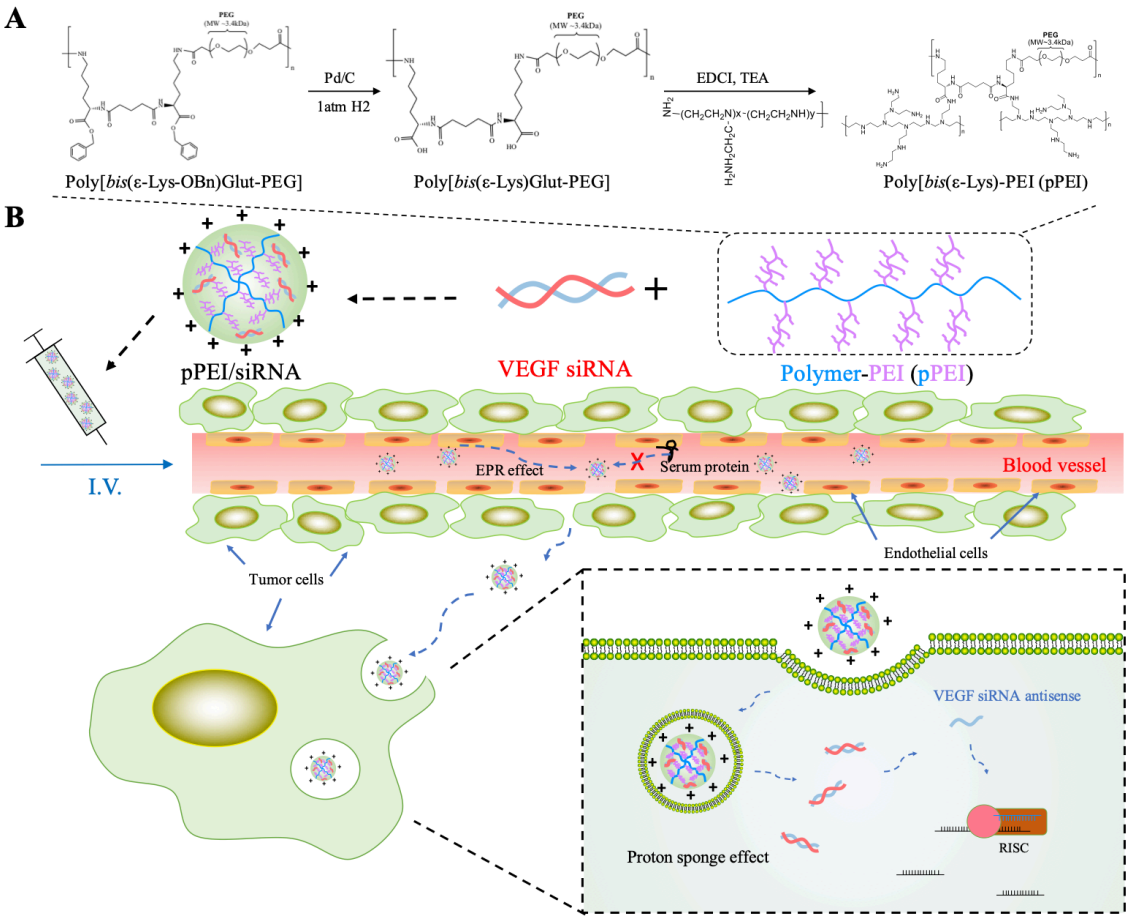

Figure 1. Synthesize scheme of polymer-PEIs, schematic illustration of pPEI/siRNA nanocomplex preparation and intended mechanism for TNBC treatment. The polymer-PEIs ($pPEI_{600}$, $pPEI_{1800}$, $pPEI_{10k}$) were synthesized by conjugated different low-molecular-weight branched PEIs to Poly[bis(ε-Lys)Glut-PEG] polymer chains and condensed VEGF siRNA into a nanocomplex structure. pPEI/siRNA nanocomplexes protected siRNA from serum protein degradation and accumulated in tumor tissue via enhanced permeability and retention (EPR) effect. The positive charge on pPEI/siRNA nanocomplex then mediated cell endocytosis and helped siRNA escape from endosome to cytosol via the "proton sponge effect".

3.2.4 Fabrication and characterization of pPEI/siRNA binary nanocomplexes

pPEIs were synthesized as mentioned above, then mixed with 20μM VEGF siRNA (sequence: 5'-GCU ACU GCC AUC CAA UCG Att-3') in different siRNA:pPEI w/w ratios (1:1, 1:5, 1:10 and 1:20) at room temperature for 30 min, and diluted to 100 nM with PBS and Opti-MEM for characterization and transfection, respectively[131]. Optimized pPEIs-siRNA ratios were measured using a gel retardation assay with a 2% agarose gel and the zeta potential was confirmed as previously reported[103]. Particle sizes of pPEI/siRNA nanocomplexes were determined using a Malvern Zetasizer Nano-ZS (Malvern Instruments, MA) in 100mM HEPES buffer (pH 7.4) and a CM12 Scanning Transmission Electron Microscope (TEM) (Philips, Germany).

3.2.5 TNBS assay

The degree of prime amine substitution of the polymer-PEIs (pPEIs) was determined with a 2,4,6-trinitrobenzene sulfonic acid (TNBS) assay. Briefly, $pPEI_{600}$, $pPEI_{1800}$ and $pPEI_{10k}$ samples synthesized at a 1:10 molar ratio were added to 96-well plates at a concentration of 1mg/ml, incubated with TNBS buffer at 37℃ for 2 hrs. After adding 10% sodium dodecyl sulfonate buffer and 1N hydrochloric acid, the absorbance of the samples was determined at 335 nm using Spectramax 190 microplate spectrophotometer (Molecular Devices, CA). A series of concentrations of PEI 600, 1800 and 10k were added as described above to generate the standard curves.

3.2.6 Serum stability

Polymer-PEIs were mixed with siRNA at a ratio of 10:1 (w/w) to form siRNA nanocomplexes and then incubated with 50% rat serum at 37℃ for various time intervals. siRNAs in the nanocomplexes were released by incubation with 40 μM heparin, electrophoresed in 2% Agarose Gel and visualized with GelRed^{TM} staining.

3.2.7 *In vitro* cytotoxicity study

Cytotoxicity of the polymer-PEI/siRNA nanocomplexes was measured by 3-(4,5-dimethylthiazol-2-yl)-2,5-diphenyltetrazolium bromide (MTT) assay. Briefly, 1×10^4 HeLa or MDA-MB-231 cells were seeded in 96-well plates and incubated at 37℃ overnight. $pPEI_{600}$, $pPEI_{1800}$ and $pPEI_{10k}$ were mixed with scrambled siRNA to form nanocomplexes, diluted in DMEM medium containing 10% FBS with a final siRNA concentration of 100 nM, and incubated with the cells for 24 and 48 h. MTT assay was performed to measure the cytotoxicity of the nanocomplexes as described before[103].

3.2.8 Cellular uptake study

HeLa and MDA-MB-231 cells (1×10^5) were seeded in 24-well plates and incubated at 37℃ overnight. The 5' end of the siRNA antisense strands were labeled with Cy5. The cells were transfected with the pPEIs/Cy5-siRNA nanocomplex at a siRNA concentration of 100 nM in Opti-MEM for 6 h. The cells were then washed with 40 μM heparin to remove non-specific bound nanocomplexes and then subjected to fluorescence analysis with a FACS II flow cytometer (BD instrument, NJ). Confocal analysis was prepared as previously described[103].

3.2.9 3D spheroid penetration study

A 3D spheroid was prepared with Spheroid Formation ECM from Amsbio (Cambridge, MA). Three thousand MDA-MB-231 cells were harvested, re-suspended in 50 μL Spheroid Formation ECM, added into a Corning™ 96-well Ultra-low attachment microplate (Pittsburgh, PA), centrifuged at 200 g for 3 min at 4℃, and incubated at 37℃ to induce spheroid formation. For the 3D spheroid penetration study, after 120 h, spheres were incubated with the pPEI/Cy5-siRNA nanocomplexes diluted in Opti-MEM medium incubated at 37℃ for 6 h. These spheres were then washed with PBS, fixed with 10% paraformaldehyde and transferred to a 4-well chamber for confocal microscopy.

3.2.10 *In vitro* transfection study

Approximately 5× 10^3 HeLa cells were seeded into each well of a 96-well plate and incubated at 37°C overnight. Sixty nanograms of Luciferase-pcDNA3 plasmid (Addgene, MA) and 30 ng pMCS-Green Renilla Luc plasmid (ThermoFisher, CA) were mixed with 0.2 μl of Lipofectamine® 2000 (ThermoFisher, CA) in 100 μl of Opti-MEM and incubated at 37°C for 6 h for the first step transfection. Luciferase siRNAs (5' CUU ACG CUG AGU ACU UCG Att 3') or scrambled siRNA formed nanocomplexes with pPEIs as mentioned above, diluted in Opti-MEM, and incubated at 37°C for 6 h in the second-step transfection. Next, the medium was replaced with normal DMEM containing 10% FBS and incubated for another 42 h. The silencing activity of siRNA/pPEI nanocomplexes was quantitated using a Dual luciferase assay kit (Promega, WI).

3.2.11 Silencing activity of pPEI/VEGF siRNA nanocomplex

A VEGF ELISA was performed to determine the silencing activity of pPEI/$VEGF_{149}$ siRNA nanocomplexes. Approximately 1×10^5 MDA-MB-231 cells were seeded in each well of a 24-well plate and incubated at 37°C overnight. pPEIs/VEGF siRNA nanocomplexes were formed as described above at a 100 nM final concentration, transfected into cells, and incubated for 24 h. The medium was replaced with normal DMEM and incubated for 24 h at 37°C. Lipofectamine® 2000 was used as a control. Then, the media were collected and the levels of the VEGF protein were quantified using a DueSet® Human VEGF ELISA kit with a Spectramax 190 plate reader.

3.2.12 Migration and invasion study

The migration and invasion assays were performed as described in a previous study[131]. For the invasion assay, 50 μg of Matrigel were coated on the top of the transwell chamber. MDA-MB-231 cells were treated with the $pPEI_{1800}$/VEGF siRNA nanocomplex as described above. Forty-eight hours after transfection, cells were detached, resuspended in DMEM supplemented with 0.5% FBS, and transferred to transwell chambers at a density of 5×10^4 cells/well. After 6 h for the migration assay and 24 h for the invasion assay, cells in the lower chamber were fixed with 10% paraformaldehyde, stained with 0.05% crystal violet, and counted at 200x magnification.

3.2.13 3D spheroid invasion study

For the 3D spheroid invasion study, 3D spheroids were prepared as described above. After 72 h of spheroid formation, 50 μL of Invasion matrix was added to the wells

and the plate was centrifuged at 300 g for 4 minutes at 4°C, followed by an incubation at 37°C for 60 minutes to induce gel formation. Then, cells were incubated with $pPEI_{1800}$/VEGF siRNA or scrambled siRNA nanocomplexes diluted in Opti-MEM at 37°C for 24 h; the medium was replaced with DMEM supplemented with 10% FBS and incubated for up to 3 days. The spheroids in each well were photographed every 24 h at 40x magnification, and the 3D cell invasion was analyzed using ImageJ software.

3.2.14 Cells proliferation study

Five thousand MDA-MB-231 cells were plated each well into a black well, clear bottom 96-well plate and incubated at 37°C overnight. After washing with PBS, cells were incubated with $pPEI_{1800}$/VEGF siRNA or scrambled siRNA nanocomplexes diluted in Opti-MEM at 37°C for totally 48 h and 72 h. One hundred microliter CellTiter-Glo buffer (Promega, WI) was added into the 96-well plate and the luminescent intensity was measured using a Spectramax M5e spectrophotometer (San Jose, CA).

For HUVEC proliferation study, 5×10^3 HUVEC cells were plated each well into a 96-well plate and grown with endothelial cell growth medium at 37°C overnight. After washing with PBS, cells were cultured in DMEM medium containing culture medium derived from $pPEI_{1800}$/siRNA transfected MDA-MB-231 cells (10%, v/v) for 24 h. Cell proliferation inhibition efficacy was evaluated by determining the luminescent intensity mentioned above.

3.2.15 Cell cycle assay

Cell cycle assay was performed as we previously reported[16]. Briefly, MDA-MB-231 cells were transfected with the $pPEI_{1800}$/siRNA nanocomplex for 24 h, incubated with fresh medium for another 24 h same as proliferation assay study, washed, suspended, and then fixed at 4℃ for 30 min in 70% cold ethanol. The cells were then incubated with propidium iodide/RNase staining solution at room temperature for 30 min, followed by cell cycle analysis using a FACS II flow cytometer.

3.2.16 *In vitro* HUVECs tube formation study

Five hundred microliter Matrigel/endothelial cell growth medium mixture (1:1, v/v) were used to pre-coat a 24-well plate[134]. HUVEC cells were suspended with culture medium derived from $pPEI_{1800}$/siRNA transfected MDA-MB-231 cells, added into Matrigel pre-coated 24-well plate with a 5×10^4 cells/well density. Tube formation was evaluated after 24 h incubation and counted at 40x magnification.

3.2.17 *In vivo* biodistribution and anti-tumor activity study

The animal protocol was approved by the Institutional Animal Care and Use Committee (IACUC) of the University of Missouri-Kansas City. Approximately 5×10^5 MDA-MB-231 cells were implanted into the right mammary gland of female nude mice to generate the orthotopic model of TNBC as previously described[135]. For *in vivo* biodistribution study, six mice were divided into two groups and intravenously injected with free Cy5 labeled siRNA or $pPEI_{1800}$/Cy5-siRNA at a siRNA dose of 0.1 mg/kg[103]. After 24 hrs, the mice were euthanized, major orangs (liver, tumor, lung, spleen, kidney,

muscle (foreleg) and heart) were collected. Organs cellular uptake and distribution were imaged and analyzed by using a Bruker MS FX PRO *In vivo* Imaging system (Billerica, CA). For the *in vivo* activity study, tumor-bearing mice were randomly divided into three groups and intravenously injected with $pPEI_{1800}$/VEGF siRNA, $pPEI_{1800}$/scrambled siRNA and saline. The injections were performed every 4 days for 4 injections with a dose of 1.5 mg siRNA/kg[136]. Tumor volumes were calculated using the formula V= longest diameter × shortest diameter^2/2.

Expressions of VEGF in tumor tissues were measured using a VEGF ELISA kit, as previously reported[30]. Tumor tissues were homogenized in RIPA buffer and centrifuged at 13,000 g for 10 min to remove the precipitate. After determining the total protein concentration using a BCA protein assay kit (ThermoFisher, CA), the concentrations of VEGF protein in tumor tissues were determined using the VEGF ELISA kit and presented as VEGF (%) in total proteins amount.

Immunohistochemical analysis was performed to determine the microvessel density in the tumor microenvironment. Briefly, tumor tissues were fixed with 4% formaldehyde and cut into 5μm section embedded in paraffin. The sections were incubated with mouse anti-human CD31 antibody (ThermoFisher, CA) at 4°C overnight after treated with histosol, 100%, 95%, 70% & 50% ethanol, DI water, and next incubated with anti-mouse biotinylated antibody, and streptavidin HRP-peroxidase. 3,3'-Diaminobenzidine (DAB) were used as chromophore and the sections were stained with hematoxylin, dehydrated and observed under microscope. Hematoxylin and Eosin (H&E) staining was also performed on tumor, liver, kidney and lung tissues sections to evaluate the *in vivo* cytotoxicity followed the protocol as previously reported[137].

3.2.18 Statistical analysis

Statistical analysis was performed using a two-way analysis of variance (ANOVA) with Tukey's *post hoc* test). $P<0.05$ was considered statically significant.

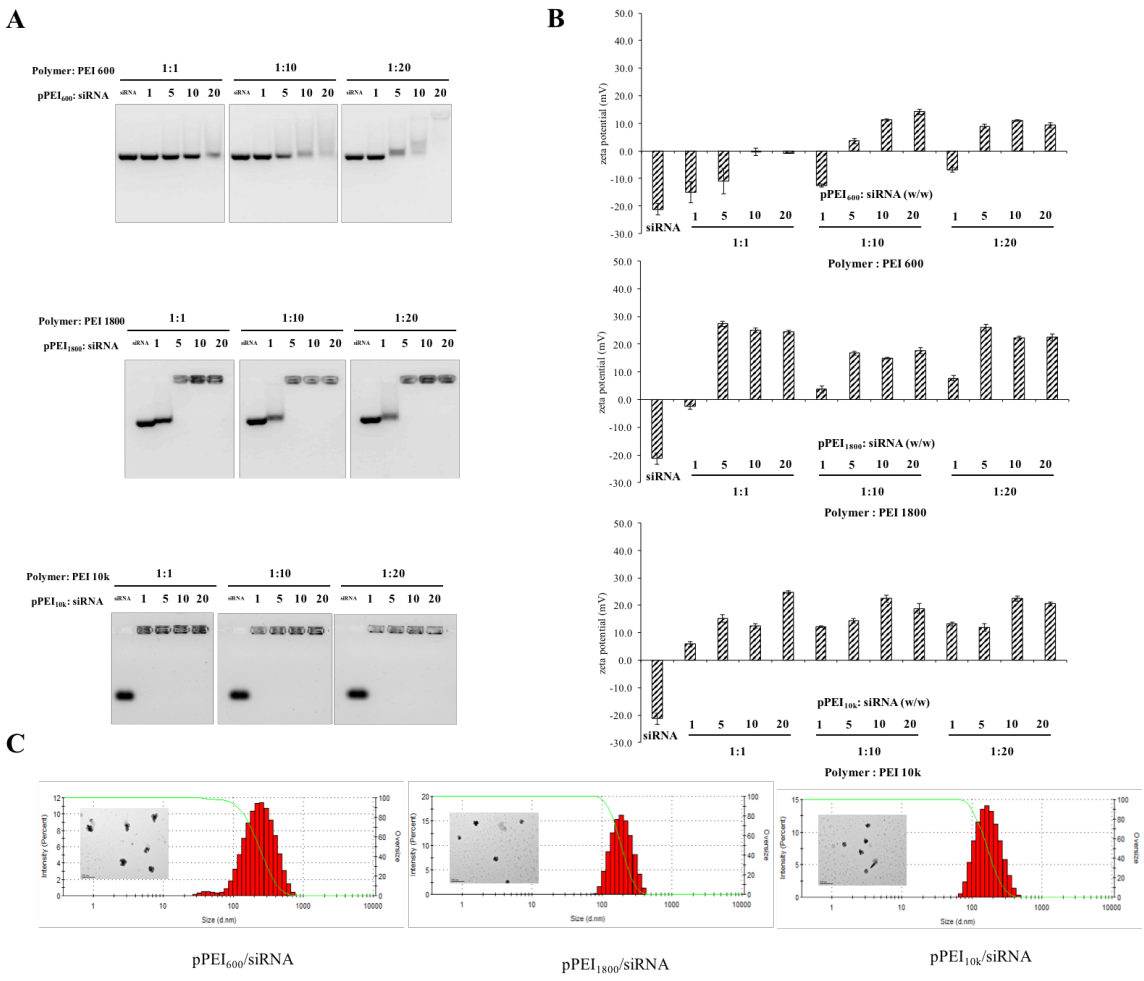

Figure 2. Characterizations of pPEI/siRNA nanocomplexes. (A) Gel retardation assay of the $pPEI_{600}$/siRNA, $pPEI_{1800}$/siRNA and $pPEI_{10k}$/siRNA at different weight ratio. (B) Zeta potential of pPEI/siRNA nanocomplexes with different weight ratio. (C) Particle size and TEM of the $pPEI_{600}$/siRNA, $pPEI_{1800}$/siRNA and $pPEI_{10k}$/siRNA nanocomplexes with a w/w ratio: 1:10.

3.3 Results

3.3.1 Fabrication and characterization of pPEI/siRNA binary nanocomplexes

The fabrication of these polymer-PEI nanocomplexes is illustrated in Figure 1B. We evaluated the condensation between synthesized pPEIs and siRNAs at different w/w ratios using a gel retardation assay. For $pPEI_{600}$, siRNAs cannot be condensed until a high w/w ratio of approximately 10 is achieved, and as shown in Figure 2A, a higher condensation is observed at higher molar ratios of the polymer to PEI. The same tendencies were also confirmed by the zeta potential results shown in Figure 2B. The same studies were performed using synthesized $pPEI_{1800}$ and $pPEI_{10k}$. $pPEI_{1800}$ condensed the siRNA at a 5:1 w/w ratio and $pPEI_{10k}$ formed the nanocomplex at 1:1 w/w ratio; similar trends were also observed in the zeta potential results. The zeta potential switched from negative to positive at a 1:1 w/w ratio for $pPEI_{1800}$ when synthesized at 1:1 molar ratio, and $pPEI_{1800}$ condensed the siRNA at 1:1 w/w ratio at higher molar ratios between PEI and the polymer. For future comparisons among different molecular weight PEIs, we chose 3 pPEIs with the same synthesized molar ratio (1:10) and same w/w ratio (10:1) to ensure that all 3 pPEIs completely formed the pPEI/siRNA nanocomplexes. The particle size of these 3 $pPEI_{600}$/siRNA, $pPEI_{1800}$/siRNA and $pPEI_{10k}$/siRNA nanocomplexes were 267, 208 and 183 nm, respectively, with PDIs of 0.263, 0.185 and 0.181, respectively, and the structures were confirmed by TEM (Figure 2C).

A TNBS assay was performed to evaluate the degree of PEI substitution in the polymer. As shown in Table 1, the grafting degree was 57.7%, 49.3% and 16.2%, respectively, for the chosen synthesized pPEIs at a molar ratio of 1:10, and molecular weight ranged from 31 to 47 kDa.

Table 1. TNBS assay for pPEIs

	Polymer-PEI mole ratio	PEI (nmole)/polymer(mg)	Degree of grafting	Molecular Weight
$pPEI_{600}$	1:10	236.8	57.7%	31471
$pPEI_{1800}$	1:10	165.8	49.3%	38487
$pPEI_{10k}$	1:10	43.6	16.2%	47844

3.3.2 Serum stability

siRNAs are easily degraded in serum in a short time; therefore, the first consideration in siRNA delivery is the method to efficiently protect siRNAs in the blood circulation[103]. We next evaluated the stability of these pPEI/siRNA nanocomplexes in 50% rat serum. As shown in Figure 3A, all three nanocomplexes protected the siRNA from serum degradation for at least 24 h. $pPEI_{600}$/siRNA nanocomplexes exhibited little degradation after 36 h incubation in serum, but both $pPEI_{1800}$/siRNA and $pPEI_{10k}$/siRNA nanocomplexes exhibited good stability and protected the siRNA in serum for up to 36 h.

3.3.3 *In vitro* cytotoxicity study

Since polymer-modified PEI reduced cytotoxicity, as mentioned above, the MTT assay was performed to evaluate the cytotoxicity of these pPEI/siRNA nanocomplexes (Figure 3B and C). $pPEI_{600}$ and $pPEI_{1800}$ were not cytotoxic to either HeLa or MDA-MB-231 cells after 24 h, and 74.0% of HeLa cells and 78.0% of MDA-MB-231 cells remained viable after a 48 h incubation with $pPEI_{1800}$, which showed much lower cytotoxicity than positive control Lipofectamine. Compared with the $pPEI_{600}$, $pPEI_{1800}$ and Lipofectamine groups, $pPEI_{10k}$ displayed higher toxicity to both cell lines after 24 and 48 h of incubation, potentially due to the considerably higher molecular weight of ethyleneimine.

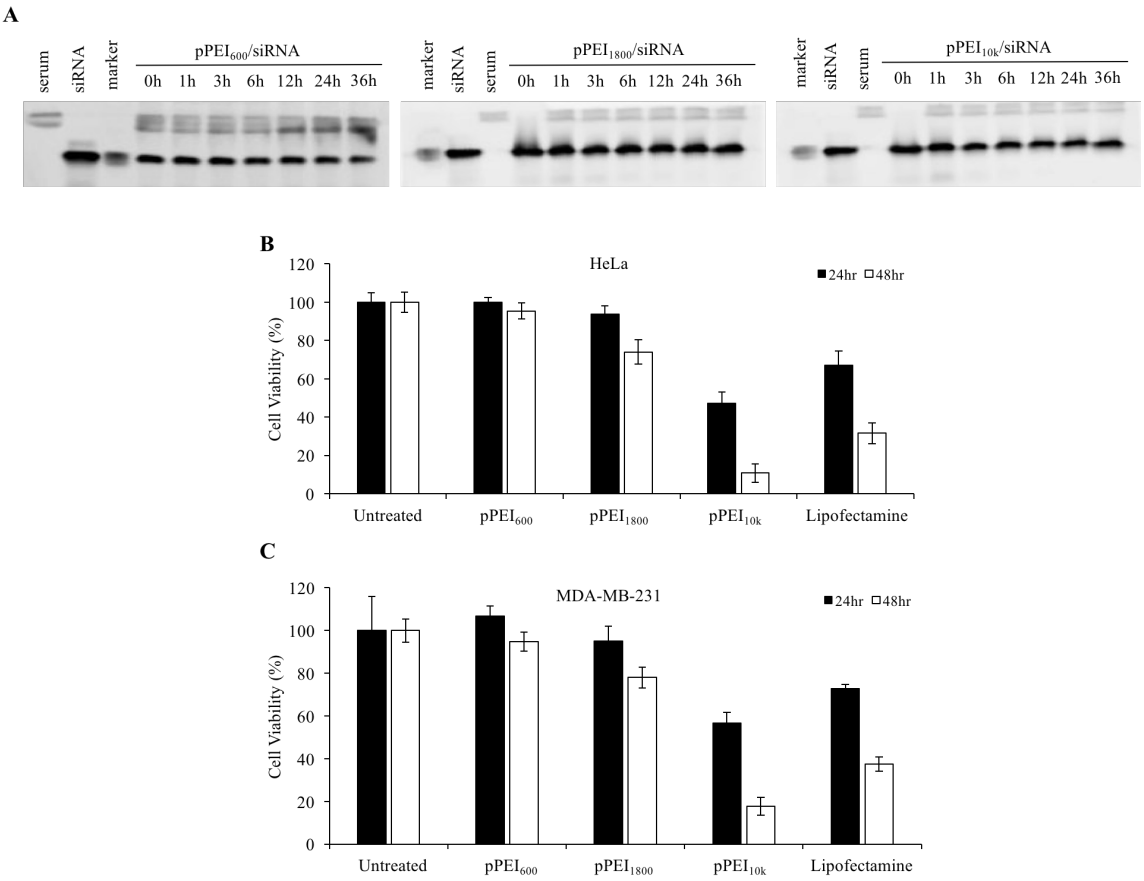

Figure 3. Serum stability and cytotoxicity of pPEI/siRNA nanocomplexes. (A) Serum stability of $pPEI_{600}$/siRNA, $pPEI_{1800}$/siRNA and $pPEI_{10k}$/siRNA nanocomplexes in 50% rat serum for 0, 1, 3, 6, 12, 24, and 36 h. (B) Cytotoxicity study of pPEI/siRNA nanocomplexes in HeLa and (C) MDA-MB-231 cell lines for 24 h and 48 h; Lipofectamine® 2000 was used as a positive control.

3.3.4 Cellular uptake study

Next, we evaluated the cellular uptake of these pPEI/siRNA nanocomplexes by determining the level of the siRNA inside the HeLa and MDA-MB-231 cells using flow cytometry. As shown in Figure 4A, $pPEI_{10k}$/siRNA nanocomplexes were taken up by HeLa cells at much higher levels 6 h after transfection, followed by the positive control Lipofectamine® and $pPEI_{1800}$/siRNA nanocomplexes. The $pPEI_{600}$/siRNA nanocomplexes group exhibited the lowest cellular uptake, and similar trends were observed in the triple negative breast cancer cell line MDA-MB-231 (Figure 4B).

Subsequently, we used confocal microscopy to compare the intracellular distributions of the pPEI/siRNA nanocomplexes in both HeLa (Figure 4C) and MDA-MB-231 cells (Figure 4D). The results are consistent with the results from the flow cytometry-based cellular uptake study. The $pPEI_{1800}$/siRNA nanocomplex has a similar cellular uptake to Lipofectamine and the $pPEI_{10k}$/siRNA nanocomplex has the highest cellular uptake in both HeLa and MDA-MB-231 cells. Moreover, in contrast to the Lipofectamine group, which displays substantial overlap between the Cy5-labeled siRNA and LysoTracker, all 3 pPEI/siRNA nanocomplexes exhibited minimal entrapment in lysosomes, and the confocal images indicate that the 3 nanocomplexes efficiently delivered the siRNA into the cytoplasm through the distinctive endosome escape capability via the “proton sponge effect”.

3.3.5 3D Spheroid penetration study

MDA-MB-231 spheroids with a diameter of approximately 500 μm were produced to mimic the *in vivo* tumor microenvironment[138, 139]. After a 6 h incubation

with the MDA-MB-231 spheroids, the $pPEI_{10k}$/siRNA nanocomplex penetrated much deeper and exhibited stronger fluorescence in the core of the spheroids compared to the other pPEIs/siRNA nanocomplexes illustrated in Figure 5A and B. The $pPEI_{600}$/siRNA nanocomplex was only observed surrounding the spheroids, with a much weaker fluorescence intensity, indicating a limited penetration capability. As shown in Figure 5A, the $pPEI_{1800}$/siRNA nanocomplex also penetrated the core of the spheroids, but the fluorescence was approximately 63% of the $pPEI_{10k}$/siRNA nanocomplex, as illustrated in Figure 5B.

3.3.6 *In vitro* transfection study

The transfection efficiency of pPEI/siRNA nanocomplexes was evaluated by transfecting luciferase and Renilla plasmids in HeLa cells, which have been widely used in transfection studies because of its high transfection efficiency[140]. Then, pPEI/luciferase siRNA nanocomplexes were transfected into HeLa cells for a total incubation of 48 h. The silencing effects of pPEI/luciferase siRNA nanocomplexes were quantified, as shown in Figure 5C, and the bioluminescence of the Renilla plasmid was determined as a control. Eighty-five percent of the expression of the luciferase plasmid was silenced by the $pPEI_{10k}$/luciferase siRNA nanocomplex, followed by 71% for $pPEI_{1800}$ and only 36% for $pPEI_{600}$. The positive control Lipofectamine displayed a 77% silencing efficiency in HeLa cells.

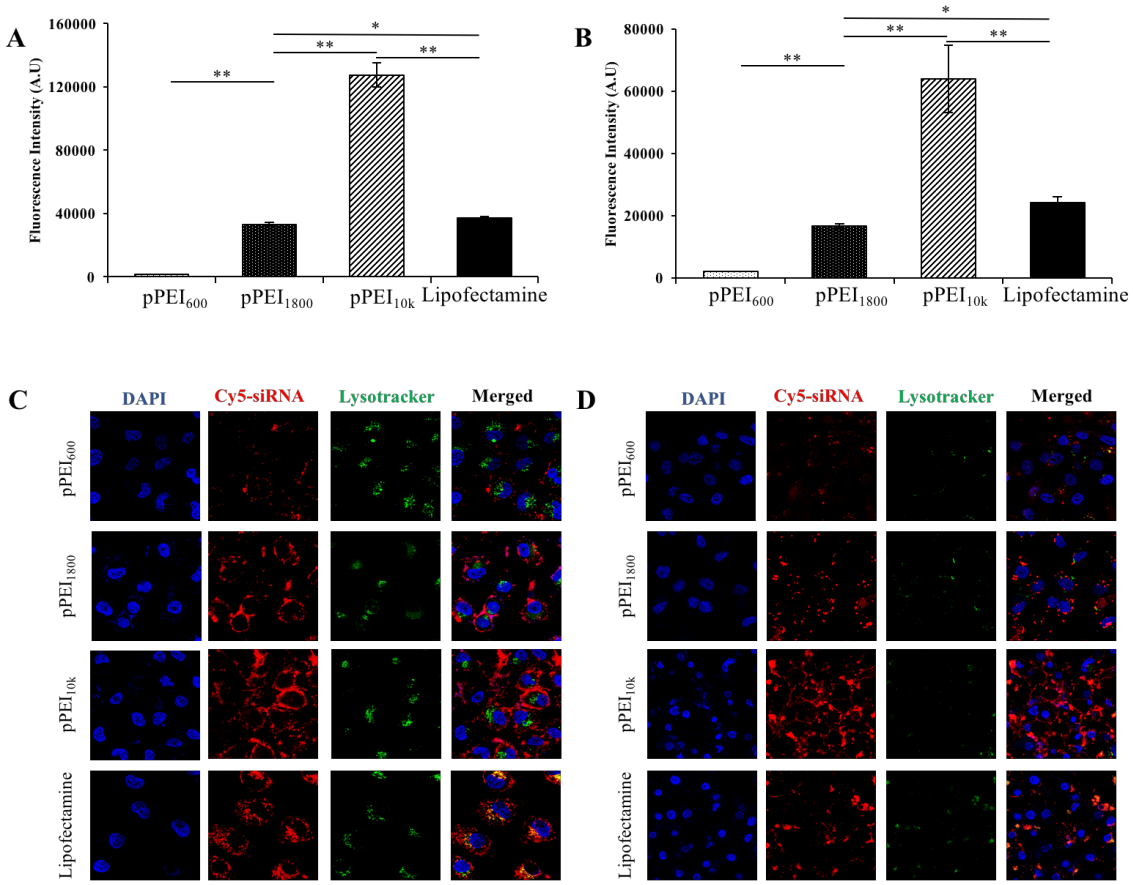

Figure 4. Quantitative cellular uptake of pPEI/siRNA nanocomplexes in HeLa and MDA-MB-231 cells for 6 h. siRNA was labeled with Cy5 for fluorescence analysis using flow cytometry (A, B) and confocal microscopy (C, D). Fluorescence intensity of the HeLa cells (A) and MDA-MB-231 cells (B) that take up the pPEI/siRNA nanocomplexes. Confocal images of the HeLa cells (C) and MDA-MB-231 cells (D) treated with these nanocomplexes. All results are presented as the mean ± SD (n = 3). (* $P < 0.05$; ** $P < 0.01$).

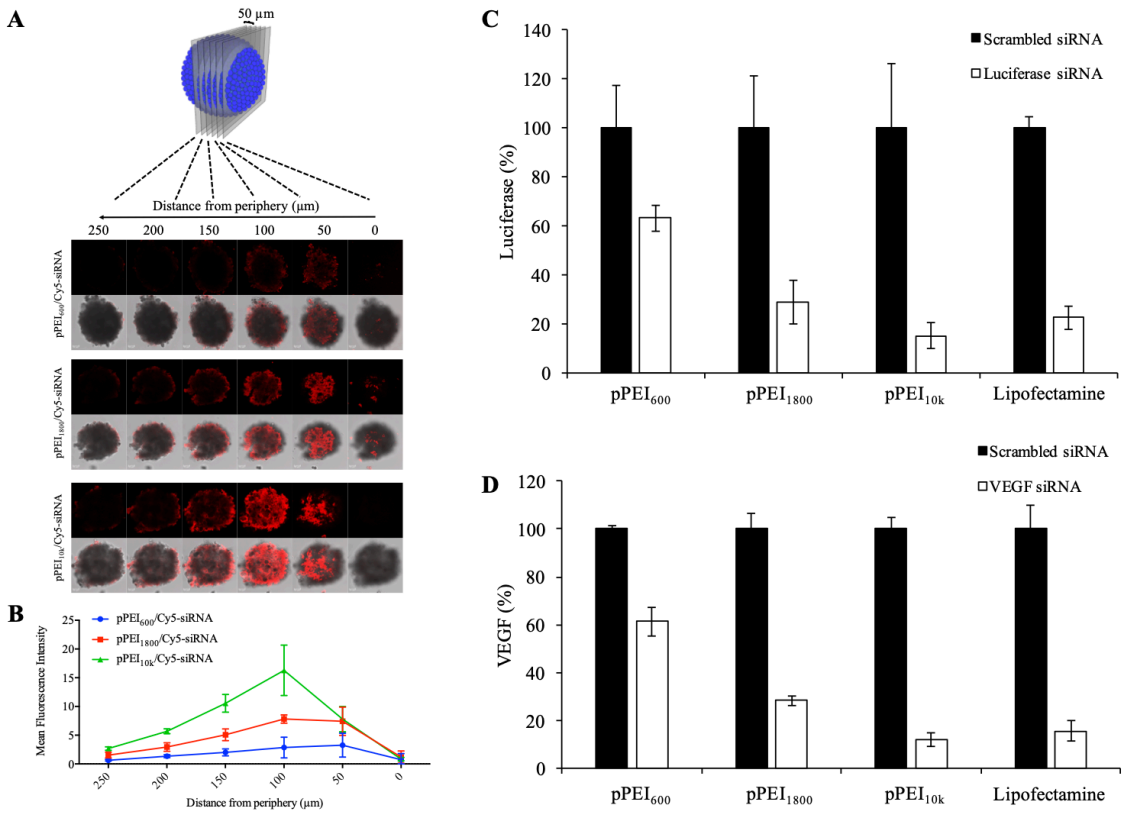

Figure 5. Penetration, transfection and silencing activities of pPEI/siRNA nanocomplexes. (A) Confocal images of the representative Z-stack penetration of pPEI/Cy5-siRNA nanocomplexes with a 50 μm step size. The scale bar represents 50 μm. (B) Mean fluorescence intensity of pPEI/Cy5-siRNA nanocomplexes vs. the distance from periphery. (C) Transfection efficacy of pPEI/Luciferase siRNA nanocomplexes on HeLa cells. (D) Silencing activities of pPEI/VEGF siRNA nanocomplexes on MDA-MB-231 cells. All results are presented as the mean ± SD (n = 3). (* P <0.05; ** P <0.01).

3.3.7 Silencing activity of pPEI/VEGF siRNA nanocomplexes

After evaluating the transfection efficiency of these three pPEI/siRNA nanocomplexes, we subsequently examined the silencing activity of pPEIs condensed with VEGF siRNA in MDA-MB-231 cells. The results illustrated in Figure 5D are consistent with the results of the cellular uptake study using MDA-MB-231 cells and transfection study using HeLa cells. The $pPEI_{10k}$/siRNA nanocomplex exhibited 88% silencing activity, which is the highest activity among all the 3 pPEI/siRNA nanocomplexes. The $pPEI_{1800}$/siRNA nanocomplex displayed 72% silencing activity, a lower value than the $pPEI_{10k}$/siRNA nanocomplex and Lipofectamine/siRNA (84%), but the value is much higher than the $pPEI_{600}$/siRNA nanocomplex, which exhibits approximately 39% silencing activity.

3.3.8 Migration and invasion study

Unlike the high transfection efficiency/high cytotoxicity of $pPEI_{10k}$, $pPEI_{1800}$ has a similar cellular uptake and transfection efficiency to Lipofectamine but a much lower cytotoxicity, indicating the $pPEI_{1800}$ represents a safe, highly efficient transfection system for delivering the siRNA cargo to cancer cells, particularly triple negative breast cancer cells. Next, we wanted to examine whether $pPEI_{1800}$ condensed with the VEGF siRNA inhibited the migration and invasion of MDA-MB-231 cells. Compared with scrambled siRNA group, the $pPEI_{1800}$/VEGF siRNA nanocomplex inhibited approximately 64% of the migration of MDA-MB-231 cells (Figure 6A and B) and 67% of the invasion of these cells (Figure 6C and D).

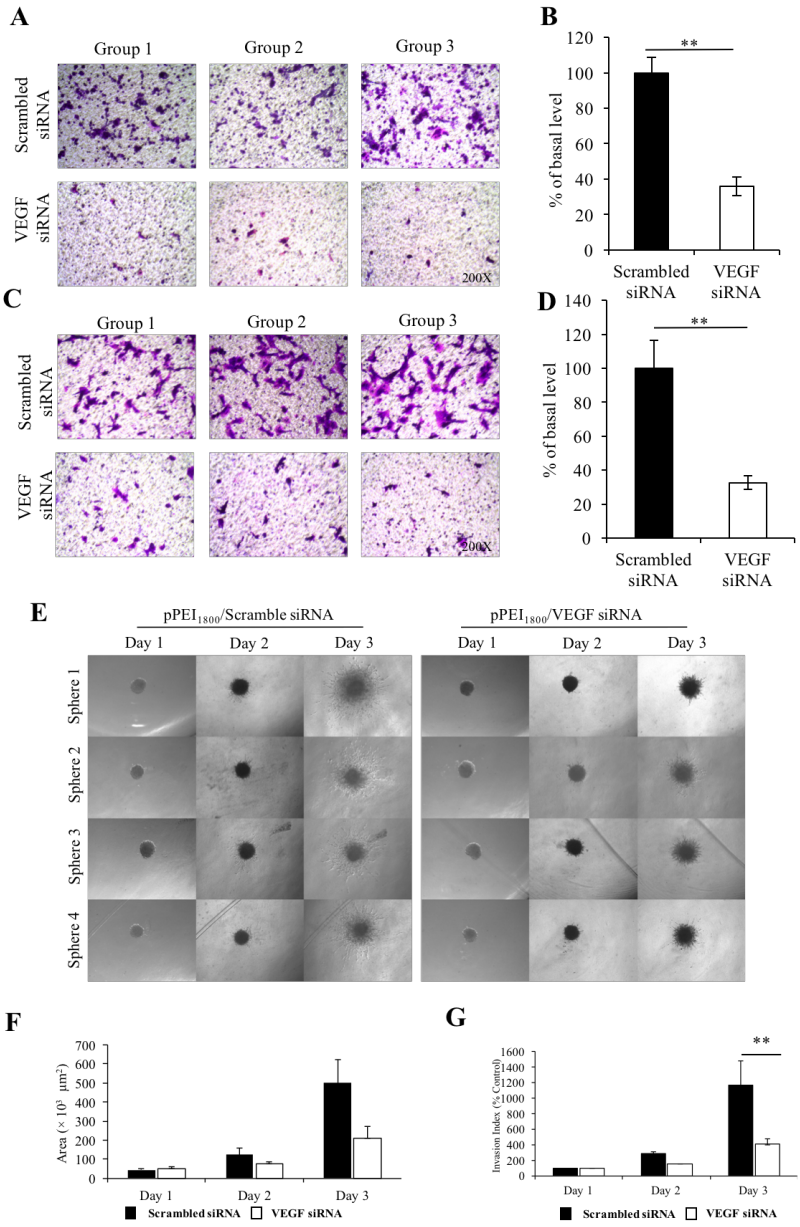

Figure 6. Inhibition of migration and invasion in MDA-MB-231 cells. (A) The migration of MDA-MB-231 cells treated with $pPEI_{1800}$/VEGF siRNA nanocomplex for 6 h. (B) Quantitative analysis of the number of migrated cells was performed by quantifying six random microscope fields. (C, D) Invasion inhibition efficacy of $pPEI_{1800}$/VEGF siRNA nanocomplex after 24 h incubation. All results are presented as the mean ± SD (n = 3). (E) 3D spheroid invasion inhibition effect of $pPEI_{1800}$/VEGF siRNA nanocomplex. Quantitative analysis of (F) cell growth and (G) invasion of MDA-MB-231 spheroid. All results are presented as the mean ± SD (n = 4). (** $P < 0.01$).

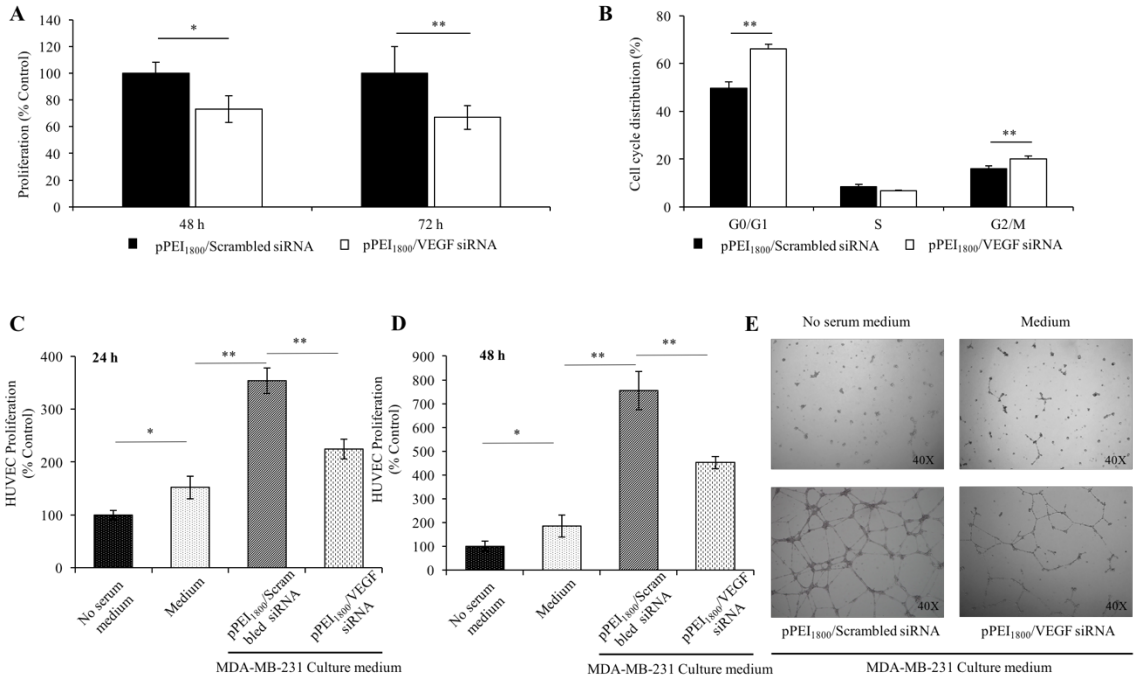

Figure 7. Inhibition of proliferation and angiogenesis of MDA-MB-231 cells *in vitro*. (A) The proliferation of MDA-MB-231 cells treated with $pPEI_{1800}$/VEGF siRNA nanocomplex for 48 h and 72 h. (B) Cell cycle distribution of MDA-MB-231 cells treated with $pPEI_{1800}$/VEGF siRNA or $pPEI_{1800}$/Scrambled siRNA nanocomplex for 48 h. The proliferation of HUVEC cells cultured with no serum medium, normal 10% FBS contained DMEM medium and culture medium from MDA-MB-231cells transfected with $pPEI_{1800}$/VEGF siRNA or $pPEI_{1800}$/Scrambled siRNA for 24 h (C) and 48 h (D). (E) Tube formation of HUVEC cells on Matrigel cultured with no serum medium, normal 10% FBS contained DMEM medium and culture medium from MDA-MB-231cells transfected with $pPEI_{1800}$/siRNA nanocomplexes for 24 h. All results are presented as the mean ± SD (n = 3). (* $P < 0.05$; ** $P < 0.01$).

A 3D spheroid invasion study was performed to determine the ability of the $pPEI_{1800}$/VEGF siRNA nanocomplex to inhibit invasion in a system mimicking the tumor microenvironment, as shown in Figure 6E. In contrast to the dramatic increase in spheroid area in the Scrambled siRNA group, the $pPEI_{1800}$/VEGF siRNA group displayed a much slower increase in invasion, with a 39% inhibition of invasion after 24 h and 58% inhibition after 48 h (Figure 6F and G). Based on these results, the $pPEI_{1800}$/VEGF siRNA nanocomplex safely and efficiently delivered the siRNA into triple negative breast cancer cells and facilitated the biological activity of the VEGF siRNA in cells.

3.3.9 Cells proliferation study

Reduced VEGF expression is reported to effectively inhibit tumor proliferation and in our previous study. Similarly, we previously demonstrated that VEGF siRNA can significantly inhibit the proliferation of HER2+ breast cancer cells[131]. We therefore treated MDA-MB-231 cells with $pPEI_{1800}$/VEGF siRNA nanocomplex for 48 h and 72 h and performed a cell proliferation study using the CellTiter-Glo luminescent cell viability assay (Figure 7A). The $pPEI_{1800}$/VEGF siRNA nanocomplex-treated group had a much lower MDA-MB-231 cell proliferation rate (73.1% for 48 h and 67.0% for 72 h) than the $pPEI_{1800}$/scrambled siRNA-treated group.

To test whether lower VEGF levels were secreted from $pPEI_{1800}$/VEGF siRNA nanocomplex-treated MDA-MB-231 cells, a cell proliferation assay was also performed on HUVECs incubated with MDA-MB-231 cell culture medium. As illustrated in Figure 7C & D, the HUVEC cell proliferation rate was significantly affected by culturing with MDA-MB-231 cell culture medium, showing a 2.5-fold increase relative to control cells

at 24 h and a 6.5-fold increase at 48 h. Meanwhile, the $pPEI_{1800}$/VEGF siRNA nanocomplex-treated group had a much lower HUVEC cell proliferation rate (63.5% for 24 h and 60.0% for 48 h) than the scrambled siRNA treated group, which indicates that silencing VEGF expression in TNBC cells can inhibit vascular endothelial cell proliferation in the tumor microenvironment.

3.3.10 Cell cycle assay

We next evaluated the cell cycle in MDA-MB-231 cells transfected with $pPEI_{1800}$/VEGF siRNA nanocomplex to identify the potential mechanism underlying the activity of VEGF siRNA in TNBC cells. Consistent with other VEGF siRNA functional studies in gastric cancer cells in a previous report, there was a significant increase in the G0/G1 phase and the G2/M phase (Figure 7B), suggesting that the $pPEI_{1800}$/VEGF siRNA nanocomplex can inhibit the growth of TNBC cells[141].

3.3.11 *In vitro* HUVEC tube formation study

VEGF plays an important role in the endothelial tube formation during tumor growth by positively regulating angiogenesis[77]. After evaluating the inhibitory effect of $pPEI_{1800}$/VEGF siRNA nanocomplex on the proliferation of vascular endothelial cells, we next performed a study to identify the role of $pPEI_{1800}$/VEGF siRNA nanocomplex in HUVEC tube formation. Similar to the proliferation study, HUVECs were seeded on a matrigel precoated 24-well plate and cultured for 24 h in the medium of MDA-MB-231 cells that were treated with the $pPEI_{1800}$/siRNA nanocomplex. Tube formation of HUVECs was significantly reduced after culturing with the medium (Figure 7E),

suggesting that silencing VEGF expression with $pPEI_{1800}$/VEGF siRNA nanocomplex in TNBC cells can diminish the function of vascular endothelial cells.

3.3.12 *In vivo* biodistribution and anti-tumor activity study

Nanomedicines have been developed to target primary and metastatic tumors through the enhanced permeability and retention (EPR) effect[142]. Cy5-labeled siRNA was used for the *in vivo* biodistribution fluorescence analysis shown in Figure 8A, and the mean fluorescence intensity of each organ was determined and presented in Figure 8B as a ratio compared to heart accumulation. As illustrated in Figure 8A, after 24 h, free siRNA was eliminated and showed low accumulation in tumors and other major organs. Compared to free siRNA, $pPEI_{1800}$/Cy5-siRNA nanocomplex showed significantly higher accumulation in tumors due to the EPR effect. Meanwhile, both free siRNA and $pPEI_{1800}$/Cy5-siRNA nanocomplex showed high accumulation in the kidney, which may be caused by the positive charge on the surface of the glomerular basement membrane[143].

After evaluating the biodistribution *in vivo*, we next performed an anti-tumor activity study that included three groups: a saline, a $pPEI_{1800}$/Scrambled-siRNA nanocomplex and a $pPEI_{1800}$/VEGF siRNA nanocomplex. As shown in Figure 8C, tumor growth in the $pPEI_{1800}$/VEGF siRNA nanocomplex-treated group was significantly inhibited, while there was no significant difference between the saline group and the scrambled siRNA-treated group. Tumor weight illustrated in Figure 8D was consistent with the tumor growth tendency. VEGF expression in tumors was also determined by utilizing a human VEGF ELISA kit (Figure 8E), and the $pPEI_{1800}$/VEGF siRNA

nanocomplex-treated group showed significantly lower VEGF expression. The lower level of VEGF expression was consistent with the reduced CD31 expression determined by IHC in tumor tissues (Figure 8F), suggesting that inhibition of VEGF expression by $pPEI_{1800}$/VEGF siRNA nanocomplex leads to diminished angiogenesis signals from TNBC cells to vascular endothelial cells in the tumor microenvironment. The inhibition of tumor angiogenesis by $pPEI_{1800}$/VEGF siRNA nanocomplex also reflected the tumor growth inhibition shown in Figure 8C. Meanwhile, H&E staining of major organs, including the liver, kidney and lung, indicated the low cytotoxicity of $pPEI_{1800}$/VEGF siRNA nanocomplex *in vivo* (Figure 8F).

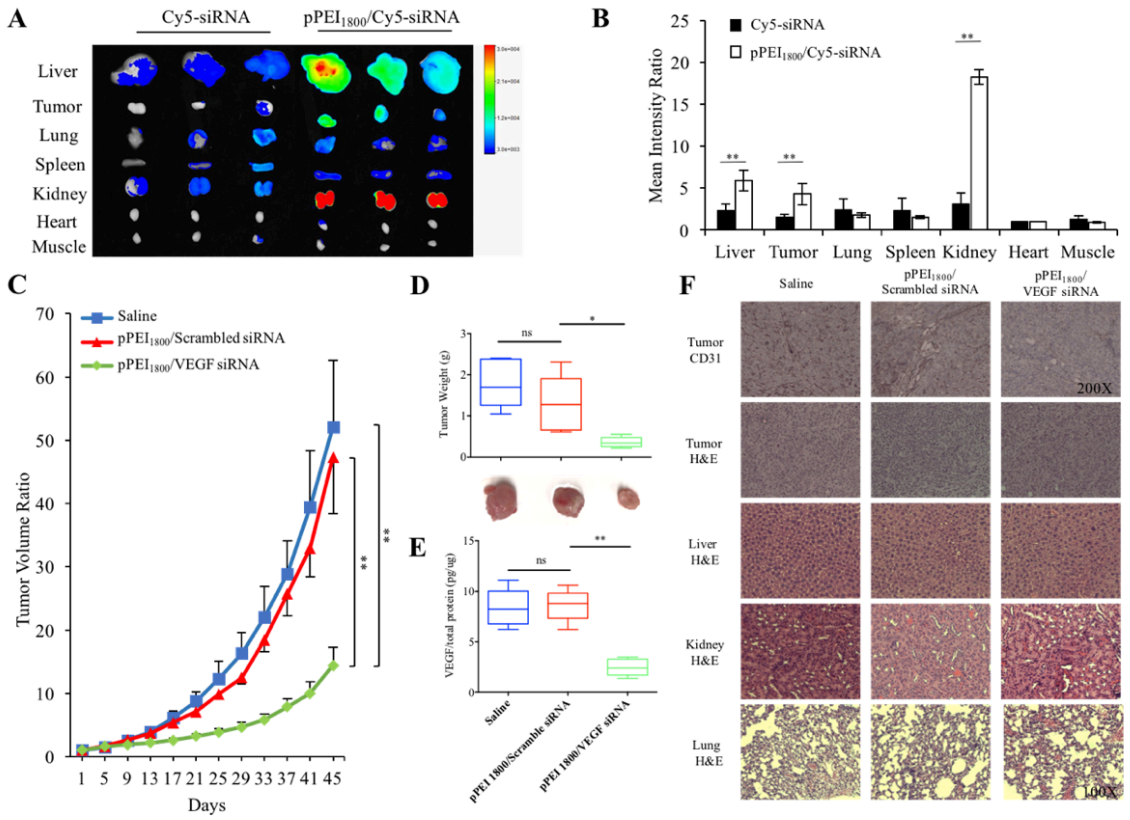

Figure 8. Biodistribution and *in vivo* anti-tumor activities in orthotopic xenograft TNBC mouse model. (A) *Ex vivo* fluorescence images of important tissues (liver, tumor, lung, spleen, kidney, heart & muscle) collected at 24 h post-injection. Free Cy5 labeled siRNA or $pPEI_{1800}$/Cy5-siRNA were injected at a siRNA dose of 0.1 mg/kg via I.V. injection. (B) Region of interest (ROI) for each organ was determined and mean fluorescence intensity ratio to heart were plotted. All results are presented as the mean ± SD (n = 3). (C) Tumor growth curve of orthotopic xenograft MDA-MB-231 tumor model presented as the mean ± SEM (n = 6). (D) Tumor weight and (E) expression of VEGF of isolated tumor tissues. All results are presented as the mean ± SD (n = 6). (* $P < 0.05$, ** $P < 0.01$). (F) CD31 immunochemistry of tumor tissues and H&E analysis in tumor, liver, kidney and lung.

3.4 Discussion

PEI has been used as a promising cationic material for nucleic acid delivery, and its molecular weight ranging between 10 to 30 kDa is a reliable transfection agent for DNA, but high cytotoxicity largely limits its application[27]. The toxicity of PEI used for nucleic acid transfection is due to two major factors: membrane destabilization caused by free PEI binding to plasma membrane proteoglycans and PEI-induced mitochondria-mediated apoptosis[144]. The use of a biodegradable polymer to modify PEI significantly reduces cytotoxicity, and PEI with a molecular weight of less than 2kDa was shown nontoxic even at high concentrations[27, 28]. Compared with linear PEIs, branched PEIs have a higher amine density and are increasingly being used to synthesize biodegradable polymer-PEI with a longer half-life and much lower toxicity[145]. PEGylation is a commonly bioactive molecular modification technique in clinic to improve pharmacokinetic and physiochemical properties[146]. Over 14 PEGylated drugs have been approved by FDA in the past twenty years, and two were approved in the 1990s as the first-generation PEGylated drugs (Oncaspar® & Adagen®). The approved PEG molecular weight started from < 1kDa (PEGylated naloxol) to maximum 40kDa PEGylated proteins and peptides shown the widely utilizing for PEGylation[146]. In this present study, a multiblock polymer was synthesized by conjugating 3.4kDa PEG with two kinds of amino acids (lysine & glutamic acid) through peptide bonds[132]. The utilizing of small molecular weight PEG and amino acids make the multiblock polymer biocompatible *in vivo* and biodegradable in the proteases-rich tumor cells. Then, as illustrated in Figure 1, we chose three branched PEIs with low molecular weights (600, 1800 & 10000 Da) for conjugation with the biodegradable multiblock polymer to

increase the siRNA transfection efficiency of the polymer-PEI nanocomplex with low cytotoxicity. These conjugated polymer-PEIs have a strong siRNA condensation capacity with slight positive surface charge and nanoscale particle size (Figure 2), enhanced siRNA protection ability from serum degradation and reduced cytotoxicity (Figure 3). *In vitro* cellular uptake (Figure 4) and *in vivo* bio-distribution study shown in Figure 8A & B indicate that pPEI/siRNA nanocomplexes can deliver siRNA into cancer cells by EPR effect and release siRNAs into cytoplasm caused by proton sponge effect.

Compared to monolayer two-dimensional cell cultures, which do not mimic the heterogeneity of *in vivo* tumor growth, cells located in a 3D spheroid mimic the complex cell-cell and cell-ECM complexity interactions similar to the tumor microenvironment[147, 148]. Due to the poor penetration ability of drugs in the clinic, particularly for large molecule drugs, cancer cells exhibit a correlation with the efficacy of a low drug concentration and the distance from blood vessels in the tumor microenvironment[138, 148]. MDA-MB-231 spheroids with a diameter of approximately 500 μm were prepared to mimic the *in vivo* tumor microenvironment and determine the ability of pPEIs delivering a 14 kDa siRNA to penetrate the spheroid[138, 139]. Cationic agents such as PEI have been reported to exhibit poor penetration, but the charge shielding effect of PEGylation significantly improves the penetration efficiency of cationic polymers[149, 150]. As shown in Figure 5A and B, the penetration efficiency of $pPEI_{1800}$ and $pPEI_{10k}$ were much higher than $pPEI_{600}$. The charges of $pPEI_{1800}$/siRNA and $pPEI_{10k}$/siRNA nanocomplexes were higher than $pPEI_{600}$/siRNA nanocomplex (Figure 2B), and these nanocomplexes also displayed a much smaller particle size, as shown in Figure 2C, and a larger polymeric molecular weight (Table 1), which also affect the

penetration efficiency[151, 152]. Moreover, the 3D penetration and transfection efficiency of nucleic acid delivery polymers are positively correlated with the monolayer cell transfection efficiency, and the transfection efficiency of $pPEI_{1800}$ and $pPEI_{10k}$ were considerably higher than $pPEI_{600}$, as shown in Figures 4 and 5C[152].

VEGF is determined highly expressed in TNBC patients, 3 times higher than ER/PR+ subtypes and 1.5 times higher than HER2+ subtypes, and effected on the proliferation and survival of TNBC cancer cells through an autocrine signaling pathway[19-22]. *Bachelder et al.,* found that the survival of metastatic breast carcinoma including TNBCs dependent on VEGF *in vitro* by specific silencing target VEGF gene with designed antisense oligodeoxynucleotide[153]. Silencing VEGF expression utilizing siRNA can inhibit proliferation and induce apoptosis *in vitro* and tumor growth *in vivo* has been reported in different cancer cell lines[154-157]. In the present study, $pPEI_{1800}$/VEGF siRNA nanocomplex can significantly inhibit TNBC tumor growth in an *in vivo* orthotopic model by specific silencing VEGF expression as illustrated in Figure 8. Metastasis is implicated in an up to 90% cancer-related mortality rate, particularly in patients with breast cancer[158, 159]. TNBCs tend to more quickly recur after surgery, and distant recurrence is more frequently observed than local recurrence, indicating a high metastasis rate[160]. VEGF not only functions in angiogenesis in the tumor microenvironment, but also promotes triple negative breast carcinoma invasion by regulating chemokine receptor type 4 (CXCR4) signaling in an autocrine manner[161]. Downregulation of VEGF expression in the TNBC microenvironment significantly inhibits tumor cell invasion[161]. The migration inhibition effect was also confirmed in our study as shown in Figure 6. The $pPEI_{1800}$/siRNA nanocomplex can significantly

silence VEGF expression with high transfection efficiency (Figure 5C & D) resulting in a migration and invasion inhibition in a 2D chamber model illustrated in Figure 6A-D. A 3D spheroid invasion inhibition was also being observed (Figure 6E-G), which may cause by the highly cellular uptake and penetration efficiency of $pPEI_{1800}$/siRNA nanocomplex.

Another role of VEGF is as a positive angiogenesis regulator of endothelial cells in new capillaries forming during tumor growth[77]. Blocking the interaction between tumor-secreted VEGF and VEGFR2 on the surface of endothelial cells utilizing anti-VEGF or anti-VEGFR2 antibodies has previously been reported to significantly inhibit the proliferation, migration, survival and adhesion of endothelial cells[162-165]. Inhibition on VEGF expression in TNBC cells by siRNA was also reported to affect the migration, proliferation and tube formation of HUVECs[134]. After transfection with $pPEI_{1800}$/VEGF siRNA nanocomplex, VEGF secreted by MDA-MB-231 cells was reduced by 72% compared to the control group (Figure 5D), and this lower VEGF level correlated with a reduced HUVEC proliferation and diminished tube formation (Figure 7 C &D). The lower VEGF level determined by ELISA and the IHC results for CD31 staining in tumor tissues (Figure 8F) suggested that inhibition of VEGF expression by $pPEI_{1800}$/VEGF siRNA nanocomplex leads to diminished angiogenesis in the tumor microenvironment.

In conclusion, siRNA nanocomplexes prepared from $pPEI_{600}$, $pPEI_{1800}$ and $pPEI_{10k}$ exhibited similar physicochemical properties, similar serum stabilities, but different transfection efficiency. The $pPEI_{1800}$/siRNA nanocomplex exhibited higher cellular uptake and deeper spheroid penetration than the $pPEI_{600}$/siRNA nanocomplex,

and a much lower cytotoxicity than the $pPEI_{10k}$/siRNA nanocomplex. The *in vitro* studies also indicated that the $pPEI_{1800}$/VEGF siRNA nanocomplex significantly inhibited the migration, invasion and proliferation of TNBC cells. Furthermore, the $pPEI_{1800}$/siRNA nanocomplex exhibited a significant anti-tumor effect by downregulating VEGF expression *in vivo*. Thus, VEGF siRNA may be a promising anti-tumor agent for TNBC therapy and a PEI 1800-conjugated biodegradable, linear multiblock polymer efficiently delivered the siRNA into tumors with a high transfection efficiency and low cytotoxicity.

CHAPTER 4

SILENCING IKBKE GENE WITH A PEPTIDE-BESED siRNA NANOCOMPLEX INHIBITS INVASIVENESS AND GROWTH OF TRIPLE NEGATIVE BREAST CANCER CELLS

4.1 Rationale

The aberrant activation of nuclear factor-kappa B (NF-κB) is reportedly a key factor in TNBC[23]. TNBC, defined as lacking the expression of ER, PR, and HER2, accounts for approximately 12-17% of all breast cancers. TNBC is more aggressive, proliferative and has poorer prognoses and survival rates than non-TNBC[35, 36]. In cancer cells, inhibitory κB kinases (IKKs) function in an activation level, the activated IKKs then phosphorylate the IκBs and induce their degradation. These activated NF-κB signaling pathways were founded to enhance cellular proliferation, invasion, and metastasis and decrease cellular apoptosis in breast cancer, especially in ER-negative breast cancers such as TNBC[78].

IκB kinase ε (IKBKE, also known as IKKε), an important mediator in the activation of the NF-κB pathway, has been identified as an oncogene in breast cancer[24]. The IKKs family contains five members: IKKα, IKKβ, IKKγ, TBK-1 (TANK-binding kinase 1) and IKKε[16]. It was reported that IKKε has 65% similarity with TBK-1, including an N-terminal kinase domain, a C-terminal leucine zipper, a helix-loop-helix motif and a ubiquitin like domain[81]. Both IKBKE and TBK-1 are related to the noncanonical NF-κB signaling pathway, but their functional and regulation of targeting proteins are different[81]. Unrelated to its regulatory roles in the interferon

response, IKBKE was found to phosphorylate serine 536 to activate the NF-κB signaling pathway in breast cancer[82]. IKBKE can also induce NF-κB activation by phosphorylating TRAF2 and CYLD, and is overexpressed in approximately 30% of breast carcinomas including TNBCs[24, 25, 83-85]. A report also demonstrated that IKBKE protected cells against DNA damage-induced death through IKKε SUMOylation[86]. As an oncogene in breast cancer, IKBKE was aberrantly amplified in TNBC cells associated with STAT3 activation and cytokine production[25]. In the previous report, we have demonstrated that silencing IKKε expression in breast cancer cell lines (MCF7 & SK-BR-3) with IKBKE siRNA can significantly suppress the proliferation, invasion [16]. By using IKBKE shRNAs and a TBK1/IKBKE, JAK signaling inhibitor (CYT387), *Thanh et al.,* identified IKBKE mediates the proliferation, migration and survival of TNBC cells by driving CCL5 and IL-6 production[25].

Generally, targeting overexpressed receptors on cancer cell surface has been proved as a promising strategy for selectively delivering anti-tumor drugs with reduced systemic toxicity[166]. CD44, a cellular surface transmembrane polymorphic glycoprotein, is highly expressed on several cancer cells, especially TNBC cells[167]. Hyaluronic acid (HA), a natural, biodegradable, non-toxic polysaccharide that can specifically bind to the extracellular domain of CD44, which has been utilized as a tumor-targeting ligand for several TNBC therapeutics[168-170]. Taxanes, including paclitaxel, docetaxel and cabazitaxel, are a group of tubulin polymerizers known as microtubule stabilizers that induce cellular apoptosis. They were reported to be more effective in TNBC patients than in non-TNBC patients[63, 64]. Cabazitaxel (XRP-6258, CTX), a novel second-generation semisynthetic taxane, was approved by the FDA to

overcome drug resistance, and for the treatment of hormone-refractory prostate cancer[69]. As a microtubule stabilizer, cabazitaxel has an equivalent potency and a similar anti-proliferation activity to docetaxel but is more potent against chemo- or taxane-resistant tumors[69, 70]. The poor affinity of cabazitaxel to P-glycoprotein, which is enrolled in the taxane resistance in cancer cells, make the treatment efficacy of cabazitaxel to metastatic prostate cancer and indicate the promising potential for the metastasis breast cancer, especially metastatic TNBC treatment[71, 72]. However, cabazitaxel was found to have a high systemic toxicity, which may limit its applications for TNBC treatment. As a result, a novel delivery strategy to alleviate its toxicity is highly needed for its clinical application[73]. Several reports have suggested that chemical modification or encapsulation of cabazitaxel into nanoparticle delivery system may significantly improve its anti-tumor efficacy with alleviated toxicity in metastatic TNBC[72-74].

Therefore, it is expected that combination therapy of IKBKE siRNA and cabazitaxel will have a synergistic inhibition on the proliferation and invasion of TNBC tumors. We have previously reported that a cholesterol-modified cationic peptide was able to self-assemble into a micelle like structure with high siRNA condensation capability[97]. In this study, cabazitaxel was encapsulated into the cholesterol-peptide micelle by hydrophobic interaction and then condensed with IKBKE siRNA to form a hybrid nanocomplex, followed by coating with cholesterol-modified hyaluronic acid (CHA), which was used as a CD44-specific targeting ligand. To further improve the release of IKBKE siRNA and cabazitaxel from endosomes, a cathepsin B-specific response dipeptide sequence (Val-Cit) was added between cholesterol and the cationic

peptide sequence[1]. The synthesis scheme for cholesterol-peptide and cholesterol-HA and the formulation procedure for this hybrid nanocomplex (CHA/CP/siRNA/CTX) are shown in Figure 9 & 11. The hybrid nanocomplexes are taken up into cancer cells through CD44-mediated endocytosis. After cleavage by cathepsin B in the cells, the micelle will dissociate and release cabazitaxel and siRNA into the cellular plasma. In summary, the multicomponent nanocomplex represents a promising strategy to co-deliver cabazitaxel and IKBKE siRNA for TNBC therapy.

4.2 Material and methods

4.2.1 Material

Lipofectamine® 2000 & RNAiMax were obtained from Invitrogen (Carlsbad, CA), Cabazitaxel was purchased from MedKoo Biosciences (Morrisville, NC), mouse and human serum were purchased from BD Biosciences (San Jose, CA). Human IKBKE ELISA kit was obtained from LifeSpan Biosciences, Inc (Seattle, WA). The CellTiter-Glo luminescent call viability assay kit was purchased from Progema (Madison, WI). BD matrigel, Annexin V-FITC apoptosis kit, chemical reagents and other materials were obtained from ThermoFisher Scientific (Pittsburgh, PA).

4.2.2 Synthesis of cholesterol-peptide (CP)

A modified cholesterol-peptide with cathepsin B specific response dipeptide sequence (Val-Cit) was synthesized through solid phase peptide synthesis method (Figure 11A)[1, 97]. Briefly, 10 mmole Fmoc protected Val-Cit-HHHKKHHHKK peptide obtained from United Peptide (Herndon, VA) was deprotected with 20% piperidine at

room temperature for 30 min. Then cholesteryl chloroformate (12.5 mmole), N,N-Diisopropylethylamine (DIPEA) (37.5 mmole), 2-(6-Chlor-1H-benzotriazol-1-yl)-1,1,3,3-tetramethylaminium-hexafluorophosphat (HCTU) (12.5 mmole) were added, and the solution was stirred continuously for 72 h at room temperature under N_2 protection. After completion of the reaction, the cholesterol conjugated peptide was cleaved from Wang resin with TFA/water/TIPS (95/2/3) at room temperature for 2 h. The cholesterol-peptide was purified by HPLC and the molecular weight (MW: 2022.5) was confirmed by mass spectrometry.

4.2.3 Synthesis of cholesteryl-linker-hyaluronic acid (CHA)

CHA was synthesized with a modified method illustrated in Figure 11B[171]. First, cholesteryl-linker was synthesized by mixing 2,2'-(ethylenedioxy)-bis-ethylamine (30 mM) with 7.5 mmole triethylamine (TEA) in DCM, then 7.5 mmole cholesteryl chloroformate were added drop by drop under N_2 protection and stirred overnight at room temperature. The product was purified by silica gel column and the molecular weight (MW: 560.5) was confirmed by mass spectrometry.

Hyaluronic acid (MW: 50kDa) obtained from Creative PEGWorks (Chapel Hill, NC) (400 mg) was dissolved in formamide with 50 ºC oil bath for 1 h with stirred. Then TEA (0.3 mM) and 1-[Bis(dimethylamino)methylene]-1H-1,2,3-triazolo[4,5-b]pyridinium 3-oxid hexafluorophosphate (HATU) (0.3 mmole) were added into the solution. Cholesteryl-linker (0.128 mmole) was dissolved in DMF and added into hyaluronic acid solution with V/V: 50/50, stirred in 50 ºC oil bath for 24 h and room temperature for another 24 h. The final product was isolated by dialysis (MWCO:

3.4kDa) against water and lyophilized. The conjugated CHA was confirmed by ^{1}H NMR spectrum in d-DMSO.

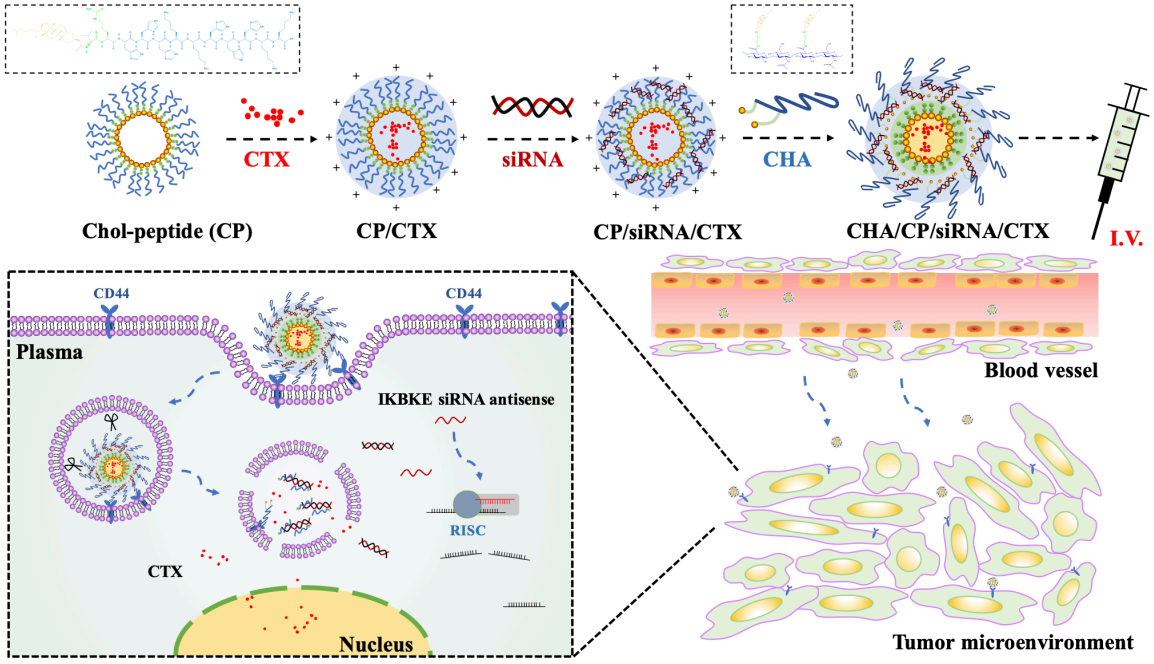

Figure 9. The schematic illustration of CHA/CP/siRNA/CTX nanocomplex preparation and intended mechanism for CD44-targeting TNBC treatment. Cholesterol-peptide (CP) was synthesized and self-assembled into a micelle-like structure loaded with cabazitaxel (CTX). Then CP/CTX micelle condensed with IKBKE siRNA. Synthesized Cholesteryl-Hyaluronic Acid (CHA) then coated on the surface of CP/siRNA/CTX to form the CHA/CP/siRNA/CTX hybrid nanocomplex. When CHA/CP/siRNA/CTX hybrid nanocomplex passes through the tumor tissue, they will be accumulated in the tumor microenvironment by passive and active targeting effect and undergo CD44-mediated endocytosis. The CHA/CP/siRNA/CTX nanocomplex can be degraded in the endosome by cathepsin B to release CTX and siRNA, thus acting in the tumor cells.

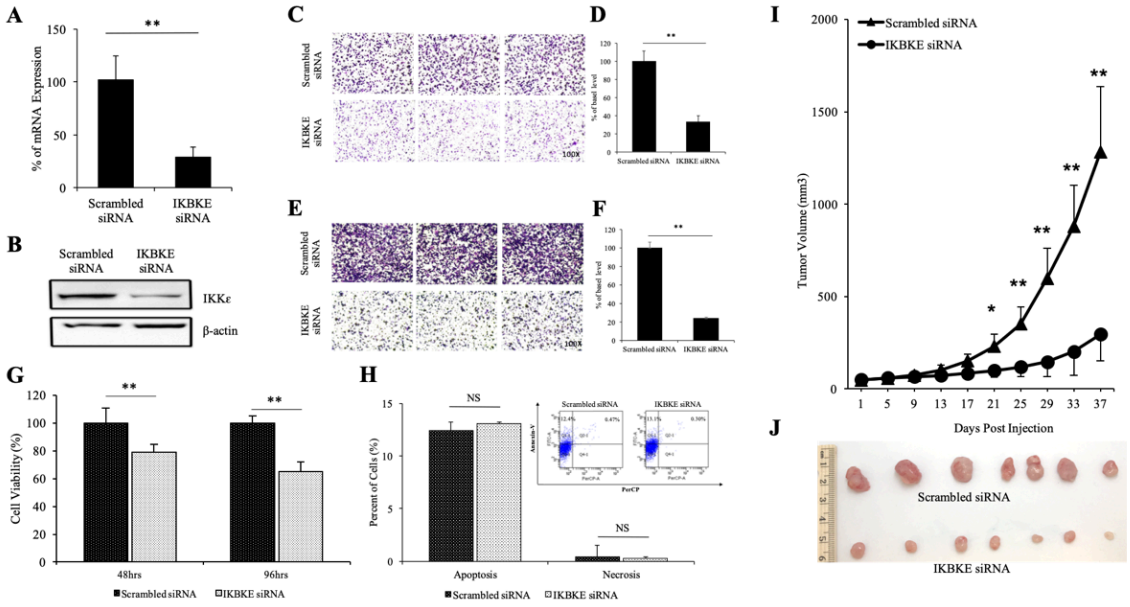

Figure 10. Bio-activities of IKBKE siRNA in TNBC MDA-MB-231 cells. (A) Silencing effect of IKBKE siRNA at the mRNA level performed by Real-time PCR. (B) Silencing activity of IKBKE siRNA at the protein level. IKBKE siRNA inhibits migration (C, D), invasion (E, F) and proliferation abilities (G) of MDA-MB-231 cells. Cell migration and invasion was assayed at 6 h and 24 h post-transfection, respectively. Quantitative analysis of the number of migrated or invasive cells was performed by quantifying six random microscope fields. Cell proliferation was determined at 48 h and 96 h post-transfection using the CellTiter-Glo Luminescent Cell Viability Assay Kit. (H) Effect of IKBKE siRNA on apoptosis and necrosis of MDA-MB-231 cells. All results are presented as the mean ± SD (n = 3). (I, J) *In vivo* anti-tumor efficacy of IKBKE siRNA in subcutaneous xenograft TNBC mouse model with intratumoral injection at a siRNA dose of 0.3 mg/kg. All results are presented as the mean ± SEM (n = 7). (* $P < 0.05$, ** $P < 0.01$).

4.2.4 Fabrication and characterization of the CHA-CP-siRNA nanocomplex

The IKBKE siRNA (sense strand sequence: 5'-GGU CUU CAA CAC UAC CAG Ctt-3') was purchased from GE Dharmacon (Lafayette, CO). For IKBKE siRNA bio-activity studies, the transfection of IKBKE siRNA mixed with Lipofectamine® RNAiMax was performed as previously described[8]. For IKBKE siRNA anti-tumor study, IKBKE siRNA was condensed with the cholesterol-peptide without Val-Cit dipeptide modification under the same conditions reported in a previous study[97].

For the CHA/CP/siRNA nanocomplex, siRNA was first condensed with modified CP (containing Val-Cit dipeptide) at different N/P ratios (1:1, 2:1, 3:1, 4:1, 5:1 & 10:1) at room temperature for 30 min to form the CP/siRNA nanocomplexes. The formation of these nanocomplexes was confirmed using a gel retardation assay. Samples were separated on a 2% agarose gel and visualized under UV light with GelRed™. Particle size and zeta potential of these nanocomplexes were determined in DI water using a Malvern Zetasizer Nano-ZS (Westborough, MA). Once the siRNA was condensed with CP, CHA was coated on the surface of the selected CP/siRNA at room temperature for 1 h with rotation at different molar ratios between CHA and CP. Two percent agarose gel was also used to confirm the nanocomplex condensation ability after coating with CHA. Zeta potential assay was performed to evaluate the changes in the surface charge of the nanocomplexes coated with different concentrations of CHA. A CM12 Scanning Transmission Electron Microscope (TEM) (Philips, Germany) was used to determine the structures of these nanocomplexes.

The critical micelle concentration (CMC) of the CHA/CP/siRNA nanocomplex was determined by using iodine as a probe[172]. Briefly, a series of sample solutions

ranging in concentration from 0.001 to 1 mg/mL were prepared in DI water, and the iodine solution was prepared by mixing iodine and potassium iodide (w/w: 1:2) in DI water. Two hundred microliter sample solutions were added into a 1.5 mL centrifuge tube, mixed with 10 μL iodine solution, and incubated at room temperature for 15 h in dark. Then, samples were transferred to a 96-well plate with black wall, and the absorbance of I_2 in the core of the micelles was determined at 366 nm using a Spectramax 190 microplate spectrophotometer (San Jose, CA).

4.2.5 Preparation of CTX-loaded micelle

Cabazitaxel-encapsulated micelle was prepared using dialysis technology, as reported in a previous report[173]. Twenty milligrams of CP were dissolved in 4 ml of DI water and stirred at room temperature for 30 min. Sixteen milligrams of cabazitaxel in ethanol (30 mg/ml) were added to the CP water solution dropwise and stirred for 30 min. Then, the mixture was ultra-sonicated for 30 min in an ice bath and centrifuged at 3000 rpm for 10 min. The solution was dialyzed against DI water for 24 h with a dialysis bag (MWCO: 3.4 kDa) and lyophilized, followed by filtration through a 0.45 μm pore-sized microporous membrane. The amount of cabazitaxel in the micelle was measured using HPLC (Shimadzu LC-20, Kyoto, Japan) by dissolving cabazitaxel and micelles in ethanol and detecting the absorbance at 274 nm. The entrapment efficiency (EE) and drug-loading (DL) capacity of cabazitaxel were calculated using the following equations:

$$\mathrm{DL}(\%) = \frac{\text{weight of cabazitaxel in micells}}{\text{weight of cabazitaxel in micelle} + \text{weight of CP fed initiallly}} \times 100\%$$

$$\mathrm{EE}(\%) = \frac{\text{weight of cabazitaxel in micells}}{\text{weight of cabazitaxel fed initially}} \times 100\%$$

4.2.6 Cell culture and siRNA transfection

MDA-MB-231 cell line was purchased from American Type Culture Collection, maintained in DMEM medium containing 10% FBS, 100 unit/ml penicillin and 100 μg/ml and culture in a 5% CO_2 filled humidified atmosphere at 37°C.

4.2.7 Silencing activity study

Five thousand MDA-MB-231 cells were seeded in a 24-well plate and incubated at 37°C for 12 h. For IKBKE bio-activity study, 50 nM IKBKE siRNA was diluted in Opti-MEM with Lipofectamine® RNAiMax as described above and transfected into cells for 24 h; the scrambled siRNA was used as a negative control. Then, RNA was isolated using a Direct-zol RNA isolation kit (ZYMO Research, CA), and Real Time RT-PCR was performed as previously reported[16]. For western blot assays, cells were first transfected with IKBKE siRNA in Opti-MEM for 24 h, and then the medium was replaced with fresh medium and cells were incubated for another 24 h. Proteins were isolated and the silencing activity was quantified by western blot with previously reported methods[16, 103].

For the CHA/CP/siRNA nanocomplex silencing activity study, 50 nM IKBKE siRNA was transfected with CP at different N/P ratios; Real Time RT-PCR and western blot assays were performed as described above. The silencing activity of CHA/CP/siRNA and CHA/CP/siRNA/CTX at the protein level was also quantitated by western blotting.

4.2.8 Cellular uptake study

Approximately 1×10^5 MDA-MB-231 cells were seeded in a 24-well plate and incubated at 37°C for 12 h. The IKBKE siRNA (50 nM) was condensed to form the CP/siRNA and CHA/CP/siRNA, and the 5' end of the siRNA antisense was labeled with Cy5. After 2, 4, and 6 h transfection, cells were treated with 40 μM heparin and cellular uptake was measured using a FACS II flow cytometer (BD Instrument, NJ)[103]. Confocal microscopy was performed 2 and 6 h after transfection[103]. For HA specific targeting efficiency, cells were pre-treated with free HA (5 mg/mL) for 2 h as previously reported[174].

4.2.9 Serum stability study

Serum stability study was performed with human and mouse serum as previously reported[103]. The CHA/CP/siRNA/CTX nanocomplex was incubated with 50% human and mouse serum for different time intervals at 37°C, then siRNAs were released form nanocomplex by incubated with heparin (40 μM) for 10 min and determined under UV stained with GelRed™ followed with electrophoresed in a 20% native PAGE gel.

4.2.10 Migration and invasion study

IKBKE siRNA was condensed with Lipofectamine® RNAiMax as described above in the silencing activity study. After 48 h incubation, treated cells were detached and re-suspended in serum-free DMEM at a concentration of 1×10^6 cells/mL for the migration assay. Then, 100 μL of the re-suspended cells were seeded into a transwell chamber with DMEM supplemented with 10% FBS. For the invasion study, the transwell

chamber was pre-coated with 50 μg of matrigel and 2×10^5 cells were seeded in the pre-coated transwell with serum-free DMEM. After 6 h (migration assay) and 24 h (invasion assay) incubation, the migrated cells were fixed with 10% paraformaldehyde and stained with 0.05% crystal violet, as previously reported[103]. The number of cells was counted at 200x magnification under a microscope (Leica, Germany).

4.2.11 *In vitro* proliferation study

Two thousand five hundred MDA-MB-231 cells were seeded in a 96-well plate, incubated at 37°C for 12 h, and treated with IKBKE siRNA/iMax for 24 h. Then, the medium was replaced with DMEM supplemented with 10% FBS, and cells were incubated at 37°C for 24 or 72 h. After 48 or 96 h of incubation, 100 μL of CellTiter-Glo buffer (Promega, WI) were added to the 96-well plate and the luminescent intensity was measured using a Spectramax M5e spectrophotometer (San Jose, CA).

4.2.12 *In vitro* apoptosis study

Approximately 2×10^5 MDA-MB-231 cells were seeded in a 6-well plate, incubated at 37°C for 12 h, and treated with IKBKE siRNA/iMax, as described in the silencing activity study. After 48 h of incubation, cells were treated according to the protocol of the Alexa Fluor® 488 Annexin V/Dead Cell Apoptosis Kit (ThermoFisher, NY) and examined using a FACS II flow cytometer. The same experiment was performed using the CHA/CP/siRNA/CTX nanocomplex; Cells were treated with free CTX, CHA/CP/siRNA and CHA/CP/siRNA/CTX for 48 h condensed with scrambled siRNA or IKBKE siRNA and apoptosis & necrosis were measured.

4.2.13 *In vivo* anti-tumor study

The animal protocol was approved by the Institutional Animal Care and Use Committee (IACUC) of the University of Missouri-Kansas City. For the IKBKE siRNA bio-activity study, 1×10^6 MDA-MB-231 cells were implanted into the back of female nude mice to create the subcutaneous xenograft tumor model. The IKBKE siRNA was condensed with the cholesterol-peptide lacking Val-Cit dipeptide under previously reported conditions[97]. The IKBKE siRNA or scrambled siRNA was injected into mice via intratumoral injection at a dose of 0.3 mg of siRNA/kg. The frequency of the injection was every 4 days/injection for 4 injections.

For the CHA/CP/siRNA/CTX nanocomplex anti-tumor study, 5×10^5 MDA-MB-231 cells were implanted into the mammary gland of female mice to set up a orthotopic TNBC model, as previously reported. Then mice were randomly divided into five groups and intravenously injected with saline, CHA/CP/IKBKE siRNA nanocomplex, cabazitaxel, CHA/CP/IKBKE siRNA nanocomplex plus free cabazitaxel and CHA/CP/IKBKE siRNA/CTX nanocomplex. The injections were performed every 4 days for totally 5 injections with a dose of 1.5 mg/kg IKBKE siRNA and 5 mg/kg cabazitaxel. Tumor volumes were calculated equal to ½ × longest diameter × shortest diameter^2. Expression of IKBKE in tumor were measured using a human IKBKE ELISA kit. Tumor tissues were homogenized in RIPA buffer and centrifuged at 13,000 g for 10 min to remove the precipitate. After determining the total protein concentration using a BCA protein assay kit (ThermoFisher, CA), the concentrations of IKBKE protein in tumor

tissues were determined using the IKBKE ELISA kit and presented as IKBKE (%) in total protein amount.

4.2.14 Statistical analysis

Data were presented as the mean ± standard deviation. Statistical analysis was performed using a two-way analysis of variance (ANOVA) with Tukey's *post hoc* test. $P < 0.05$ was considered statically significant.

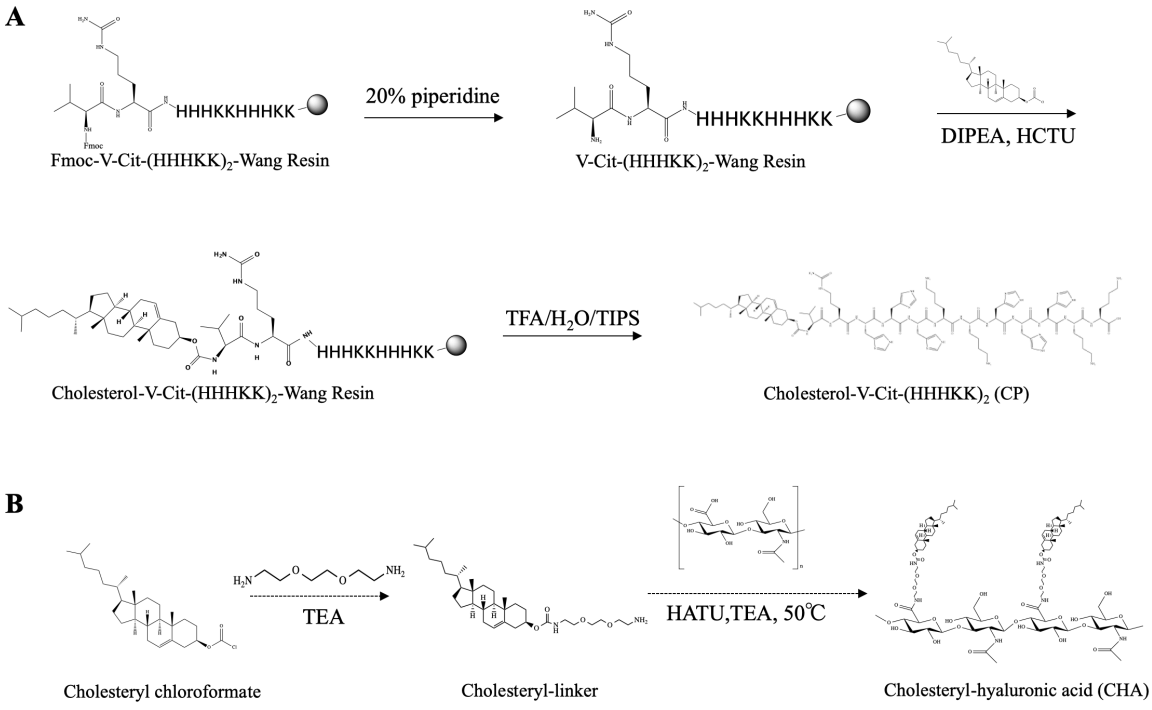

Figure 11. The synthesis of (A) cholesterol-peptide and (B) cholesteryl-hyaluronic acid. (A) The cationic peptide (V-Cit-HHHKKHHHKK) was modified at N-terminal with cholesterol by HCTU/DIPEA system. (B) Cholesteryl-hyaluronic acid (CHA) was synthesized by linked cholesteryl-chloroformate to the HA chains with a small linker 2,2'-(ethylenedioxy)-bis-(ethylamine) by HATU/TEA system.

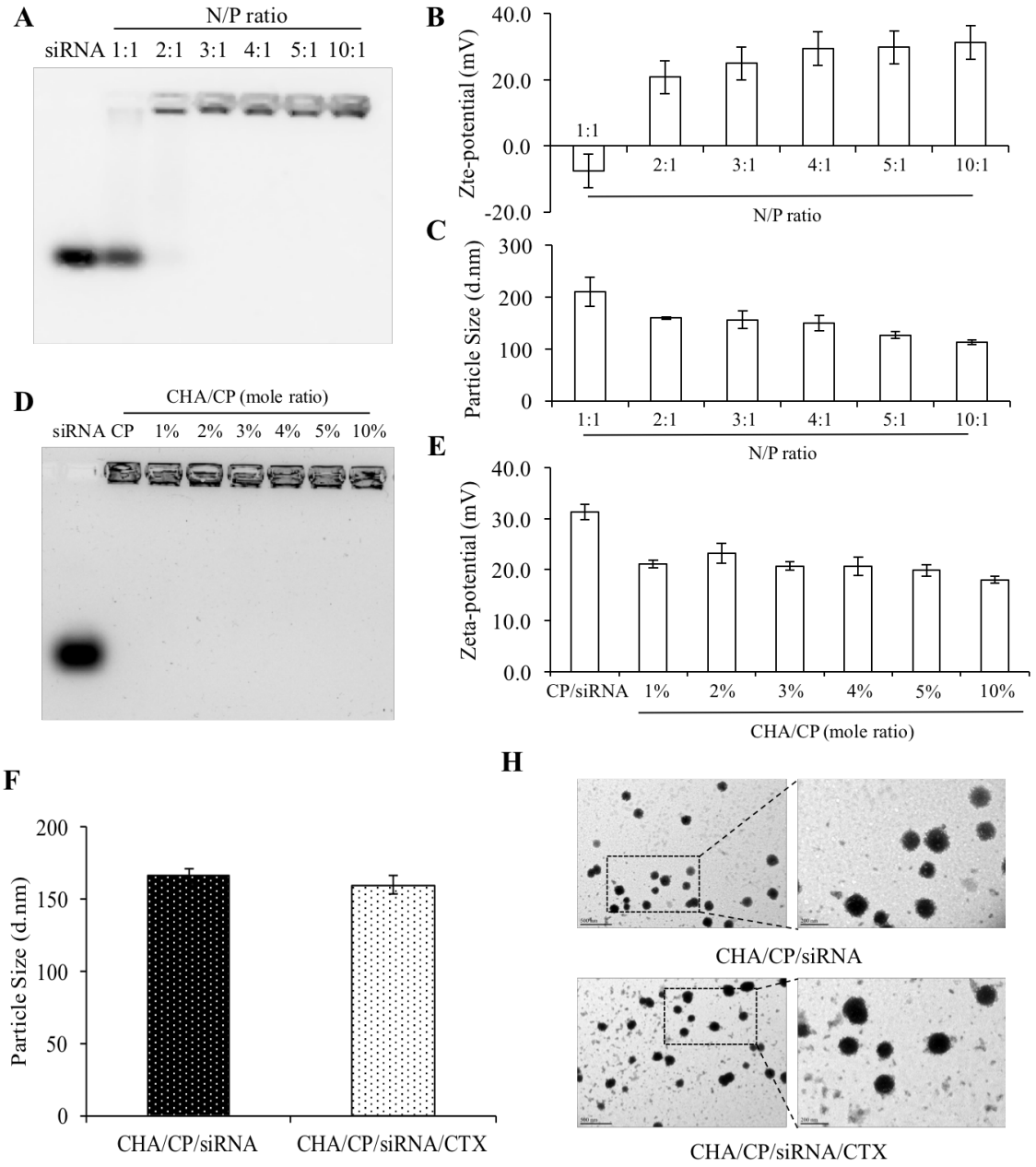

Figure 12. Characterization of CHA/CP/siRNA/CTX nanocomplex. (A) Gel retardation assay of the CP/siRNA at different N/P ratio. (B) Zeta-potential and (C) particle size of the CP/siRNA at different N/P ratio. (D) Gel retardation assay of the CHA/CP/siRNA at different CHA/CP mole ratio. (E) Zeta-potential of the CHA/CP/siRNA at different CHA/CP mole ratio. (F) Particle size and TEM images (H) of CHA/CP/siRNA and CTX loaded CHA/CP/siRNA/CTX nanocomplexes.

4.3 Results

4.3.1 Bio-activities of IKBKE siRNA for TNBC cell line

In our previous report, we evaluated the silencing effect of the IKBKE siRNA on HER2+ breast cancer cell lines (MCF7 and SK-BR-3)[16]. In this study, we condensed the IKBKE siRNA with Lipofectamine® RNAiMax to evaluate the bio-activities of the IKBKE siRNA on a TNBC cell line (MDA-MB-231) by the same method reported as previous studies[16, 111]. As shown in Figure 10A, IKBKE siRNA silenced 71% of the expression of the IKKε in MDA-MB-231 cells with 24 h transfection, and the silencing effect was confirmed by a western blot assay after 48 h transfection, as illustrated in Figure 10B.

After evaluating the silencing effect of IKBKE siRNA on TNBC cell line, we next performed the migration and invasion assay to determine whether IKBKE siRNA inhibits the migration and invasion on TNBC cells, as determined in the HER2+ cell lines in our previous report[16]. Compared to scrambled siRNA, only 33% of MDA-MB-231 cells treated with IKBKE siRNA migrating from FBS-free medium to 10% FBS-containing medium in 6 h, as shown in Figure 10C & D. Similar trends were observed in the invasion assay, the invasion of approximately 76% of IKBKE siRNA-treated cells was inhibited after 24 h compared to the control group, as illustrated in Figure 10E & F.

A CellTiter-Glo assay was performed to measure the inhibitory effect of IKBKE siRNA on the proliferation of TNBC cells. Forty-eight and 96 hours after transfection and incubation, IKBKE siRNA significantly inhibited the proliferation of MDA-MB-231 cells by 21% and 35%, respectively, as shown in Figure 10G.

Furthermore, we used flow cytometry to determine the apoptosis of TNBC cells treated with the IKBKE siRNA. Similar to our previous study of HER2+ breast cancer, we did not observe a significant difference in the number of apoptotic TNBC cells between IKBKE siRNA and scrambled siRNA groups. As shown in Figure 10H, IKBKE siRNA induced the apoptosis of 13.1% of MDA-MB-231 cells, while scrambled siRNA induced the apoptosis of 12.4% of cells, with a P value of 0.432, suggesting that knockdown of the IKKε gene alone in TNBC cells may not induce apoptosis.

Next, we performed an *in vivo* study to determine the anti-tumor effect of IKBKE siRNA alone on an MDA-MB-231 xenograft tumor model. IKBKE siRNA or scrambled siRNA was condensed into a micelle structure by N-terminal cholesterol-modified cationic peptide (HHHKKHHHKK) because of its high transfection efficiency and low cytotoxicity[97]. Micelles containing siRNAs were injected into the tumor at a dose of approximately 0.3 mg/kg for 4 times. As illustrated in Figure 10I & J, tumor growth was significantly inhibited in the IKBKE siRNA-treated group as compared to scrambled siRNA.

4.3.2 Fabrication and characterization of the CHA/CP/siRNA nanocomplex

Furtherly, to improve the endosome escape and tumor targeting effect of siRNA, the cathepsin B specific dipeptide (Val-Cit) was added between the cationic peptide and cholesterol, which can be degraded in the endosome and the CD44-targeting HA was coated on the surface of nanocomplex. Modified CP was used to condense the siRNA at different N/P ratios and examined on a 2% agarose gel. As shown in Figure 12A, CP completely condensed the siRNA at an N/P ratio of 2:1, and this result was confirmed by

the zeta potential results shown in Figure 12B; the surface charge of CP/siRNA micelles switched from negative (N/P ratio 1:1) to positive (N/P ratio 2:1) and increased as the N/P ratio increasing. In Figure 12C, the particle sizes decreased as the N/P ratio increasing, which might be attributed to the enhanced interaction between the siRNA and CP. We coated the complex with cholesteryl modified HA, which targets CD44 on the surface of TNBC cells, as ligand added into CP/siRNA micelle. The HA modified with cholesterol (CHA) coated on the surface of the CP/siRNA nanocomplex by charge interaction due to the negatively charged of HA and the interaction between CP/siRNA and CHA were also strengthened by hydrophobic interaction between the cholesterol linked to the HA and cholesterol linked to the CP. We performed another gel retardation assay with a 2% agarose gel to evaluate the stability of CHA/CP/siRNA nanocomplex. As illustrated in Figure 12D, no free siRNA was detected as the molar ratio of CP to CHA increasing from 1% to 10%. The zeta potentials of CP/CHA/siRNA nanocomplexes were reduced as the amount of CHA increasing, as shown in Figure 12E.

To furtherly improve the antitumor efficacy, cabazitaxel was encapsulated into the CHA/CP/siRNA nanocomplex to inhibit the proliferation of tumor cells, which was induced by apoptosis. The drug loading (DL%) of cabazitaxel was 18.3% and the entrapment efficiency (EE%) was 19.8%. The CMCs of the above-mentioned groups were measured. As shown in Figure 13A, CMCs of CP, CP/siRNA and CP/CHA/siRNA were 72 μg/ml, 76 μg/ml and 82 μg/ml, respectively. The condensation of siRNA and coating with CHA hardly changed the CMC and the low CMC value suggested that CHA/CP/siRNA delivery system might maintain stability in diluted condition, which was beneficial to the application *in vivo*. The particle sizes of CHA/CP/siRNA and CTX-

loaded CHA/CP/siRNA/CTX nanocomplexes were 165 nm and 160 nm, respectively, and the structure were furtherly confirmed by TEM illustrated in Figure 12F.

4.3.3 Serum stability of CHA/CP/siRNA/CTX nanocomplex

CHA/CP/IKBKE siRNA/CTX nanocomplex were incubated with 50% human and mouse serum for 0, 1, 6, and 24 h at 37°C. After treated with heparin, released siRNAs were determined in a 20% native PAGE gel. The results shown in Figure 13B indicated that CHA/CP/IKBKE siRNA/CTX hybrid nanocomplex protected siRNA from human and mouse serum degradation up to 24 h.

4.3.4 Silencing activity study of CHA/CP/siRNA/CTX nanocomplex

A Real-time PCR assay was performed to evaluate the silencing activity of the IKBKE siRNA condensed at different N/P ratios 24 h after transfection. As illustrated in Figure 14A, the expression of IKKε gene in MDA-MB-231 cells was reduced as the N/P ratio increasing. Similar results were exhibited at the protein level by western blot assay, as shown in Figure 14B. Another western blot experiment was performed to evaluate the silencing effect of CHA/CP/siRNA/CTX, as shown in Figure 14C, and there is no significant difference in silencing efficiency between CHA/CP/IKBKE siRNA nanocomplex with or without loading cabazitaxel and both showed effective silencing effect on IKKε.

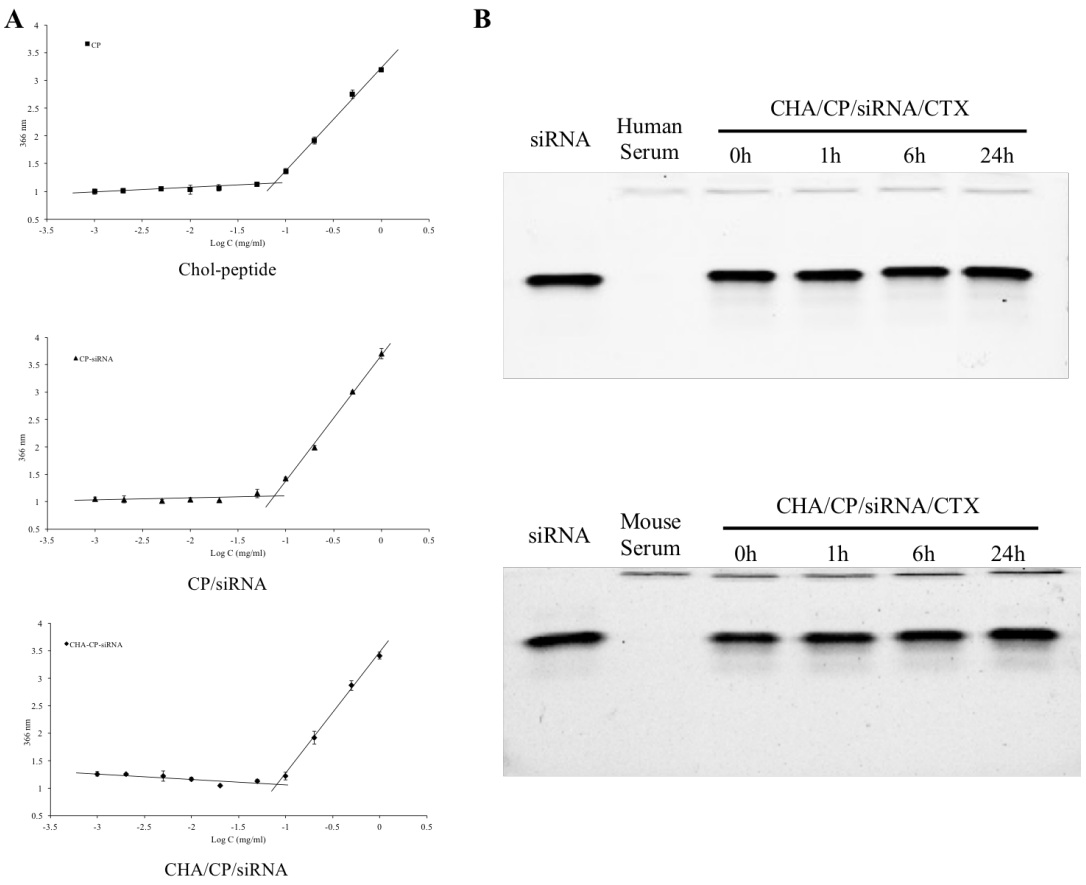

Figure 13. Critical micelle concentration (CMC) and serum stability of CHA/CP/siRNA/CTX nanocomplexes. (A) CMC of Chol-peptide, CP/siRNA and CHA/CP/siRNA were determined using iodine as a probe and measured at 366 nm. (B) Serum stability of CHA/CP/siRNA/CTX nanocomplex in 50% human or mouse serum for 0, 1, 6, and 24 h.

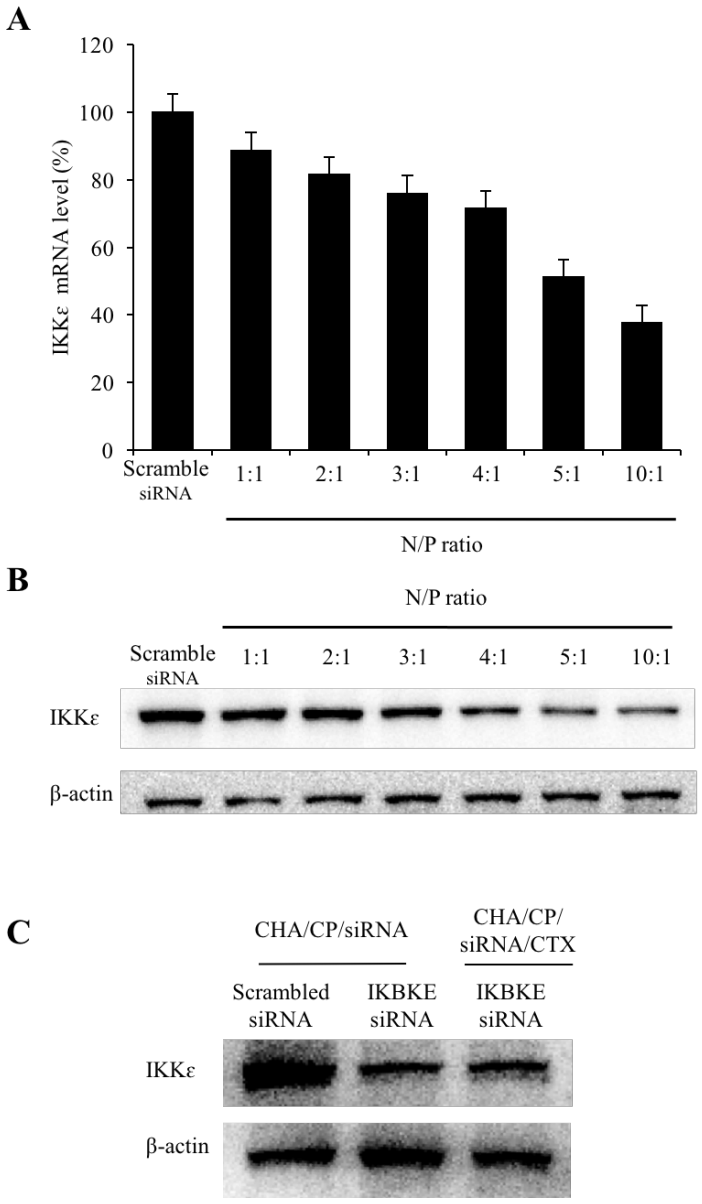

Figure 14. Silencing activities of CHA/CP/siRNA/CTX nanocomplexes. (A) Silencing activities at IKKε mRNA level of CP/IKBKE siRNA at different N/P ratio. All results are presented as the mean ± SD (n = 3). (B) Western Blot assay performed IKKε protein level of CP/IKBKE siRNA at different N/P ratio. (C) Silencing activities at protein level for IKKε of CHA/CP/siRNA and CHA/CP/siRNA/CTX nanocomplexes.

4.3.5 Cellular uptake study of CHA/CP/siRNA/CTX nanocomplex

The siRNA was labeled with Cy5 dye at the 5' end to evaluate the cell uptake effect of the CHA/CP/siRNA/CTX nanocomplexes. Flow cytometry was used to determine the cellular uptake of micelles at different time points. Compared to the free siRNA, both CP/siRNA and CHA/CP/siRNA exhibited a higher cellular uptake, as illustrated in Figure 15A. The fluorescence intensity was also determined to quantify the cellular uptake. As shown in Figure 15B, the fluorescence intensity of CHA/CP/siRNA was 3.06-, 2.80- and 2.18-fold higher than CP/siRNA at 2, 4 and 6 h of incubation, respectively, indicating that the coated CHA significantly enhanced the cellular uptake of the CP/siRNA nanocomplexes. Meanwhile, the CHA-mediated increase in fluorescence intensity was reduced from 3.06- to 2.18-fold over time, potentially due to the non-passive accumulation of nanoparticles. We also performed a confocal microscopy study to confirm the increase in the cellular uptake of the CHA/CP/siRNA nanocomplex delivery system after 2 and 6 h of incubation. Cells were pre-treated with free HA to specifically determine the HA targeting efficiency. As illustrated in Figure 15C & D, the cellular uptake of CHA/CP/siRNA was higher than CP/siRNA 2 and 6 h after transfection, similar to the flow cytometry results. CHA/CP/siRNA exhibited much less cellular uptake after the pre-treatment, which indicated the specific targeting efficiency of HA in the CHA/CP/siRNA nanocomplex.

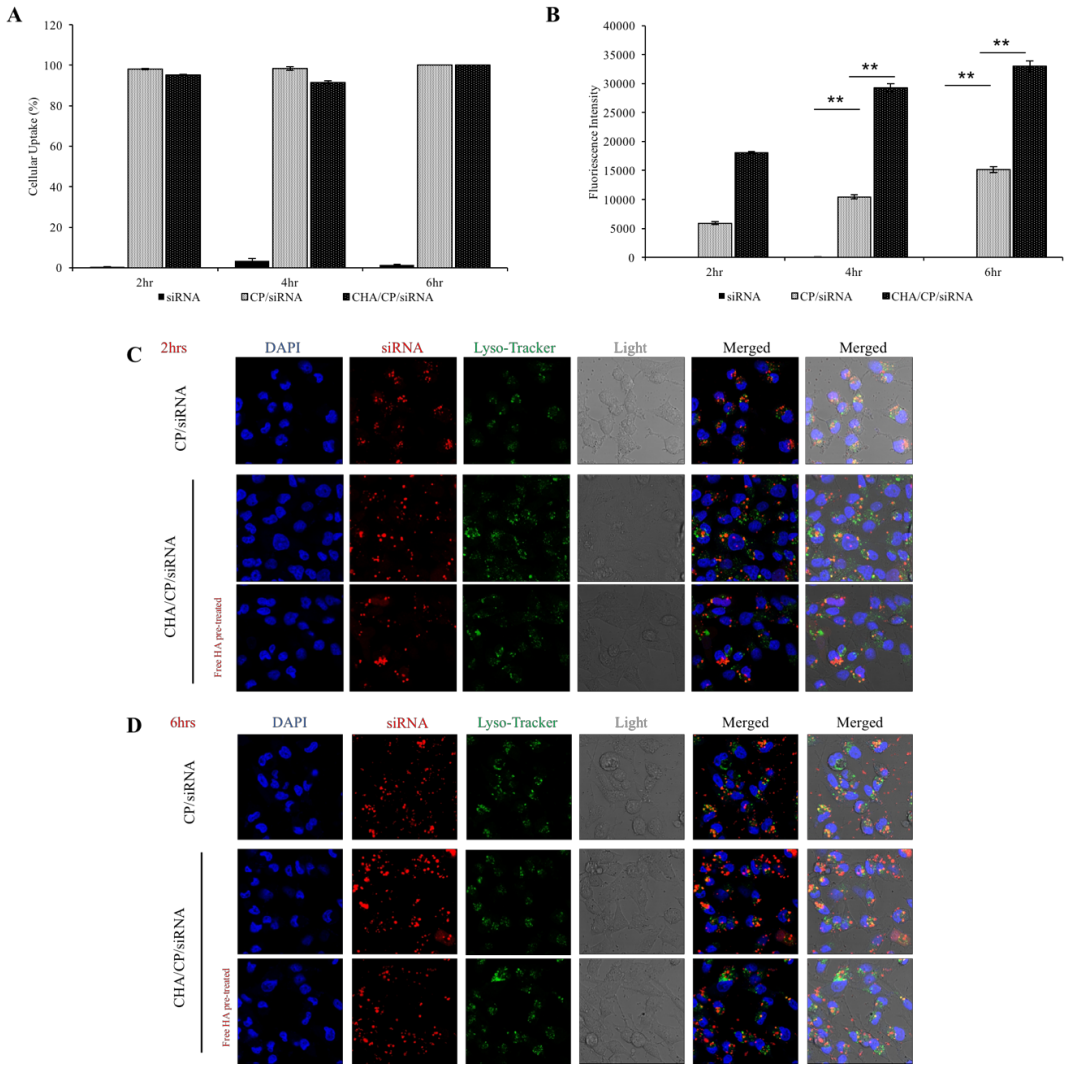

Figure 15. Quantitative cellular uptake of CHA/CP/siRNA nanocomplex. siRNA was labeled with Cy5 for fluorescence analysis using flow cytometry (A, B) and confocal microscopy (C, D). (A) Percent of the cells that take up free siRNA, CP/siRNA and CHA/CP/siRNA nanocomplexes after 2, 4, and 6 h transfection. (B) Fluorescence intensity of the cells that take up the nanocomplex after 2, 4, and 6 h transfection. Confocal images of the cells treated with CP/siRNA and CHA/CP/siRNA nanocomplexes after 2 h (C) and 6 h (D) incubation. Free HA (5 mg/ml) was used to pre-treated cells.

4.3.6 Apoptosis study of CHA/CP/siRNA/CTX nanocomplex

We used same flow cytometry method to evaluate the apoptosis of CHA/CP/siRNA/CTX nanocomplexes on MDA-MB-231 cells, as shown in Figure 16A & B. Compared to free cabazitaxel, both CHA/CP/IKBKE siRNA/CTX and CHA/CP/scrambled siRNA/CTX exhibited enhanced apoptosis of TNBC cells, which may due to the high cellular uptake of CHA/CP/siRNA/CTX nanocomplex.

4.3.7 *In vivo* study of CHA/CP/siRNA/CTX nanocomplex

In this study, an orthotopic xenograft mouse model of TNBC was established to mimic the natural tumor microenvironment. The effect of different preparations on antitumor activities was evaluated. The nanocomplexes were administered via tail vein every 4 days for a total of 5 times at a dose of 1.5 mg/kg IKBKE siRNA and 5 mg/kg cabazitaxel. There were five groups in total (Saline, CHA/CP/IKBKE siRNA nanocomplex, CTX, CHA/CP/IKBKE siRNA nanocomplex plus free CTX and CHA/CP/IKBKE siRNA/CTX nanocomplex). The tumor volume from saline treated control group increased 40.9-fold compared to that on the first day treatment illustrated in Figure 17A. In contrast, the tumor volume in the group of CHA/CP/IKBKE siRNA nanocomplex was approximately 28.1-fold suggest the similar tumor growth inhibition of illustrated in Figure 9I; however, the inhibition efficacy is lower (31.3% vs 78.0%) than the intratumoral injected IKBKE siRNA. Meanwhile, free CTX group also performed a 39.1% tumor growth inhibition efficacy at a dose of 5 mg/kg and confirmed by examining the weight of isolated tumor tissues (Figure 17A & B). Additionally, a 13.2-fold change of tumor volume was observed in CHA/CP/IKBKE siRNA nanocomplex

plus free CTX group and an 8.7-fold change in CHA/CP/IKBKE siRNA/CTX nanocomplex treated group to the initial volumes. All these indicate the tumor growth inhibition efficacy of IKBKE siRNA & CTX. The significantly difference between CHA/CP/IKBKE siRNA nanocomplex plus free CTX (67.7%) and CHA/CP/IKBKE siRNA/CTX nanocomplex (78.7%) further indicate that CHA/CP/siRNA/CTX can be a promising strategy for TNBC therapy by combined IKBKE siRNA and cabazitaxel. Human IKBKE ELISA kit was used to determine the level of IKBKE protein in each group (Figure 17C). Compared to control saline treated group, both CHA/CP/IKBKE siRNA nanocomplex, CHA/CP/IKBKE siRNA nanocomplex plus free CTX and CHA/CP/IKBKE siRNA/CTX nanocomplex treated groups performed a similar and significant reduced IKBKE protein expression in tumor tissues; meanwhile, there are no difference between cabazitaxel and saline treated groups. All these results indicate that this multifunctional drug co-delivery system for cabazitaxel and IKBKE siRNA may offer a promising option for TNBC therapy.

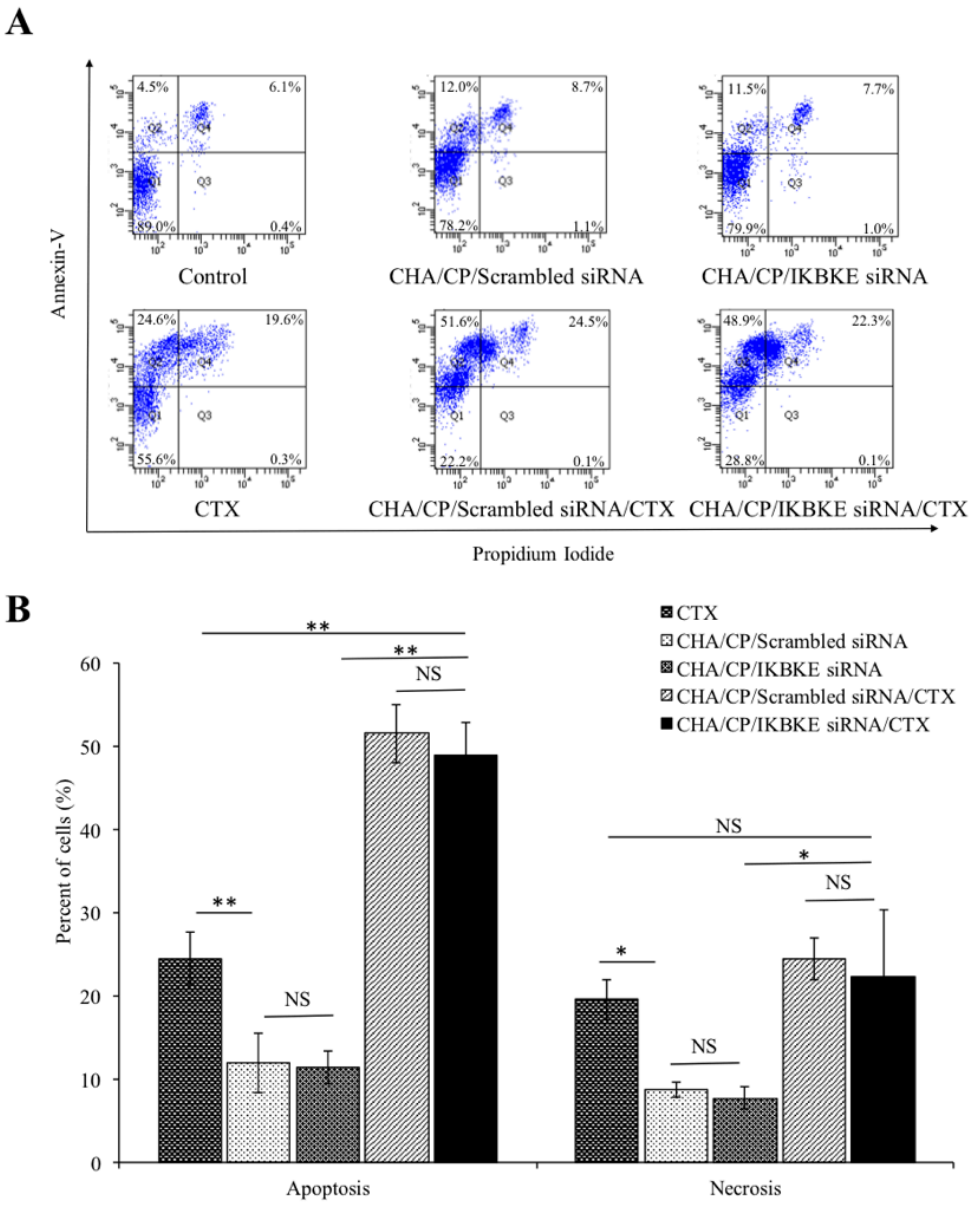

Figure 16. Apoptosis and necrosis in MDA-MB-231 cells. (A) Alexa Fluor® 488 Annexin V/Dead Cell Apoptosis Kit and FACS II flow cytometer were used to determine the effect of free CTX, CHA/CP/siRNA with scramble siRNA or IKBKE siRNA, CHA/CP/siRNA/CTX nanocomplexes with scramble siRNA or IKBKE siRNA on apoptosis in MDA-MB-231 cells after 48 h transfection. (B) Percent of apoptotic and necrotic cells after 48 h transfection. All results are presented as the mean ± SD (n = 3). (* $P < 0.05$, ** $P < 0.01$).

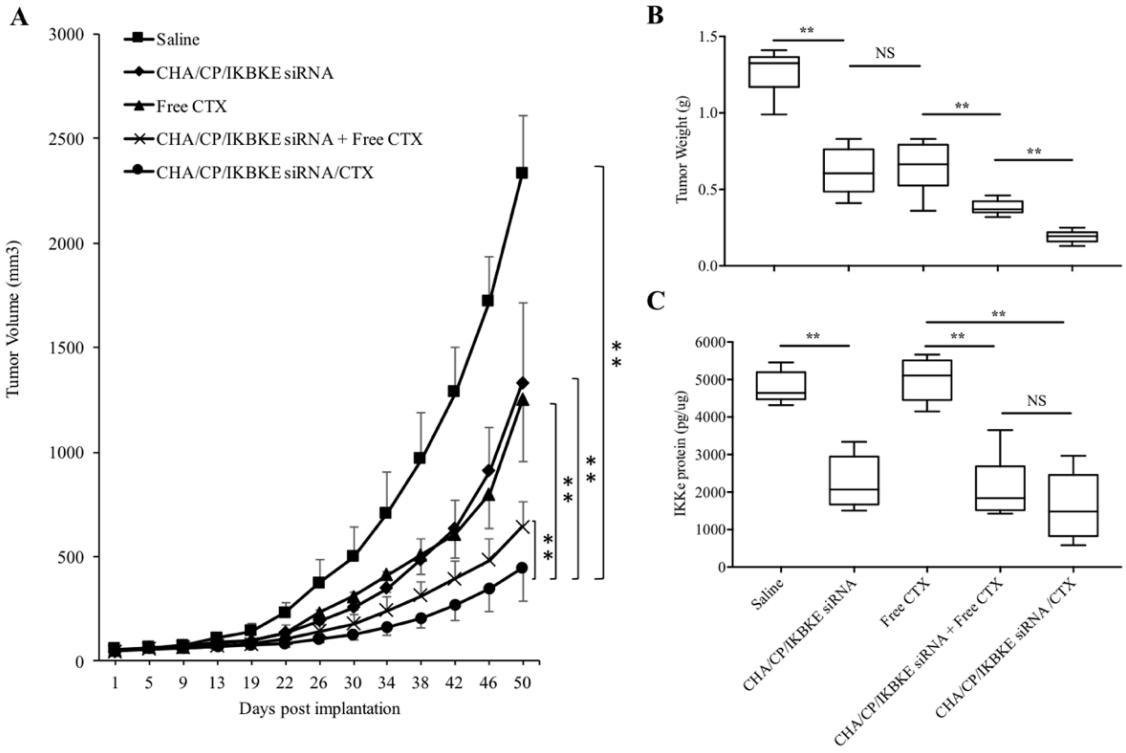

Figure 17. Anti-tumor activity of CHA/CP/siRNA/CTX nanocomplex. (A) Tumor growth curve of orthotopic xenograft MDA-MB-231 tumor model presented as the mean ± SEM (n = 6) for five groups: Saline, CHA/CP/IKBKE siRNA nanocomplex, CTX, CHA/CP/IKBKE siRNA nanocomplex plus free CTX and CHA/CP/IKBKE siRNA/CTX nanocomplex. (D) Tumor weight and (E) expression of IKBKE of isolated tumor tissues. All results are presented as the mean ± SD (n = 6). (** $P < 0.01$).

4.4 Discussion

IKBKE, an important mediator that functions in the NF-κB activation process by phosphorylating TRAF2 and CYLD, is identified as an oncogene and overexpressed in approximately 30% of breast carcinomas and aberrantly overexpressed in TNBCs[24, 25]. IKBKE overexpression is associated with STAT3 activation and contributes to the proliferation and survival of TNBCs[25]. Meanwhile, IKBKE-mediated production of the cytokines CCL5A and IL-6 also induces a migration effect on both TNBC cells and endothelial cells through autocrine and paracrine activities[25]. *Barble et al.,* reported that the proliferation and migration of TNBC cells can be impaired by treatment with a multitargeted IKBKE/JAK signaling inhibitor (CYT387) but not with ruxolitinib (another JAK signaling inhibitor)[25]. Our finding regarding the bioactivities of IKBKE siRNA supports the hypothesis regarding IKBKE function in TNBCs. Similar to its roles in HER2+ breast cancer cell lines, silencing IKBKE significantly inhibited the proliferation, migration and invasion of TNBC cells, but no apoptosis was induced (Figure 10A to H). An *in vivo* study also showed the tumor growth inhibition effect of IKBKS siRNA (Figure 10I & J). The findings revealed that targeting IKBKE by utilizing siRNA can be a potential therapeutic strategy for TNBC.

To further improve the anti-tumor efficacy of the IKBKE siRNA towards TNBC, we developed a cathepsin B-specific dipeptide-modified, HA surface-coated nanocomplex as a cargo for the co-delivery of IKBKE siRNA and cabazitaxel (Figure 9). Cabazitaxel, a novel semi-synthetic taxane, hormone-refractory prostate cancer treatment drug, is more potent than docetaxel in breast cancer[69, 175]. Moreover, cabazitaxel demonstrates increased antiproliferation and greater apoptosis induction than docetaxel

by raising more sustained G_2-M arrest over treatment for 48 or 72 hrs [175]. *Zhong et al.,* loaded cabazitaxel into polymeric micelles and found that cabazitaxel-loaded micelles significantly inhibited 4T1 (a mouse TNBC cell line) tumor growth and metastasis[72].

The combination of cabazitaxel with IKBKE siRNA has a better anti-tumor efficacy against TNBC. Currently, the limitation of cabazitaxel therapy is mainly attributable to its cytotoxicity[73]. Free cabazitaxel injection at doses over 10 mg/kg showed increased systemic toxicity, and a 20 mg/kg dose was sufficient to cause mouse death in an *in vivo* animal study[73]. Encapsulated cabazitaxel with polymeric micelles or PEGylation to nanoparticles has been reported to significantly reduce systemic toxicity[73, 176]. Meanwhile, the application of IKBKE siRNA has been limited due to its high negative charge and serum instability[15]. In this study, cholesterol and a cathepsin B-specific response dipeptide-modified cationic peptides self-assembled into a micelle-like structure and encapsulated cabazitaxel in the hydrophobic center. The micelles were then condensed with IKBKE siRNA to form nanocomplexes, followed by coating with cholesterol-HA to target CD44 on TNBC. The nanocomplex protected IKBKE siRNA from both human and mouse serum degradation for up to 24 h, as shown in Figure 13B. Meanwhile, the hybrid nanocomplex had a low CMC value (0.082 mg/ml, Figure 13A), indicating that it may be a promising cargo for hydrophobic cabazitaxel. As illustrated in Figure 17A, cabazitaxel-loaded CHA/CP/siRNA/CTX nanocomplex can significantly inhibited tumor growth at a cabazitaxel dose of 5 mg/kg in combination with IKBKE siRNA, which was much lower than the systemic toxicity toleration dose of cabazitaxel.

In conclusion, IKBKE siRNA can significantly inhibit the proliferation, migration and invasion of TNBC cells but has no apoptosis-inducing effect. The *in vivo* study also indicated that IKBKE siRNA can inhibit TNBC tumor growth. CD44-targeting CHA/CP/siRNA/CTX nanocomplex showed the synergistic effect of IKBKE siRNA and cabazitaxel on the inhibition of invasiveness and growth of TNBC tumors with an enhanced CD44 specific targeting effect. CHA/CP/siRNA/CTX nanocomplexes also exhibited a significant anti-tumor effect through IKBKE siRNA and cabazitaxel *in vivo*. Thus, IKBKE siRNA may be a promising anti-tumor agent for TNBC therapy, and co-delivery of IKBKE siRNA and cabazitaxel through a CD44-targeting nanocomplex is a potential strategy for TNBC treatment.

CHAPTER 5

DEVELOPMENT OF A PEPTIDE-MODIFIED siRNA NANOCOMPLEX FOR HEPATIC STELLATE CELLS

5.1 Rationale

Liver fibrosis is a wound healing process characterized by the accumulation of excess extracellular matrix (ECM) in the liver. It is induced by chronic liver injuries caused by nonalcoholic steatohepatitis, hepatitis, alcohol abuse, and metal poisoning[3, 4]. If left untreated, liver fibrosis will develop into liver cirrhosis, which is irreversible and affects nearly 633,233 adults in the United States[105].

The expression of ECM increases dramatically when quiescent hepatic stellate cells (HSCs) are activated to myofibroblast-like cells[3, 5-7]. Although HSCs only constitute approximately 5-8% of total liver cells[109], they are the major contributors for liver fibrosis and are able to cover the entire microcirculatory network of hepatic sinusoidal[110]. Type I collagen is the most abundant protein in ECM, and its abnormal accumulation is primarily due to the increased half-life of its collagen α1(I) mRNA[112, 113]. We recently discovered an siRNA to silence the poly(rC) binding protein 2 (PCBP2) gene in HSCs to inhibit the expression of αCP2 protein, which is responsible for stabilization of the collagen α1(I) mRNA. Silencing of the PCBP2 gene reduced the expression of type I collagen in activated HSCs[8]. We also developed an avidin-based siRNA nanocomplex for the PCBP2 siRNA and discovered that neutravidin is the best avidin analogue for siRNA delivery[17, 32].

Targeted delivery of antifibrotic agents to HSCs is a major challenge in liver fibrosis therapy. Therapeutic agents cannot easily reach HSCs because of the excessive

accumulation of ECM, the closure of endothelial fenestrae, and the reduced flow exchange between sinusoid blood and liver cells[9]. The delivery of antifibrotic agents to HSCs is also limited by the reduced perisinusoidal space (or space of Disse)[31]. One promising strategy to improve the delivery of antifibrotic agents to HSCs is to modify drug carriers with a specific ligand that binds to a moiety on activated HSCs[32-34]. Three targeting moieties, including cellular-binding protein type I (CRBP-1), low-density lipoprotein receptor (LDLR) and insulin-like growth factor 2 receptor (IGF2R) have been studied for HSC-specific drug delivery. IGF2R, also known as mannose-6-phosphate receptor (M6PR), is a 300k Da glycoprotein that plays a critical role in the insulin-like growth signaling system. IGF2R contains three domains, including an extracellular domain, a transmembrane domain and a cytoplasmic domain[125]. Because its expression is upregulated during liver fibrogenesis[126, 127], IGF2R has been utilized as a targeting moiety for HSC-specific drug delivery. For example, M6P was used as a ligand to deliver a triplex-forming oligonucleotides to fibrotic liver [33]. We recently discovered an IGF2R-specific peptide, peptide-431, using a novel combinatorial biopanning strategy. Peptide-431 and its dimeric form showed high and specific affinity to activated human and rat HSCs[127]. In this disseration, dimeric peptide-431 will used as a targeting ligand of the siRNA nanocomplex to specifically deliver the nanocomplex to activated HSCs in fibrotic liver and compared to free siRNA and the nanocomplexes coupled with vitamin A and cholesterol *in vitro* and *in vivo*.

5.2 Materials and methods

5.2.1 Materials

PCBP2 and scramble siRNAs were ordered from Invitrogen (Carlsbad, CA) and Shanghai Genepharm (Shanghai, China). Neutravidin, and BCA protein assay kit were obtained from Pierce (Rockford, IL). Protamine sulfate (salmon X grade), all-trans-retinoic acid and anti-β actin antibody were purchased from Sigma-Aldrich (St. Louis, MO). GelRed™ was purchased from Biotium (Hayward, CA). Anti-IGF2R antibody and anti-α-SMA antibody were purchased from R&D system (Minneapolis, MN). Biotin-PEG-amine and biotin-PEG-acid were purchased from BroadPharm (San Diego, CA). Lipofectamine® RNAiMAX, cell culture media, and all other chemical reagents were purchased from Fisher Scientific (Grand Land, NY).

5.2.2 Synthesis of biotin-PEG-ligands

Biotin was conjugated to various ligands (IGF2R-specific peptide, vitamin A, and cholesterol) via a low molecular weight (1 kDa) polyethylene glycol (PEG) linker. The reaction schemes were presented in Figure 18 (A, B, C).

The biotin-PEG-IGF2R peptide was synthesized using solid phase peptide synthesis. Briefly, the N-(1-(4,4-dimethyl-2,6-dioxocyclohexylidene)ethyl) (Dde) protecting group in the dimeric peptide-431 (0.1 mmole) was removed by washing with 2% hydrazine in N,N-dimethylformamide (DMF) for 3 times, each for 10 minutes. Next, 2-(6-Chlor-1H-benzotriazol-1-yl)-1,1,3,3-tetramethylaminium-hexafluorophosphat (HCTU) (0.2 mmole) and biotin-PEG-acid (0.2 mmole) were added, and the solution was stirred continuously at room temperature for 24 h. After completion of the reaction, the peptide was cleaved

from Wang resin with TFA/phenol/water/TIPS (88/5/5/2) at room temperature for 2 h. The biotin-PEG-peptide product was then purified by HPLC, and the molecular weight (Mw:5015.1) was confirmed by Matrix Assisted Laser Desorption/Ionization Time of Flight (MALDI-TOF).

For biotin-PEG-cholesterol, biotin-PEG-amine (0.12 mmole) and cholesterol chloroformate (0.1 mmole) were dissolved in 2 mL Dichloromethane (DCM) and stirred continuously at room temperature for 24 h. Next, 0.2 mmole Triethylamine (TEA) was added, and the reaction was continued at room temperature for another 24 h. The biotin-PEG-cholesterol product was purified by silica gel column, and its molecular weight (Mw:1729.1) was confirmed by MALDI-TOF.

For biotin-PEG-vitamin A, all-trans-retinoic acid (0.2 mmole) were dissolved in 2 mL DCM with 0.3 mmole 1-Ethyl-3-(3-dimethylaminopropyl) carbodiimide (EDC), 0.3mmole Hydroxybenzotriazole (HOBt) and 0.3 mmole N, N-Diisopropylethylamine (DIEA). The solution was stirred continuously at room temperature for 24 h. After adding 0.1 mmole biotin-PEG-amine, the reaction was continued for another 24 h, and the final product was purified by silica gel column. The molecular weight (Mw:1582.0) was confirmed by mass spectrometry (MS).

5.2.3 Fabrication and characterization of the neutravidin-based siRNA nanocomplex

Biotin-conjugated PCBP2 siRNA (sense strand sequence: 5'-GUC AGU GUG GCU CUC UUA Utt-3') was purchased from Shanghai Genepharm (Shanghai, China). Biotin was linked to the 3' end of the sense strand via a disulfide linker. Biotin-siRNA,

neutravidin and biotin-conjugated ligands were mixed in a 2:1:2 ratio at room temperature for 10 min to form the siRNA-neutravidin-IGF2R peptide (SNP) complex, the siRNA-neutravidin-cholesterol (SNC) complex, and the siRNA-neutravidin-vitamin A (SNV) complex. These complexes were then condensed with protamine at different N/P ratios (1:1. 2:1, 5:1 and 10:1) at room temperature for 30 min to form the multicomponent siRNA-nuetriavidin-peptide-protamine nanocomplex (SNPP), siRNA-neutravidin-cholesterol-protamine nanocomplex (SNCP), and siRNA-neutravidin-vitamin A-protamine nanocomplex (SNVP).

Formation of the nanocomplexes were confirmed using a gel retardation assay. Briefly, 10 μL of the nanocomplex was separated on 20% native polyacrylamide gel electrophoresis (PAGE) and visualized with GelRed^{TM} under UV light. Particle size and zeta potential of the nanocomplexes were measured in HEPES buffer (pH 7.4) using a Malvern Zetasizer Nano-ZS (Malvern Instruments, Westborough, MA).

5.2.4 Serum stability of the neutravidin-based siRNA nanocomplex

The nanocomplexes were incubated with 50% rat serum at 37°for various time intervals. Half of the samples were separated by a 20 % native PAGE gel and visualized with GelRed^{TM}. To demonstrate that the siRNAs encapsulated inside the nanocomplex are still intact, another half of the samples were incubated with 40 μM heparin and 100 mM DTT for 10 min to dissociate free siRNA from the nanocomplex[177]. Dissociated siRNA samples were electrophoresed in a 20% native PAGE and visualized with GelRed^{TM}.

5.2.5 Cytotoxicity study of the neutravidin-based siRNA nanocomplex

Cytotoxicity of the siRNA nanocomplex in HSC-T6 cells was evaluated using MTT assay as described[111, 178]. HSC-T6 cells seeded in 96-well plate (2500 cells/well) were incubated with SNCP, SNVP and SNPP nanocomplexes at 37 °C for 24 h and 48 h, followed by adding MTT to measure cytotoxicity.

5.2.6 Cell culture

The rat hepatic stellate cell line HSC-T6 and human hepatic stellate cell line LX-2 were kindly provided by Dr. Scott L. Friedman (Mount Sinai School of Medicine, New York University) and cultured as previously reported[127].

Primary rat HSCs were isolated as we reported before[123, 179]. The animal protocol was approved by the Institutional Animal Care and Use Committee (IACUC), University of Missouri-Kansas City. Primary rat HSCs were cultured in DMEM with 10% FBS, 100 units/mL penicillin, and 100 μg/mL streptomycin. The primary rat HSCs in the 5^{th} and 15^{th} passage generations were used for cellular uptake study.

5.2.7 Cellular uptake of the siRNA nanocomplex

Cellular uptake of the nanocomplexes were evaluated in HSC-T6, LX-2 and primary rat HSCs (the 5^{th} and 16^{th} passage generations) using flow cytometry and confocal microscopy. The 5' end of the siRNA antisense strand was labeled with Alex Flour 647. The cells were incubated with the nanocomplexes at 37 °C for various time intervals and then washed with Opti-MEM containing 1mg/mL heparin to remove nonspecifically bound nanocomplexes.

Following heparin treatment, the cells were detached with 0.25% trypsin, washed, suspended, and subjected to fluorescence analysis using a BD FACS II flow cytometer (BD instruments, NJ). For confocal analysis, the cells were stained with 150 nM LysoTracker in Opti-MEM at room temperature for 30mins, fixed with 10% formalin, and examined under a confocal microscope (Leica TCS SP5, Germany).

5.2.8 Silencing activity of the siRNA nanocomplex

HSC-T6 cells, primary rat HSCs (the 5^{th} and 16^{th} passage generations) were cultured and transfected with the siRNA nanocomplex as described before[17]. SNCP, SNVP and SNPP nanocomplexes were prepared as described above with the N/P ratio of 2:1 and incubated with the cells at a final concentration of 50 nM siRNA. After incubation for 6 h, the medium was replaced with DMEM with 10% FBS, and the cells were harvested 48 h post-transfection. Silencing activity was quantitated using western blot assay as previously reported.

5.2.9 Invasion assay

The invasion assay was performed as described with modifications.[16, 180] Briefly, matrigel (50 μg/mL) and type I collagen (50 μg/mL) were coated on the top and bottom, respectively, of transwell chambers. HSC-6 cells were transfected with the siRNA nanocomplexes at a concentration of 50 nM siRNA for 24 h, followed by incubation in DMEM with 0.5% FBS (for serum starvation) and 100 mM alcohol for another 24 h. The cells were detached, resuspended in DMEM with 0.5% FBS, and loaded into the transwell chambers at a density of 30,000 cells/chamber. The wells were

filled with DMEM containing 10% FBS as attractant. After 4 h invasion, the cells were fixed with 10% paraformaldehyde and stained with 0.05% crystal violet. The migrated cells on the bottom were counted at 100x magnification under a microscope.

5.2.10 *In-vivo* biodistribution study

The animal protocol was approved by the Institutional Animal Care and Use Committee (IACUC) at the University of Missouri-Kansas City. Male Sprague Dawley rats were housed in a humidity and temperature controlled room with a 12 h light–dark cycle. Liver fibrosis was induced by intraperitoneal injection with the mixture of carbon tetrachloride (CCl_4) and olive oil (1:1, v/v) at a dose of 1 mL/kg CCl_4 twice a week for five consecutive weeks. The rats were then randomly divided into four groups and intravenously injected with Cy5-labeled siRNA or the siRNA nanocomplexes encapsulating Cy5-labeled siRNA at a dose of 0.1 mg/Kg. After 2 h, the rats were euthanized, and major organs including the liver, lungs, spleen, kidneys, heart, muscle (thigh), and blood were harvested for imaging analysis using a Bruker MS FX PRO In vivo Imaging System (Billerica, MA).

5.2.11 Statistical analysis

All data were presented as the mean ± standard deviation. Statistical analysis was performed using two-way analysis of variance (ANOVA) with Tukey's post hoc test. $P<0.05$ was considered statistically significant.

5.3 Results

5.3.1 Fabrication and characterization of the neutravidin-based siRNA nanocomplexes

The nanocomplexes were fabricated as illustrated in Figure 18D. Biotin-PEG-peptide-431 and biotin-labeled siRNA were mixed with neutravidin in a 2:2:1 molar ratio to form the siRNA-neutravidin-peptide complex by noncovalent neutravidin-biotin interaction, followed by condensation with protamine at different N/P ratios to form the SNPP nanocomplex. Similarly, SNCP and SNVP nanocomplexes coupled with cholesterol and vitamin A, respectively, were fabricated using the same procedure. In our previous studies, we developed an avidin-based siRNA nanocomplex at the N/P ration 10:1, but it showed somewhat non-specific accumulation in the lung[177]. This could be due to its high positive charge (+18 mV)[114]. Moreover, high positive charge of nanoparticles may cause significant systemic toxicity[181]. Therefore, we aimed to reduce the N/P ratio of the nanocomplex to minimize its non-specific accumulation in the lung.

We evaluated the complexation and condensation of the siRNA nanocomplexes using gel retardation assay. As illustrated in Figure 19A, complexation of the biotin-labeled siRNA, neutravidin, and biotin-labeled ligands shifted siRNA bands, indicating a complete complexation of the siNRA, neutravidin, and biotin-labeled ligands. Condensation of the siRNA-neutravidin-ligand complex with protamine at high N/P ratios (2:1 to 10:1) completely shielded the siRNA from staining, suggesting complete encapsulation of siRNA inside the nanocomplex. Zeta potential of the siRNA-neutravidin-ligand complexes was negative, while zeta potential of the nanocomplexes

was slightly positive (+4mV) at the N/P ratio 2:1 (Figure 19B). This is consistent with the gel retardation results in Figure 19A. All the three nanocomplexes, SNCP, SNVP, and SNPP, showed similar results in complexation and zeta potential, suggesting that different targeting ligands do not affect the fabrication of the s nanocomplexes. Based on these results, N/P ratio of 2:1 was selected for the neutravidin-based siRNA nanocomplex for subsequent studies.

Particle size of the SNCP, SNVP and SNPP nanocomplexes was 191, 167 and 228 nm, respectively, and the polydispersity index (PDI) values were 0.132, 0.114 and 0.249, respectively (Figure 19C). The relatively large particle size of the SNPP nanocomplex is possibly because of the higher molecular weight of the peptide ligand compared to cholesterol and vitamin A.

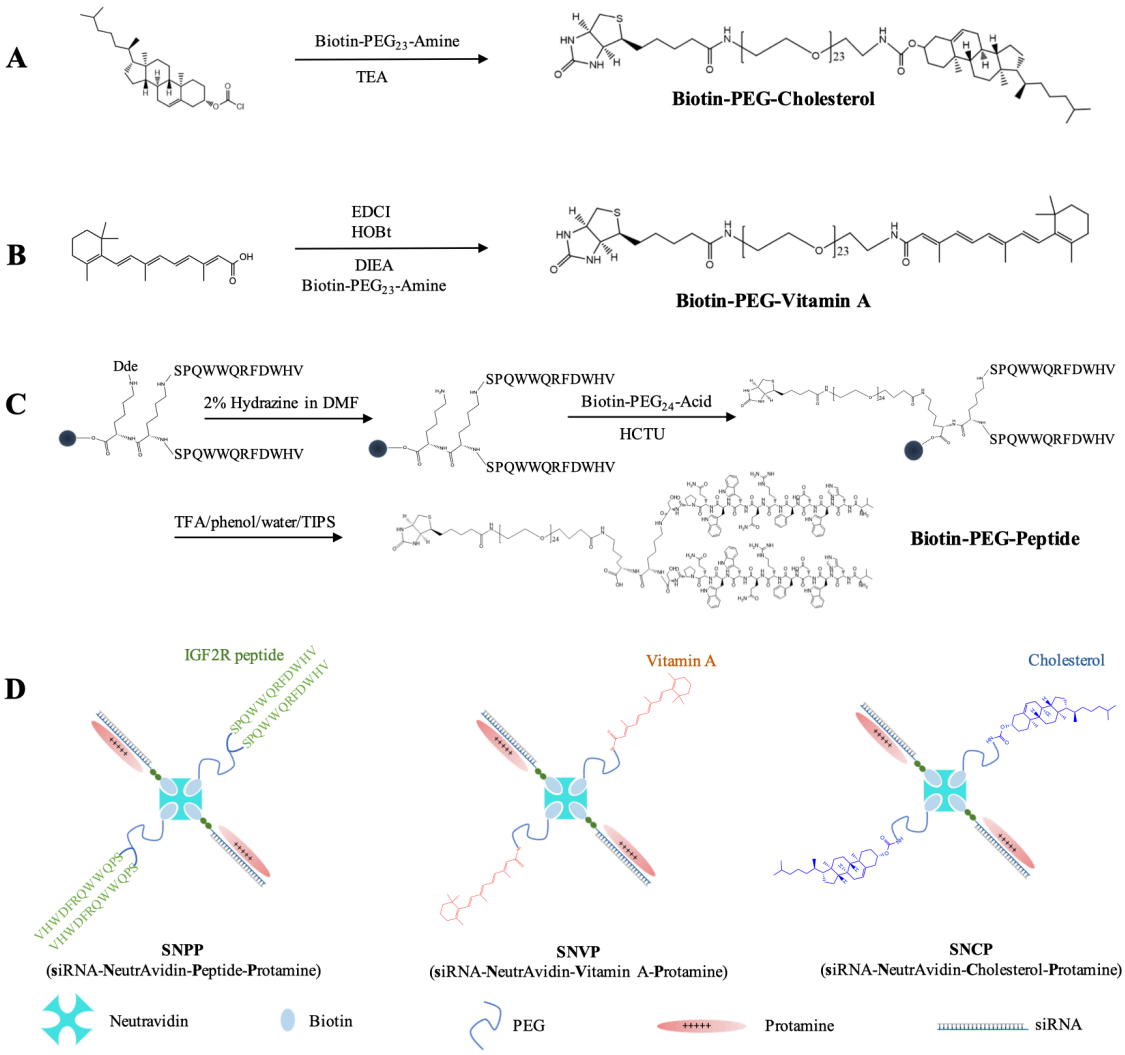

Figure 18. The synthesis and fabrication schemes of (A) biotin-conjugated cholesterol, (B) biotin-conjugated vitamin A, (C) biotin-conjugated IGF2R-speific peptide, and (D) the neutravidin-based siRNA nanocomplex. Biotin-conjugated PCBP2 siRNA, neutravidin and biotin-conjugated ligands were mixed in a 2:1:2 ratio at room temperature to form the siRNA-neutravidin-ligand complex, followed by condensation with protamine to form the final nanocomplex.

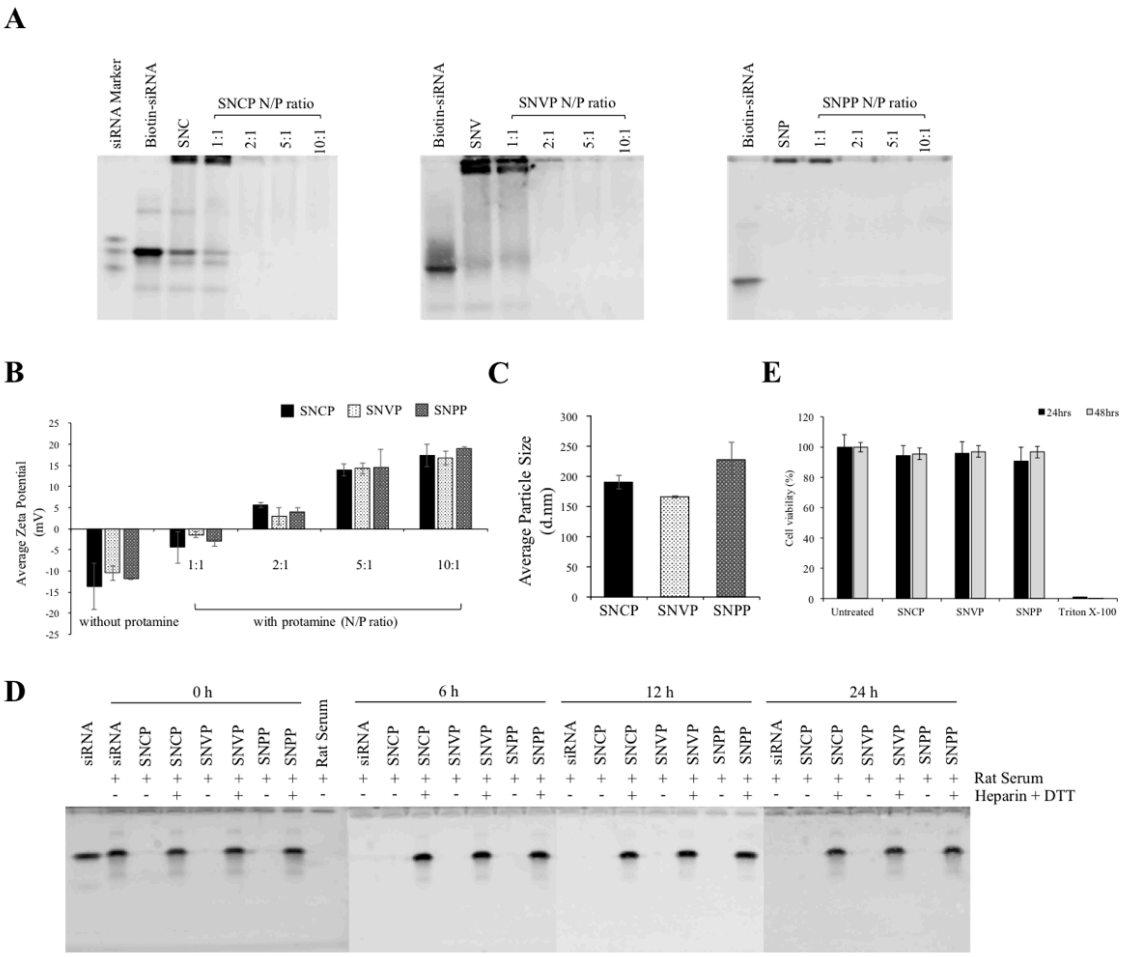

Figure 19. Characterization and silencing activity of the nanocomplex. (A) Gel retardation assay of the SNCP, SNVP and SNPP nanocomplexes at different N/P ratios. (B) Zeta potential of the nanocomplexes with different N/P ratios. (C) Particle size of the nanocomplexes. (SNC: siRNA-neutravidin-cholesterol complex; SNV: siRNA-neutravidin- vitamin A complex; SNP: siRNA-neutravidin-peptide-431 complex). (D) Serum Stability of the nanocomplex in 50% rat serum for 0, 6, 12, and 24 h. (E) Cytotoxicity study of the nanocomplexes. MTT assay was performed for 24 h and 48 h.

5.3.2 Serum stability of the neutravidin-based siRNA nanocomplex

Serum stability of the nanocomplexes was examined in 50% rat serum. As Figure 19D showed, free siRNA was rapidly degraded in the serum, and no siRNA was detected after 6 h. Consistent with the results in Figure 19A, the nanocomplexes shielded siRNA from GelRed^{TM} staining at all time intervals, indicating a good stability of the nanocomplexes in the serum up to 24 h. Treatment of the nanocomplexes with heparin and DTT released intact siRNA even after 24 h incubation in the serum. This data revealed that the neutravidin-based nanocomplexes can efficiently protect siRNA from degradation in the serum. Moreover, MTT assay demonstrated that the SNCP, SNVP and SNPP nanocomplexes do not induce cytotoxicity in HSC-T6 cells (Figure 19E).

5.3.3 Cellular uptake

We next examined cellular uptake of the nanocomplexes in HSC-T6 cells. Flow cytometry was used to determine the percentage of cells that take up the nanocomplex (Figure 20A) and intensity of the siRNA inside the cells (Figure 20B). Compared to free siRNA, all the three nanocomplexes demonstrated substantially higher uptake in HSC-T6 cells. This is in accordance with our previous findings that neutravidin-based nanocomplexes can efficiently deliver siRNA to HSCs[177]. In addition, the results indicated that targeting ligand plays an important role in the cellular uptake of the nanocomplex. Compared to nanocomplexes modified with cholesterol (SNCP) and vitamin A (SNVP), the nanocomplex modified with the IGF2R-specific peptide (SNPP) showed the highest cellular uptake, suggesting a high affinity of the IGF2R-specific peptide to HSCs. Particularly, the fluorescence intensity of the Alexa Fluor 647-labeled

siRNA in SNPP transfected cells is approximately 3.6 folds higher than that in SNCP and SNVP transfected cells.

Subsequently, confocal microscopy was used to compare intracellular distribution of these nanocomplexes in HSC-T6 cells (Figure 20C, D, E). The results are consistent with the flow cytometry results, in which SNPP showed the highest cellular uptake. Moreover, the confocal images showed that all the three nanocomplexes efficiently deliver the siRNA into the cytoplasm with minimal entrapment inside lysosomes, indicating their distinctive capabilities to escape endosomes.

We subsequently examined cellular uptake of these nanocomplexes in quiescent primary rat HSCs (5^{th} passage generation) and activated primary rat HSC cells (16^{th} passage generation). As illustrated in quiescent primary rat HSCs (Figure 21 A, B, and C), SNPP nanocomplex exhibited similar uptake as SNCP and SNVP nanocomplexes. By contrast, SNPP nanocomplex showed the highest uptake in activated primary rat HSCs (Figure 4 D, E, F). These results indicated that the high uptake of SNPP nanocomplex is mediated by the overexpressed IGF2R in activated HSCs.

To explore the potential applications of SNPP nanocomplex in the future for human patients, we also evaluated the uptake of these nanocomplexes in a spontaneously immortalized human hepatic human HSC cell line LX-2. As shown in Figure 23 A, after incubation for 6 and 24 h, SNPP nanocomplex demonstrated the highest cellular uptake compared to SNCP and SNVP nanocomplexes. More importantly, SNPP nanocomplex exhibited approximately 3.04-fold and 4.3-fold increase of the siRNA fluorescence intensity in the cells compared to SNCP and SNVP, respectively, at 6 h (Figure 23B).

Confocal microscopy (Figure 23C) revealed the same results as flow cytometry in Figure 23A and 23B.

HSC-T6 is an activated HSC cell line with fibroblast-like phenotype and proliferates rapidly in cell culture[116]. We hypothesized that the high uptake of SNPP nanocomplex in HSC-T6 is mainly mediated by IGF2R. We tested this hypothesis by conducting a similar cellular uptake study in quiescent and activated primary rat HSCs. Quiescent primary rat HSCs were activated by continuous passaging in cell culture. We first quantified the expression of IGF2R in primary rat HSCs at different passages. As Figure 22A showed, the expression of IGF2R and α-SMA, a marker for activated fibroblasts, in primary rat HSCs increased with the number of passaging. The primary rat HSCs at the 16^{th} passage generation exhibited similar expression of α-SMA and higher expression of IGF2R as compared to HSC-T6 cells.

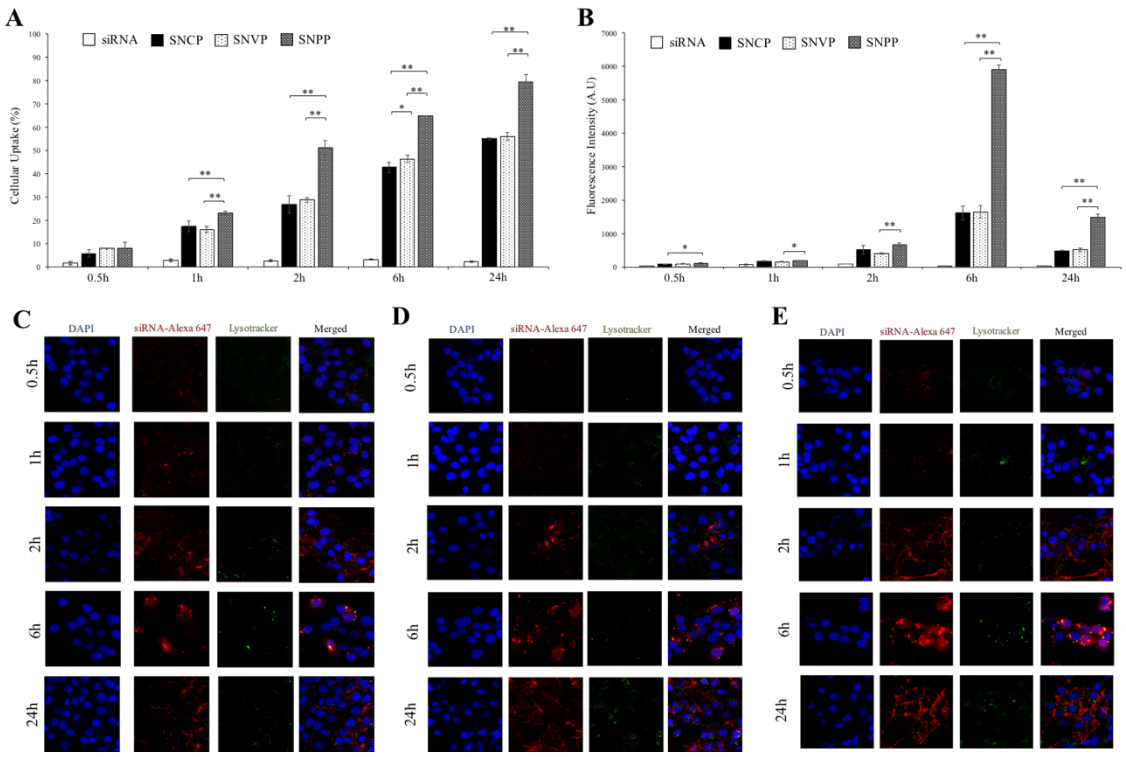

Figure 20. Quantitative cellular uptake of SNCP, SNVP and SNPP nanocomplexes in HSC-T6 cells. siRNA was labeled with Alexa Flour 647 for fluorescence analysis using flow cytometry (A, B) and confocal microscopy (C, D, E). (A) Percent of the cells that take up the nanocomplexes. (B) Fluorescence intensity of the cells that take up the nanocomplexes. Confocal images of the cells treated with SNCP (C), SNVP (D) and SNPP (E) nanocomplexes at various time intervals. All results are presented as the mean ± SD (n=3). (*P<0.05; **P<0.01).

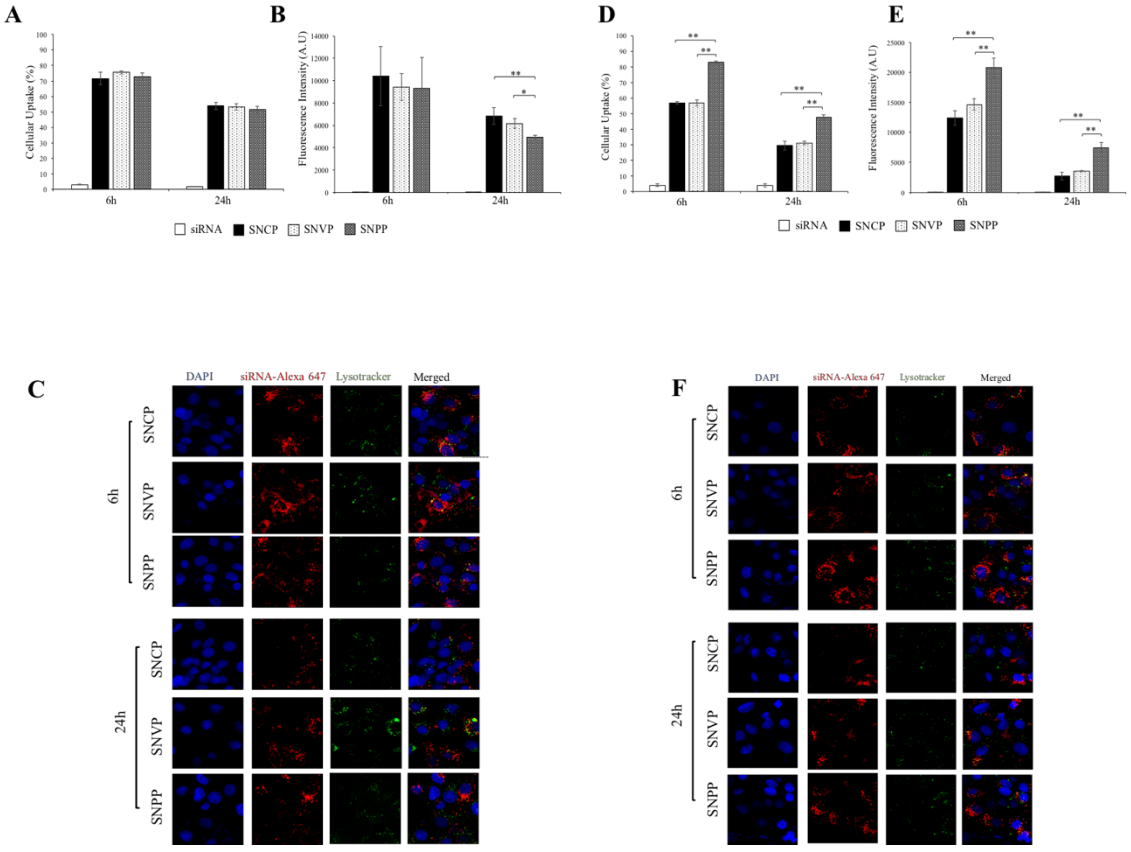

Figure 21. Cellular uptake of the nanocomplexes in quiescent and activated primary rat HSCs. Cellular uptake of the SNCP, SNVP and SNPP nanocomplexes containing Alexa Flour 647 labeled siRNA were evaluated in quiescent primary rat HSCs at the 5th passage generation (A, B, and C) and activated primary rat HSCs at the 16th passage generation (D, E, and F). (A, D) Percent of the cells that take up the nanocomplexes; (B, E) Fluorescence intensity of the cells that take up the nanocomplexes; (C, F) Confocal images of the cells. All results are presented as the mean ± SD (n=3). (*P<0.05; **P<0.01).

5.3.4 Silencing activity

In accordance with the cellular uptake results in Figure 20 and 21, the nanocomplexes exhibited significantly silencing activity at the protein level in HSC-T6 and primary rat HSCs (Figure 22B, C and D). Compared to SNCP and SNVP, SNPP exhibited higher silencing activity in activated HSCs, such as HSC-T6 and primary rat HSCs (16^{th} passage generation), suggesting the important role of IGF2R in the uptake of SNPP.

5.3.5 Invasion assay

Having shown the high cellular uptake of the SNPP nanocomplex in activated HSCs, we next wanted to demonstrate its antifibrotic activity in HSCs. During liver fibrogenesis, various fibrogenic cytokines, such as TGF-β1, PDGF, and VEGF, activate HSCs and increase their migratory behavior[182, 183]. Alcohol abuse is another stimuli that can cause chronic liver injuries and subsequently result in liver fibrosis[5]. We recently demonstrated that alcohol stimulation increased the migration capability of HSCs, and transfection of PCBP2 siRNA can efficiently reverse the migration of HSCs[184]. To determine whether the SNPP nanocomplex loaded with PCBP2 siRNA inhibits the migration of HSCs, we transfected HSC-T6 cells with SNPP for 24 h and then incubated the cells with 100mM alcohol for another 24 h. As shown in Figure 24, SNPP nanocomplex inhibited approximately 55% of the invasion of the HSC-T6 cells. This result proved that SNPP nanocomplex can efficiently deliver siRNA to HSCs and subsequently exert its biological activity in the cells.

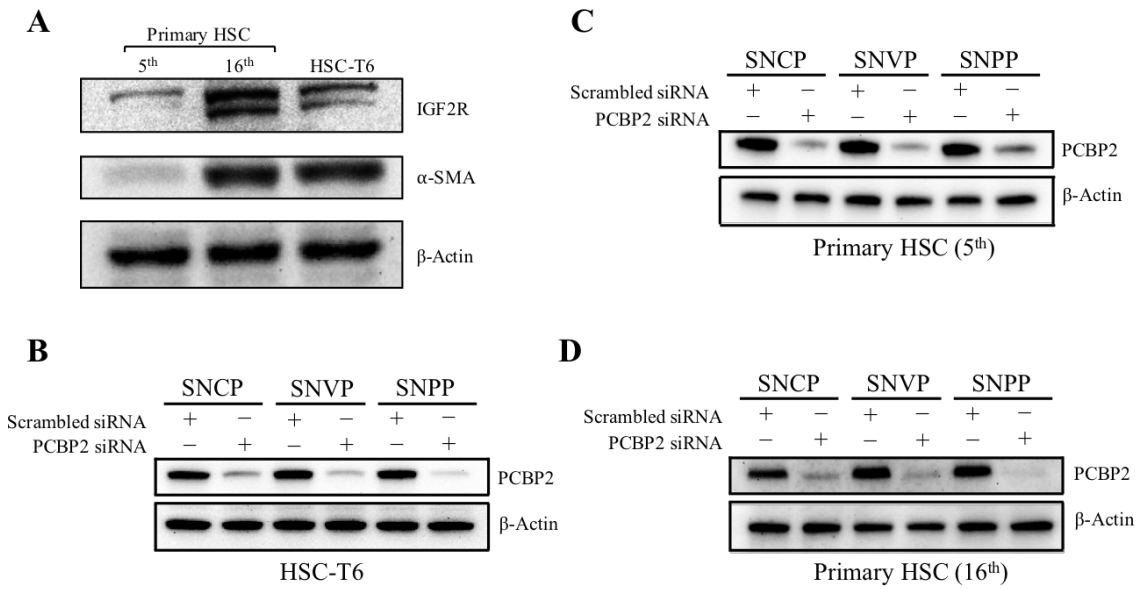

Figure 22. Activation of primary rat HSCs increases the expression of IGF2R and α-SMA and silencing activity of nanocomplexes. (A) Quiescent primary rat HSCs were activated by continuous passaging in cell culture. The protein expressions of IGR2R and α-SMA in primary rat HSCs (the 5th and 16th passage generations) were detected using western blot. (B, C, D) Silencing activity of SNCP, SNVP and SNPP nanocomplexes were detected for PCBP2 protein by using western blot in HSC-T6 (B), quiescent primary rat HSCs (C) and activated primary rat HSCs (D).

5.3.6 *In-vivo* biodistribution

Hepatic uptake of antifibrotic agents *in vivo* is always a challenge because of the extensive accumulation of collagen and dramatic changes of sinusoids during liver fibrogenesis[123, 179]. As a result, it is of utmost importance to evaluate biodistribution of the nanocomplexes in rats with CCl_4-induced liver fibrosis, which is the most widely used animal model for liver fibrosis study[5, 185]. The nanocomplexes were prepared with Cy5-labeled PCBP2 siRNA for fluorescence analysis. Two hours after systemic administration of the nanocomplexes, the rats were euthanized and major organs, including the liver, lungs, kidneys, spleen, muscle, and blood were harvested for fluorescence analysis using a small animal imaging system. As illustrated in Figure 25, free siRNA was eliminated rapidly and showed low accumulation in the fibrotic liver. Compared to free siRNA, all the three nanocomplexes showed higher uptake in the liver. This is because of two reasons: the protection of siRNA by the nanocomplex, and the targeting effect of cholesterol, vitamin A, and peptide-431 for their corresponding receptors in HSCs. Consistent with the *in vitro* cellular uptake results in Figures 20, 22, and 23, SNPP nanocomplex showed the highest liver uptake compared to SNCP and SNVP nanocomplexes. More importantly, SNPP nanocomplex showed negligible accumulation in the lung and kidney, in which SNCP and SNVP nanocomplexes showed non-specific accumulations. Taken together, these data provided compelling evidence that the SNPP nanocomplex could be a promising carrier to specifically deliver antifibrotic siRNAs to HSCs *in vitro* and *in vivo*.

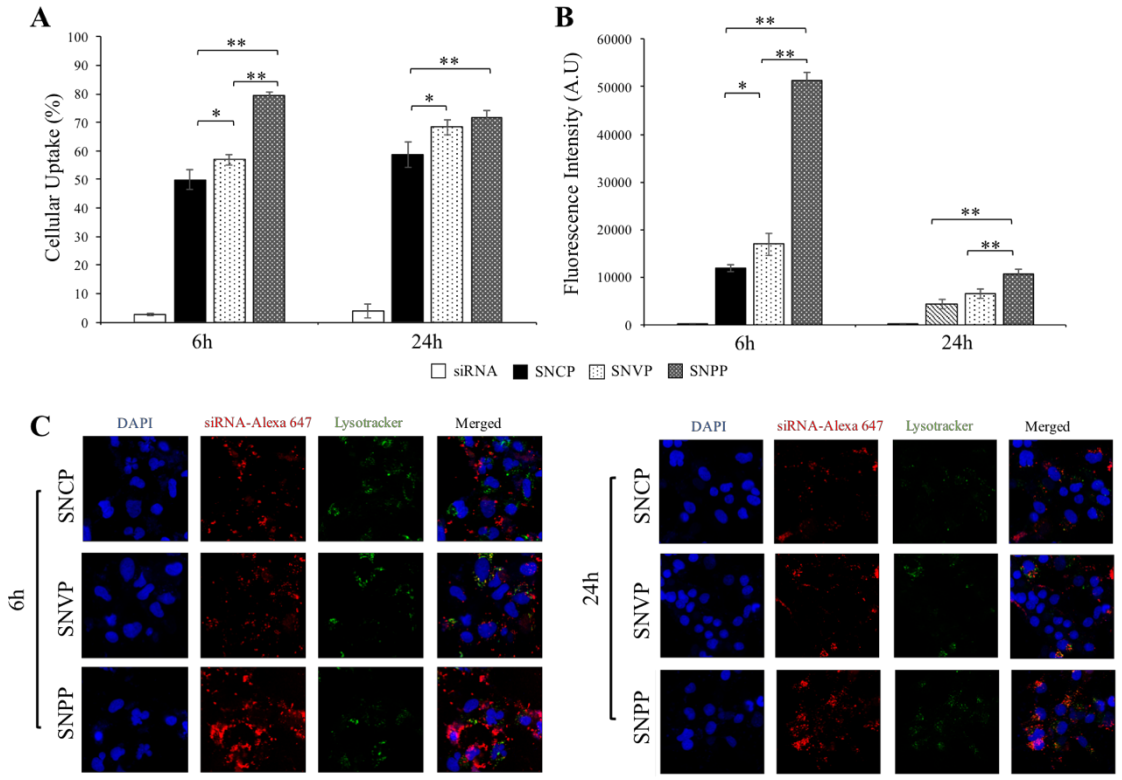

Figure 23. Cellular uptake of the nanocomplexes in human HSC LX-2 cells. The SNCP, SNVP and SNPP nanocomplexes were incubated with LX-2 cells for 6 and 24h. (A) Percent of the cells that take up the nanocomplexes. (B) Fluorescence intensity of the cells that take up the nanocomplexes; (C) Confocal images of the cells. All results are presented as the mean ± SD (n=3). (*P<0.05; **P<0.01).

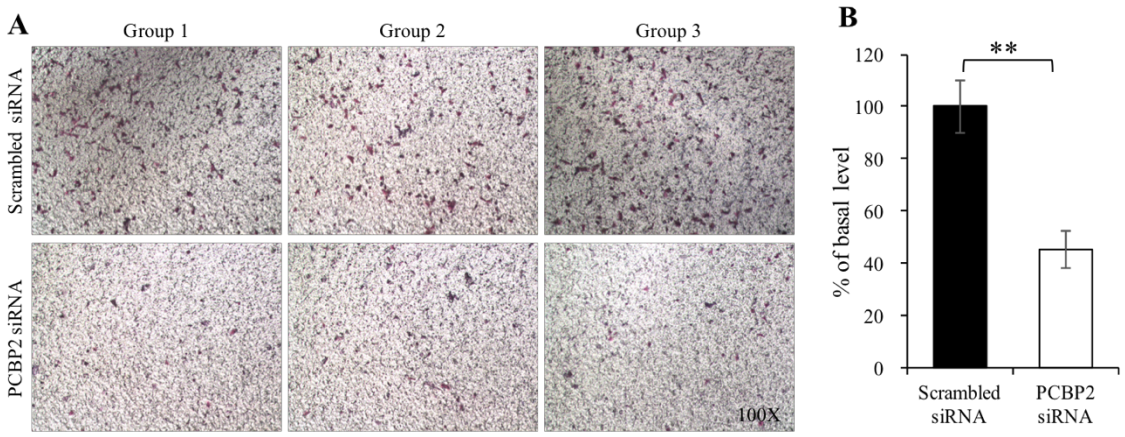

Figure 24. SNPP nanocomplex containing PCBP2 siRNA inhibits the migration effect of alcohol on HSC-T6. HSC-T6 cells were transfected with the SNPP nanocomplex at a concentration of 50 nM siRNA for 24 h, followed by stimulation with 100 mM alcohol for another 24 h. The cells weMre then harvested for migration assay using transwell chambers. All results are presented as the mean ± SD (n=3). (**P<0.01).

5.4 Discussion

In our previous studies, we prepared an avidin-based siRNA nanocomplex with an N/P ratio of 10:1. The siRNA nanocomplex showed somewhat non-specific accumulation in the lung[177], which could be due to its high positive charge (+18 mV)[114]. In addition, high positive charge of a carrier may cause significant systemic toxicity[181]. We therefore optimized the N/P ratio and selected 2:1 as the best ratio to form the siRNA nanocomplex with a slightly positive charge (Figure 19B). By reducing the N/P ratio from 10:1 to 2:1, the amount of protamine in the nanocomplex was also reduced from 66% to 28%, leading to a higher loading of the siRNA in the nanocomplex.

Another improvement in the current siRNA nanocomplex is the incorporation of PEG (Figure 18). PEG has long been used to prolong the blood circulation time and minimize systemic toxicity of a drug carrier[186]. Unmodified nanoparticles tend to accumulate in the reticuloendothelial system (RES), particularly in the Kupffer cells of the liver[187, 188]. For example, PEGylation of an oligonucleotide enhanced its antifibrotic activity by avoiding capture by Kupffer cells and subsequently accumulating in HSCs[189]. In our study, a 1 kDa PEG was used as a linker between biotin and ligands to increase binding affinity to HSCs, prolong circulation time, and avoid nonspecific uptake by the RES.

The major challenge in liver fibrosis therapy is how to specifically deliver antifibrotic agents to HSCs *in vivo*, which are the major contributors for liver fibrosis but only constitute approximately 5-8% of total liver cells[109]. Various receptors including LDLR, CRBP-1, and IGF2R have been exploited to enhance drug delivery to HSCs. We recently discovered an IGF2R-specific peptide with a high specificity and affinity to HSCs. The objective of this study is to compare the cellular uptake and activity of the

siRNA nanocomplexes coupled with three different ligands, including cholesterol, vitamin A and the IGF2R-specific peptide (Figure 18). Despite having different ligands, the nanocomplexes exhibited similar complexation, zeta potential, particle size and serum stability (Figures 19). This clearly indicated the robustness and flexibility of the neutravidin-based siRNA nanocomplex for various ligands and applications.

The *in vitro* cellular uptake and activity studies revealed that the neutravidin-based nanocomplex is an efficient platform to deliver siRNA to HSCs and exert its biological activity (Figures 20-24). This is consistent with our previous studies using streptavidin-based siRNA nanocomplex[17, 32]. Targeting ligand also plays an important role in the cellular uptake of the nanocomplex. The nanocomplexes coupled with cholesterol and vitamin A exhibited similar uptake in activated human and rat HSCs, while the nanocomplex coupled with the IGF2R-specific peptide showed the highest cellular uptake (Figure 20). However, the nanocomplexes with different ligands exhibited similar cellular uptake in quiescent rat primary HSCs (Figure 21A). This could be explained by the low expression of IGF2R in quiescent HSCs but upregulated expression of IGF2R in activated HSCs (Figure 22A, 22B). The expression of IGF2R could be increased by ~20 folds in activated HSCs compared to quiescent HSCs[128]. Moreover, approximately 16% of the IGF2R are located on the cell membrane surface, and IGF2R-mediated endocytosis is 3 times faster in activated HSCs compared to quiescent HSCs[128]. All these characteristics of IGF2R contribute to its important role in HSC-specific drug delivery.

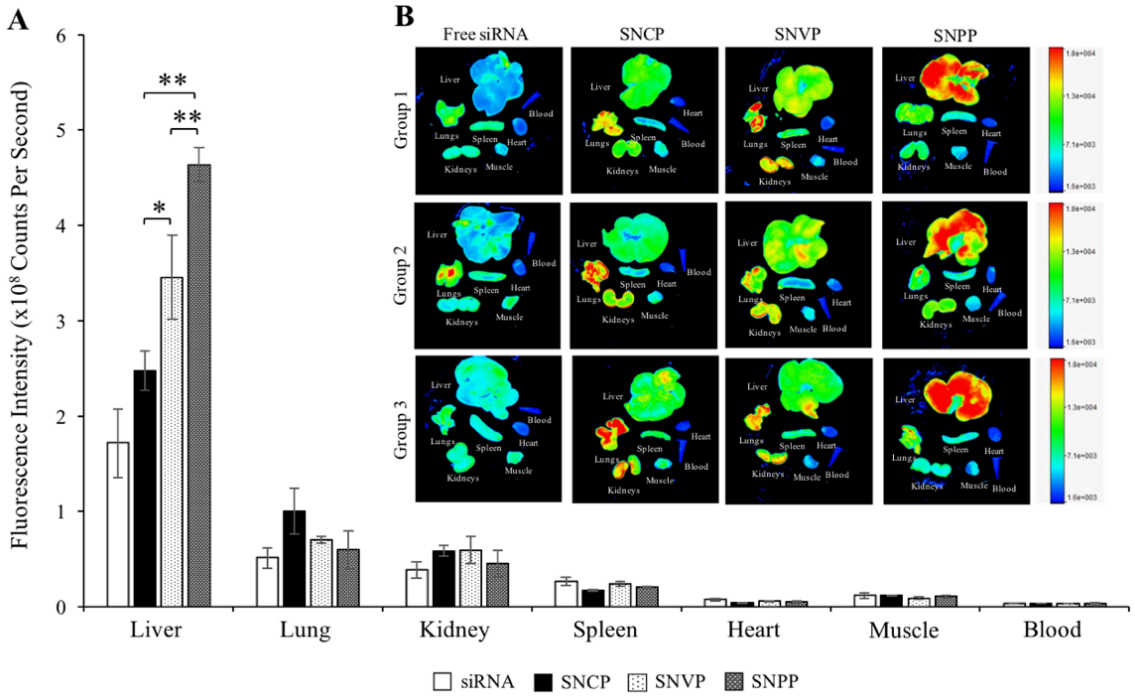

Figure 25. Biodistribution of the SNCP, SNVP and SNPP nanocomplexes in rats with CCl4-induced liver fibrotic. Fluorescence images of the major organs from three rats were presented. Region of interest (ROI) for each organ was determined by the Bruker molecular imaging software, and fluorescence intensities with respect to the area under the ROI were plotted. All results are presented as the mean ± SD (n=3). (*P<0.05; **P<0.01).

Similarly, *in vivo* biodistribution study revealed that IGF2R-specific peptide is the best ligand to deliver the siRNA nanocomplex to the fibrotic liver of rats with CCl_4-induced liver fibrosis (Figure 25). SNPP nanocomplex showed significantly high uptake in the liver and very low uptake in other organs, indicating a high specificity of the nanocomplex to the liver. This result also provides compelling evidence that the IGF2R-specific peptide is highly specific to activated HSCs *in vivo*. By contrast, SNCP and SNVP nanocomplexes exhibited low uptake in the liver but high uptake in the lung and kidney.

Cholesterol has long been used as a ligand to enhance liver uptake because of the high expression of its receptors, LDLR and SR-B1, in liver cells including HSCs, hepatocytes, and Kupffer cells[32, 120, 122]. However, the nanocomplex coupled with cholesterol showed the highest uptake in the lung of the rats with liver fibrosis. This could be due to the fact that the lung can act as a uptake organ for cholesterol[190]. In addition, the physiologic changes during liver fibrogenesis also limited hepatic uptake of the nanocomplex coupled with cholesterol. On the other hand, cholesterol's receptors, LDLR and SR-BI, are not HSC-specific and also expressed in hepatocytes and Kupffer cells, thus limiting its specificity to HSCs[120, 179].

Approximately 50-80% of vitamin A in the body is stored as retinyl palmitate in lipid droplets in HSCs, and they are taken up through CRBP-1[116, 118]. Vitamin A has therefore been utilized as a targeting ligand to deliver therapeutic agents to HSCs. For example, *Sato et al.,* developed vitamin A coupled liposome to deliver gp46 siRNA to fibrotic liver[34]. However, the expression of CRBP-1 in HSCs is downregulated during liver fibrogenesis[115-117]. As a result, HSCs lose retinyl lipid droplets during the

process of fibrosis by exocytosis[117, 191]. This is possibly the major reason for the moderate liver uptake of the vitamin A modified nanocomplex in the rats with liver fibrosis (Figure 25). On the other hand, other retinol-binding proteins also exist in hepatocytes and serum[192-194], which may limit the specificity of vitamin A to HSCs. Our biodistribution study revealed moderate uptake of the vitamin A coupled nanocomplex in the liver but also nonspecific uptake in the lung and kidney (Figure 25). This could be due to the expression of retinol-binding proteins in these organs. For example, lipid droplet-containing stellate cells were identified in the lung and kidney of rats[195].

In this study, we demonstrated that IGF2R-specific peptide can efficiently deliver the siRNA nanocomplex to activated HSCs *in vitro* and *in vivo*. Compared to nanocomplexes coupled with cholesterol and vitamin A, the IGF2R-specific peptide coupled nanocomplex showed the highest uptake in the liver and lowest uptake in the lung and kidney of the rats with CCl_4-induced liver fibrosis. The IGF2R-specific peptide modified nanocomplex is therefore a promising delivery platform for antifibrotic siRNAs.

Chapter 5 has been submitted to Nanomedicine: Nanotechnology, Biology and Medicine, and it was accepted and published in Volume 14, Issus 1, January 2018, Page 51-61 in Nanomedicine: Nanotechnology, Biology and Medicine, which is original source of Chapter 5.

CHAPTER 6

SUMMARY AND CONCLUSION

Triple-negative breast cancer (TNBC) is a subtype of breast cancer that lacks expression of ER, PR and HER2. Compared to other breast cancers, TNBC grows more rapidly and is more likely to metastasize. As a result, there is a great need to develop novel therapies for TNBC[2]. RNA interference, which uses small 19-23 nucleotides RNA (siRNA) to knock down target genes by binding to their complementary mRNA and triggering mRNA degradation, has been showing considerable promise for cancer therapy. VEGF plays important roles in the angiogenesis process and is correlated with high metastasis of breast cancer. Particularly, VEGF is highly expressed in TNBC[19-22]. Thus, silence VEGF expression in TNBC cells can be a promising strategy for the treatment of TNBC. In our previous study, we developed a VEGF siRNA and reported its inhibitory effect on breast cancer by knocking down VEGF expression[131]. In this dissertation, we conjugated low-molecular-weight branched PEIs with different molecular weights (600 Da, 1800 Da, and 10k Da) to a linear, bio-degradable multiblock polymer to form a highly positively charged carrier for targeted delivery of the VEGF siRNA. Interestingly, polymer conjugated with PEIs can form a nanocomplex to delivery VEGF siRNA into cells with a high transfection efficiency and a much lower cytotoxicity. The *in vitro* cellular uptake and 3D spheroid penetration studies demonstrated that pPEIs/siRNA nanocomplex exhibited significantly higher siRNA accumulation. Moreover, the migration and 3D spheroid invasion studies showed that $pPEI_{1800}$/VEGF siRNA nanocomplex dramatically inhibited the invasiveness ability of TNBC cells. More importantly, $pPEI_{1800}$/VEGF siRNA nanocomplex performed a

significant tumor growth inhibition efficiency *in vivo* by downregulation of VEGF expression as compared with saline and scrambled siRNA. These results suggested that the VEGF siRNA was a promising anti-tumor agent for TNBC therapy and PEI 1800 conjugated bio-degradable, linear multiblock polymer was efficient delivery system of VEGF siRNA into tumor with a high transfection efficiency and a much lower cytotoxicity.

The aberrant activation of nuclear factor-kappa B (NF-κB) was reported to be regulated as a key factor in TNBC[23]. IKKε, an important mediator in the activation of the NF-κB pathway, has been identified as an oncogene in breast cancer[24], and aberrantly amplified in TNBC cells associated and related with the proliferation, migration and survival in TNBC cells by driving CCL5 and IL-6 production[25]. In our previous study, we developed a IKBKE siRNA and reported its inhibitory effect on breast cancer by knocking down IKBKE expression[16]. In this dissertation, we first evaluated the bio-activities of IKBKE siRNA on TNBC cells, then cabazitaxel was encapsulated into a cholesterol-peptide micelle by hydrophobic interaction and condensed with IKBKE siRNA to form a hybrid nanocomplex, followed by coating with cholesterol-modified hyaluronic acid (CHA), which was used as a CD44-specific targeting ligand. To future improve the release of IKBKE siRNA and cabazitaxel from endosomes, a cathepsin B-specific response dipeptide sequence (Val-Cit) was added between cholesterol and the cationic peptide sequence. The hybrid nanocomplex (CHA/CP/siRNA/CTX) can protect siRNA from serum degradation and specific targeting to TNBC cells. Moreover, CHA/CP/siRNA/CTX nanocomplex exhibited an anti-tumor effect for TNBC *in vivo*. In future studies, we will generate a TNBC metastasis model using luciferase-expressing

MDA-MB-231 cells and then investigate the anti-metastasis efficiency of the IKBKE siRNA nanocomplex.

Liver fibrosis is a wound healing process characterized by the accumulation of excess extracellular matrix in the liver. The expression of ECM increases dramatically when quiescent hepatic stellate cells are activated to myofibroblast-like cells[3, 5-7]. Targeted delivery of antifibrotic agents to HSCs is a major challenge in liver fibrosis therapy. Therapeutic agents cannot easily reach HSCs because of the excessive accumulation of ECM, the closure of endothelial fenestrae, and the reduced flow exchange between sinusoid blood and liver cells[9]. The delivery of antifibrotic agents to HSCs is also limited by the reduced perisinusoidal space (or space of Disse)[31]. One promising strategy to improve the delivery of antifibrotic agents to HSCs is to modify drug carriers with a specific ligand that binds to a moiety on activated HSCs[32-34]. In this dissertation, we develop a peptide ligand-modified siRNA nanocomplex and compared to other two ligands modified siRNA nanocomplex for specific targeting HSCs. Compared to free siRNA and the nanocomplexes coupled with vitamin A and cholesterol, the nanocomplex coupled with the IGF2R-specific peptide exhibited the highest silencing activity of PCBP2 and the best inhibition on the migration of activated HSCs. The IGF2R-specific peptide coupled nanocomplex also showed the highest uptake in the liver of the rats with CCl_4-induced liver fibrosis.

APPENDIX

LETTER OF PERMISSION

Title: Development of a peptide-modified siRNA nanocomplex for hepatic stellate cells

Author: Zhen Zhao,Yuanke Li,Akshay Jain,Zhijin Chen,Hao Liu,Wei Jin,Kun Cheng

Publication: Nanomedicine: Nanotechnology, Biology and Medicine

Publisher: Elsevier

Date: January 2018

Logged in as:
Zhen Zhao
University of Missouri-Kansas City
LOGOUT

Please note that, as the author of this Elsevier article, you retain the right to include it in a thesis or dissertation, provided it is not published commercially. Permission is not required, but please ensure that you reference the journal as the original source. For more information on this and on your other retained rights, please visit: https://www.elsevier.com/about/our-business/policies/copyright#Author-rights

BACK CLOSE WINDOW

REFERENCES

1. Foulkes, W.D., I.E. Smith, and J.S. Reis-Filho, *Triple-negative breast cancer.* N Engl J Med, 2010. **363**(20): p. 1938-48.
2. Friedman, S.L., *Liver fibrosis -- from bench to bedside.* J Hepatol, 2003. **38 Suppl 1**: p. S38-53.
3. Lee, Y.A., M.C. Wallace, and S.L. Friedman, *Pathobiology of liver fibrosis: a translational success story.* Gut, 2015. **64**(5): p. 830-41.
4. Cheng, K. and R.I. Mahato, *Gene modulation for treating liver fibrosis.* Crit Rev Ther Drug Carrier Syst, 2007. **24**(2): p. 93-146.
5. Raghow, R., *The role of extracellular matrix in postinflammatory wound healing and fibrosis.* FASEB J, 1994. **8**(11): p. 823-31.
6. Senoo, H., et al., *Molecular mechanisms in the reversible regulation of morphology, proliferation and collagen metabolism in hepatic stellate cells by the three-dimensional structure of the extracellular matrix.* J Gastroenterol Hepatol, 1998. **13 Suppl**: p. S19-32.
7. Shukla, R.S., et al., *PCBP2 siRNA reverses the alcohol-induced pro-fibrogenic effects in hepatic stellate cells.* Pharm Res, 2011. **28**(12): p. 3058-68.
8. Garcia-Banuelos, J., et al., *Cirrhotic rat livers with extensive fibrosis can be safely transduced with clinical-grade adenoviral vectors. Evidence of cirrhosis reversion.* Gene Ther, 2002. **9**(2): p. 127-34.
9. Hudis, C.A. and L. Gianni, *Triple-negative breast cancer: an unmet medical need.* Oncologist, 2011. **16 Suppl 1**: p. 1-11.

10. Sanford, M., *Subcutaneous trastuzumab: a review of its use in HER2-positive breast cancer.* Target Oncol, 2014. **9**(1): p. 85-94.

11. Amiri-Kordestani, L., et al., *First FDA approval of neoadjuvant therapy for breast cancer: pertuzumab for the treatment of patients with HER2-positive breast cancer.* Clin Cancer Res, 2014. **20**(21): p. 5359-64.

12. Turner, N.C., et al., *Palbociclib in Hormone-Receptor-Positive Advanced Breast Cancer.* N Engl J Med, 2015. **373**(3): p. 209-19.

13. Kalimutho, M., et al., *Targeted Therapies for Triple-Negative Breast Cancer: Combating a Stubborn Disease.* Trends Pharmacol Sci, 2015. **36**(12): p. 822-846.

14. Wittrup, A. and J. Lieberman, *Knocking down disease: a progress report on siRNA therapeutics.* Nat Rev Genet, 2015. **16**(9): p. 543-52.

15. Qin, B. and K. Cheng, *Silencing of the IKKepsilon gene by siRNA inhibits invasiveness and growth of breast cancer cells.* Breast Cancer Res, 2010. **12**(5): p. R74.

16. Shukla, R.S., et al., *Intracellular trafficking and exocytosis of a multi-component siRNA nanocomplex.* Nanomedicine, 2016. **12**(5): p. 1323-34.

17. Titze-de-Almeida, R., C. David, and S.S. Titze-de-Almeida, *The Race of 10 Synthetic RNAi-Based Drugs to the Pharmaceutical Market.* Pharm Res, 2017. **34**(7): p. 1339-1363.

18. Kristensen, T.B., et al., *Anti-vascular endothelial growth factor therapy in breast cancer.* Int J Mol Sci, 2014. **15**(12): p. 23024-41.

19. Linderholm, B.K., et al., *Significantly higher levels of vascular endothelial growth factor (VEGF) and shorter survival times for patients with primary operable triple-negative breast cancer.* Ann Oncol, 2009. **20**(10): p. 1639-46.

20. Mohammed, R.A., et al., *Lymphatic and blood vessels in basal and triple-negative breast cancers: characteristics and prognostic significance.* Mod Pathol, 2011. **24**(6): p. 774-85.

21. Dales, J.P., et al., *[Prognostic significance of VEGF receptors, VEGFR-1 (Flt-1) and VEGFR-2 (KDR/Flk-1) in breast carcinoma].* Ann Pathol, 2003. **23**(4): p. 297-305.

22. Ossovskaya, V., et al., *Exploring molecular pathways of triple-negative breast cancer.* Genes Cancer, 2011. **2**(9): p. 870-9.

23. Boehm, J.S., et al., *Integrative genomic approaches identify IKBKE as a breast cancer oncogene.* Cell, 2007. **129**(6): p. 1065-79.

24. Barbie, T.U., et al., *Targeting an IKBKE cytokine network impairs triple-negative breast cancer growth.* J Clin Invest, 2014. **124**(12): p. 5411-23.

25. Godbey, W.T., K.K. Wu, and A.G. Mikos, *Size matters: molecular weight affects the efficiency of poly(ethylenimine) as a gene delivery vehicle.* J Biomed Mater Res, 1999. **45**(3): p. 268-75.

26. Chiper, M., et al., *Self-aggregating 1.8kDa polyethylenimines with dissolution switch at endosomal acidic pH are delivery carriers for plasmid DNA, mRNA, siRNA and exon-skipping oligonucleotides.* J Control Release, 2017. **246**: p. 60-70.

27. Thomas, M., et al., *Cross-linked small polyethylenimines: while still nontoxic, deliver DNA efficiently to mammalian cells in vitro and in vivo.* Pharm Res, 2005. **22**(3): p. 373-80.

28. Yin, T., et al., *Tumor-penetrating codelivery of siRNA and paclitaxel with ultrasound-responsive nanobubbles hetero-assembled from polymeric micelles and liposomes.* Biomaterials, 2014. **35**(22): p. 5932-43.

29. Feng, Q., et al., *Synergistic inhibition of breast cancer by co-delivery of VEGF siRNA and paclitaxel via vapreotide-modified core-shell nanoparticles.* Biomaterials, 2014. **35**(18): p. 5028-38.

30. Varin, F. and P.M. Huet, *Hepatic microcirculation in the perfused cirrhotic rat liver.* J Clin Invest, 1985. **76**(5): p. 1904-12.

31. Shukla, R.S., et al., *Development of streptavidin-based nanocomplex for siRNA delivery.* Mol Pharm, 2013. **10**(12): p. 4534-45.

32. Ye, Z., et al., *Receptor-mediated hepatic uptake of M6P-BSA-conjugated triplex-forming oligonucleotides in rats.* Bioconjug Chem, 2006. **17**(3): p. 823-30.

33. Sato, Y., et al., *Resolution of liver cirrhosis using vitamin A-coupled liposomes to deliver siRNA against a collagen-specific chaperone.* Nat Biotechnol, 2008. **26**(4): p. 431-42.

34. Morris, G.J., et al., *Differences in breast carcinoma characteristics in newly diagnosed African-American and Caucasian patients: a single-institution compilation compared with the National Cancer Institute's Surveillance, Epidemiology, and End Results database.* Cancer, 2007. **110**(4): p. 876-84.

35. Wang, C., et al., *MicroRNA-203 suppresses cell proliferation and migration by targeting BIRC5 and LASP1 in human triple-negative breast cancer cells.* J Exp Clin Cancer Res, 2012. **31**: p. 58.

36. Kumar, P. and R. Aggarwal, *An overview of triple-negative breast cancer.* Arch Gynecol Obstet, 2016. **293**(2): p. 247-69.

37. Rakha, E.A., et al., *Triple-negative breast cancer: distinguishing between basal and nonbasal subtypes.* Clin Cancer Res, 2009. **15**(7): p. 2302-10.

38. Tischkowitz, M., et al., *Use of immunohistochemical markers can refine prognosis in triple negative breast cancer.* BMC Cancer, 2007. **7**: p. 134.

39. DeSantis, C.E., et al., *Breast cancer statistics, 2017, racial disparity in mortality by state.* CA Cancer J Clin, 2017. **67**(6): p. 439-448.

40. Steward, L.T., et al., *Impact of radiation therapy on survival in patients with triple-negative breast cancer.* Oncol Lett, 2014. **7**(2): p. 548-552.

41. Parvani, J.G. and M.W. Jackson, *Silencing the roadblocks to effective triple-negative breast cancer treatments by siRNA nanoparticles.* Endocr Relat Cancer, 2017. **24**(4): p. R81-R97.

42. Penault-Llorca, F. and G. Viale, *Pathological and molecular diagnosis of triple-negative breast cancer: a clinical perspective.* Ann Oncol, 2012. **23 Suppl 6**: p. vi19-22.

43. Hammond, M.E., et al., *American Society of Clinical Oncology/College Of American Pathologists guideline recommendations for immunohistochemical testing of estrogen and progesterone receptors in breast cancer.* J Clin Oncol, 2010. **28**(16): p. 2784-95.

44. Wolff, A.C., et al., *American Society of Clinical Oncology/College of American Pathologists guideline recommendations for human epidermal growth factor receptor 2 testing in breast cancer.* J Clin Oncol, 2007. **25**(1): p. 118-45.

45. Wolff, A.C., et al., *Recommendations for human epidermal growth factor receptor 2 testing in breast cancer: American Society of Clinical Oncology/College of American Pathologists clinical practice guideline update.* Arch Pathol Lab Med, 2014. **138**(2): p. 241-56.

46. Chacon, R.D. and M.V. Costanzo, *Triple-negative breast cancer.* Breast Cancer Res, 2010. **12 Suppl 2**: p. S3.

47. Harbeck, N. and M. Gnant, *Breast cancer.* Lancet, 2017. **389**(10074): p. 1134-1150.

48. Moran, M.S., *Radiation therapy in the locoregional treatment of triple-negative breast cancer.* Lancet Oncol, 2015. **16**(3): p. e113-22.

49. Abdulkarim, B.S., et al., *Increased risk of locoregional recurrence for women with T1-2N0 triple-negative breast cancer treated with modified radical mastectomy without adjuvant radiation therapy compared with breast-conserving therapy.* J Clin Oncol, 2011. **29**(21): p. 2852-8.

50. Lowery, A.J., et al., *Locoregional recurrence after breast cancer surgery: a systematic review by receptor phenotype.* Breast Cancer Res Treat, 2012. **133**(3): p. 831-41.

51. Solin, L.J., W.T. Hwang, and N. Vapiwala, *Outcome after breast conservation treatment with radiation for women with triple-negative early-stage invasive breast carcinoma.* Clin Breast Cancer, 2009. **9**(2): p. 96-100.

52. Panoff, J.E., et al., *Risk of locoregional recurrence by receptor status in breast cancer patients receiving modern systemic therapy and post-mastectomy radiation.* Breast Cancer Res Treat, 2011. **128**(3): p. 899-906.

53. Chen, J., et al., *The efficacy of molecular subtyping in predicting postoperative recurrence in breast-conserving therapy: a 15-study meta-analysis.* World J Surg Oncol, 2014. **12**: p. 212.

54. Early Breast Cancer Trialists' Collaborative, G., et al., *Effect of radiotherapy after breast-conserving surgery on 10-year recurrence and 15-year breast cancer death: meta-analysis of individual patient data for 10,801 women in 17 randomised trials.* Lancet, 2011. **378**(9804): p. 1707-16.

55. Overgaard, M., *Overview of randomized trials in high risk breast cancer patients treated with adjuvant systemic therapy with or without postmastectomy irradiation.* Semin Radiat Oncol, 1999. **9**(3): p. 292-9.

56. Recht, A., et al., *Postmastectomy radiotherapy: clinical practice guidelines of the American Society of Clinical Oncology.* J Clin Oncol, 2001. **19**(5): p. 1539-69.

57. Wang, J., et al., *Adjuvant chemotherapy and radiotherapy in triple-negative breast carcinoma: a prospective randomized controlled multi-center trial.* Radiother Oncol, 2011. **100**(2): p. 200-4.

58. Saini, A., et al., *Outcomes by molecular subtype after accelerated partial breast irradiation using single-entry catheters.* Brachytherapy, 2018. **17**(2): p. 415-424.

59. Stover, D.G. and E.P. Winer, *Tailoring adjuvant chemotherapy regimens for patients with triple negative breast cancer.* Breast, 2015. **24 Suppl 2**: p. S132-5.

60. O'Reilly, E.A., et al., *The fate of chemoresistance in triple negative breast cancer (TNBC).* BBA Clin, 2015. **3**: p. 257-75.

61. Andreopoulou, E., et al., *Therapies for triple negative breast cancer.* Expert Opin Pharmacother, 2015. **16**(7): p. 983-98.

62. Martin, M., et al., *Molecular predictors of efficacy of adjuvant weekly paclitaxel in early breast cancer.* Breast Cancer Res Treat, 2010. **123**(1): p. 149-57.

63. Sparano, J.A., et al., *Weekly paclitaxel in the adjuvant treatment of breast cancer.* N Engl J Med, 2008. **358**(16): p. 1663-71.

64. von Minckwitz, G. and M. Martin, *Neoadjuvant treatments for triple-negative breast cancer (TNBC).* Ann Oncol, 2012. **23 Suppl 6**: p. vi35-9.

65. Sparano, J.A., et al., *Long-Term Follow-Up of the E1199 Phase III Trial Evaluating the Role of Taxane and Schedule in Operable Breast Cancer.* J Clin Oncol, 2015. **33**(21): p. 2353-60.

66. Swain, S.M., et al., *Longer therapy, iatrogenic amenorrhea, and survival in early breast cancer.* N Engl J Med, 2010. **362**(22): p. 2053-65.

67. Alba, E., et al., *A randomized phase II trial of platinum salts in basal-like breast cancer patients in the neoadjuvant setting. Results from the GEICAM/2006-03, multicenter study.* Breast Cancer Res Treat, 2012. **136**(2): p. 487-93.

68. Vrignaud, P., et al., *Preclinical profile of cabazitaxel.* Drug Des Devel Ther, 2014. **8**: p. 1851-67.

69. Vrignaud, P., et al., *Preclinical antitumor activity of cabazitaxel, a semisynthetic taxane active in taxane-resistant tumors.* Clin Cancer Res, 2013. **19**(11): p. 2973-83.

70. Gottesman, M.M., T. Fojo, and S.E. Bates, *Multidrug resistance in cancer: role of ATP-dependent transporters.* Nat Rev Cancer, 2002. **2**(1): p. 48-58.

71. Zhong, T., et al., *Treating breast cancer metastasis with cabazitaxel-loaded polymeric micelles.* Acta Pharmacol Sin, 2017. **38**(6): p. 924-930.

72. Wang, H., et al., *New Generation Nanomedicines Constructed from Self-Assembling Small-Molecule Prodrugs Alleviate Cancer Drug Toxicity.* Cancer Res, 2017. **77**(24): p. 6963-6974.

73. Mahdaviani, P., et al., *Peptide functionalized poly ethylene glycol-poly caprolactone nanomicelles for specific cabazitaxel delivery to metastatic breast cancer cells.* Mater Sci Eng C Mater Biol Appl, 2017. **80**: p. 301-312.

74. Sledge, G.W., *Anti-vascular endothelial growth factor therapy in breast cancer: game over?* J Clin Oncol, 2015. **33**(2): p. 133-5.

75. Cameron, D., et al., *Adjuvant bevacizumab-containing therapy in triple-negative breast cancer (BEATRICE): primary results of a randomised, phase 3 trial.* Lancet Oncol, 2013. **14**(10): p. 933-42.

76. Lee, T.H., et al., *Vascular endothelial growth factor mediates intracrine survival in human breast carcinoma cells through internally expressed VEGFR1/FLT1.* PLoS Med, 2007. **4**(6): p. e186.

77. Wang, W., S.A. Nag, and R. Zhang, *Targeting the NFkappaB signaling pathways for breast cancer prevention and therapy.* Curr Med Chem, 2015. **22**(2): p. 264-89.

78. Liu, M., et al., *The canonical NF-kappaB pathway governs mammary tumorigenesis in transgenic mice and tumor stem cell expansion.* Cancer Res, 2010. **70**(24): p. 10464-73.

79. Oeckinghaus, A. and S. Ghosh, *The NF-kappaB family of transcription factors and its regulation.* Cold Spring Harb Perspect Biol, 2009. **1**(4): p. a000034.

80. Shen, R.R. and W.C. Hahn, *Emerging roles for the non-canonical IKKs in cancer.* Oncogene, 2011. **30**(6): p. 631-41.

81. Adli, M. and A.S. Baldwin, *IKK-i/IKKepsilon controls constitutive, cancer cell-associated NF-kappaB activity via regulation of Ser-536 p65/RelA phosphorylation.* J Biol Chem, 2006. **281**(37): p. 26976-84.

82. Eddy, S.F., et al., *Inducible IkappaB kinase/IkappaB kinase epsilon expression is induced by CK2 and promotes aberrant nuclear factor-kappaB activation in breast cancer cells.* Cancer Res, 2005. **65**(24): p. 11375-83.

83. Hutti, J.E., et al., *Phosphorylation of the tumor suppressor CYLD by the breast cancer oncogene IKKepsilon promotes cell transformation.* Mol Cell, 2009. **34**(4): p. 461-72.

84. Shen, R.R., et al., *IkappaB kinase epsilon phosphorylates TRAF2 to promote mammary epithelial cell transformation.* Mol Cell Biol, 2012. **32**(23): p. 4756-68.

85. Renner, F., R. Moreno, and M.L. Schmitz, *SUMOylation-dependent localization of IKKepsilon in PML nuclear bodies is essential for protection against DNA-damage-triggered cell death.* Mol Cell, 2010. **37**(4): p. 503-15.

86. D'Andrea, A.D. and M. Grompe, *The Fanconi anaemia/BRCA pathway.* Nat Rev Cancer, 2003. **3**(1): p. 23-34.

87. Gonzalez-Angulo, A.M., et al., *Incidence and outcome of BRCA mutations in unselected patients with triple receptor-negative breast cancer.* Clin Cancer Res, 2011. **17**(5): p. 1082-9.

88. Farmer, H., et al., *Targeting the DNA repair defect in BRCA mutant cells as a therapeutic strategy.* Nature, 2005. **434**(7035): p. 917-21.

89. Berrada, N., S. Delaloge, and F. Andre, *Treatment of triple-negative metastatic breast cancer: toward individualized targeted treatments or chemosensitization?* Ann Oncol, 2010. **21 Suppl 7**: p. vii30-5.

90. Leng, Q., et al., *Advances in Systemic siRNA Delivery.* Drugs Future, 2009. **34**(9): p. 721.

91. Liu, Y., et al., *Triple negative breast cancer therapy with CDK1 siRNA delivered by cationic lipid assisted PEG-PLA nanoparticles.* J Control Release, 2014. **192**: p. 114-21.

92. Parvani, J.G., et al., *Silencing beta3 Integrin by Targeted ECO/siRNA Nanoparticles Inhibits EMT and Metastasis of Triple-Negative Breast Cancer.* Cancer Res, 2015. **75**(11): p. 2316-2325.

93. Deng, Z.J., et al., *Layer-by-layer nanoparticles for systemic codelivery of an anticancer drug and siRNA for potential triple-negative breast cancer treatment.* ACS Nano, 2013. **7**(11): p. 9571-84.

94. Hu, Y., et al., *Gene delivery of PEI incorporating with functional block copolymer via non-covalent assembly strategy.* Acta Biomater, 2013. **9**(2): p. 5003-12.

95. Guan, J., et al., *Hypoxia-induced tumor cell resistance is overcome by synergistic GAPDH-siRNA and chemotherapy co-delivered by long-circulating and cationic-interior liposomes.* Nanoscale, 2017.

96. Qin, B., et al., *Development of cholesteryl peptide micelles for siRNA delivery.* J Control Release, 2013. **172**(1): p. 159-68.

97. Nel, A.E., et al., *Understanding biophysicochemical interactions at the nano-bio interface.* Nat Mater, 2009. **8**(7): p. 543-57.

98. Akinc, A., et al., *Exploring polyethylenimine-mediated DNA transfection and the proton sponge hypothesis.* J Gene Med, 2005. **7**(5): p. 657-63.

99. Zhong, Z., et al., *Low molecular weight linear polyethylenimine-b-poly(ethylene glycol)-b-polyethylenimine triblock copolymers: synthesis, characterization, and in vitro gene transfer properties.* Biomacromolecules, 2005. **6**(6): p. 3440-8.

100. Itaka, K., et al., *Biodegradable polyamino acid-based polycations as safe and effective gene carrier minimizing cumulative toxicity.* Biomaterials, 2010. **31**(13): p. 3707-14.

101. Barrett, S.E., et al., *Development of a liver-targeted siRNA delivery platform with a broad therapeutic window utilizing biodegradable polypeptide-based polymer conjugates.* J Control Release, 2014. **183**: p. 124-37.

102. Zhao, Z., et al., *Development of a Peptide-modified siRNA Nanocomplex for Hepatic Stellate Cells.* Nanomedicine, 2018. **14**(1): p. 51-61.

103. Song, E., et al., *Antibody mediated in vivo delivery of small interfering RNAs via cell-surface receptors.* Nat Biotechnol, 2005. **23**(6): p. 709-17.

104. Scaglione, S., et al., *The Epidemiology of Cirrhosis in the United States: A Population-based Study.* J Clin Gastroenterol, 2015. **49**(8): p. 690-6.

105. Sun, M. and T. Kisseleva, *Reversibility of liver fibrosis.* Clin Res Hepatol Gastroenterol, 2015. **39 Suppl 1**: p. S60-3.

106. Meissner, E.G., et al., *Simtuzumab treatment of advanced liver fibrosis in HIV and HCV-infected adults: results of a 6-month open-label safety trial.* Liver Int, 2016. **36**(12): p. 1783-1792.

107. Pellicoro, A., et al., *Liver fibrosis and repair: immune regulation of wound healing in a solid organ.* Nat Rev Immunol, 2014. **14**(3): p. 181-94.

108. Geerts, A., *History, heterogeneity, developmental biology, and functions of quiescent hepatic stellate cells.* Semin Liver Dis, 2001. **21**(3): p. 311-35.

109. Marra, F. and M. Pinzani, *Role of hepatic stellate cells in the pathogenesis of portal hypertension.* Nefrologia, 2002. **22 Suppl 5**: p. 34-40.

110. Liu, H., et al., *Silencing of alpha-complex protein-2 reverses alcohol- and cytokine-induced fibrogenesis in hepatic stellate cells.* Liver Res, 2017. **1**(1): p. 70-79.

111. Lindquist, J.N., B. Stefanovic, and D.A. Brenner, *Regulation of collagen alpha1(I) expression in hepatic stellate cells.* J Gastroenterol, 2000. **35 Suppl 12**: p. 80-3.

112. Sato, M., S. Suzuki, and H. Senoo, *Hepatic stellate cells: unique characteristics in cell biology and phenotype.* Cell Struct Funct, 2003. **28**(2): p. 105-12.

113. Blanco, E., H. Shen, and M. Ferrari, *Principles of nanoparticle design for overcoming biological barriers to drug delivery.* Nat Biotechnol, 2015. **33**(9): p. 941-51.

114. Motoyama, H., et al., *Cytoglobin is expressed in hepatic stellate cells, but not in myofibroblasts, in normal and fibrotic human liver.* Lab Invest, 2014. **94**(2): p. 192-207.

115. Vogel, S., et al., *An immortalized rat liver stellate cell line (HSC-T6): a new cell model for the study of retinoid metabolism in vitro.* J Lipid Res, 2000. **41**(6): p. 882-93.

116. Senoo, H., et al., *Hepatic stellate cell (vitamin A-storing cell) and its relative--past, present and future.* Cell Biol Int, 2010. **34**(12): p. 1247-72.

117. Higashi, N., et al., *Vitamin A storage in hepatic stellate cells in the regenerating rat liver: with special reference to zonal heterogeneity.* Anat Rec A Discov Mol Cell Evol Biol, 2005. **286**(2): p. 899-907.

118. Fortuna, V.A., et al., *Hepatic stellate cells uptake of retinol associated with retinol-binding protein or with bovine serum albumin.* J Cell Biochem, 2003. **90**(4): p. 792-805.

119. Wolfrum, C., et al., *Mechanisms and optimization of in vivo delivery of lipophilic siRNAs.* Nat Biotechnol, 2007. **25**(10): p. 1149-57.

120. Gao, R. and D.R. Brigstock, *Low density lipoprotein receptor-related protein (LRP) is a heparin-dependent adhesion receptor for connective tissue growth factor (CTGF) in rat activated hepatic stellate cells.* Hepatol Res, 2003. **27**(3): p. 214-220.

121. Bijsterbosch, M.K., et al., *bis-Cholesteryl-conjugated phosphorothioate oligodeoxynucleotides are highly selectively taken up by the liver.* J Pharmacol Exp Ther, 2002. **302**(2): p. 619-26.

122. Cheng, K., et al., *Enhanced hepatic uptake and bioactivity of type alpha1(I) collagen gene promoter-specific triplex-forming oligonucleotides after conjugation with cholesterol.* J Pharmacol Exp Ther, 2006. **317**(2): p. 797-805.

123. Bijsterbosch, M.K., et al., *Modulation of plasma protein binding and in vivo liver cell uptake of phosphorothioate oligodeoxynucleotides by cholesterol conjugation.* Nucleic Acids Res, 2000. **28**(14): p. 2717-25.

124. Morgan, D.O., et al., *Insulin-like growth factor II receptor as a multifunctional binding protein.* Nature, 1987. **329**(6137): p. 301-7.

125. de Bleser, P.J., et al., *Insulinlike growth factor-II/mannose 6-phosphate receptor is expressed on CCl4-exposed rat fat-storing cells and facilitates activation of latent transforming growth factor-beta in cocultures with sinusoidal endothelial cells.* Hepatology, 1995. **21**(5): p. 1429-37.

126. Chen, Z., et al., *Discovery of Peptide ligands for hepatic stellate cells using phage display.* Mol Pharm, 2015. **12**(6): p. 2180-8.

127. Mousavi, S.A., et al., *Enhanced activity of lysosomal proteases in activated rat hepatic stellate cells is associated with a concomitant increase in the number of the mannose-6-phosphate/insulin-like growth factor II receptor.* Cell Biol Int, 2013. **37**(7): p. 703-12.

128. Li, F., et al., *Effects of interferon-gamma liposomes targeted to platelet-derived growth factor receptor-beta on hepatic fibrosis in rats.* J Control Release, 2012. **159**(2): p. 261-70.

129. Bartneck, M., K.T. Warzecha, and F. Tacke, *Therapeutic targeting of liver inflammation and fibrosis by nanomedicine.* Hepatobiliary Surg Nutr, 2014. **3**(6): p. 364-76.

130. Tai, W., B. Qin, and K. Cheng, *Inhibition of breast cancer cell growth and invasiveness by dual silencing of HER-2 and VEGF.* Mol Pharm, 2010. **7**(2): p. 543-56.

131. Tai, W., et al., *A novel rapamycin-polymer conjugate based on a new poly(ethylene glycol) multiblock copolymer.* Pharm Res, 2014. **31**(3): p. 706-19.

132. Zhao, G., et al., *Smart pH-sensitive nanoassemblies with cleavable PEGylation for tumor targeted drug delivery.* Sci Rep, 2017. **7**(1): p. 3383.

133. Ray, A., S. Dhar, and B.K. Ray, *Control of VEGF expression in triple-negative breast carcinoma cells by suppression of SAF-1 transcription factor activity.* Mol Cancer Res, 2011. **9**(8): p. 1030-41.

134. Tavera-Mendoza, L.E. and M. Brown, *A less invasive method for orthotopic injection of breast cancer cells into the mouse mammary gland.* Lab Anim, 2017. **51**(1): p. 85-88.

135. Essex, S., et al., *Phospholipid-modified PEI-based nanocarriers for in vivo siRNA therapeutics against multidrug-resistant tumors.* Gene Ther, 2015. **22**(3): p. 257-266.

136. Li, Y., et al., *Sigma receptor-mediated targeted delivery of anti-angiogenic multifunctional nanodrugs for combination tumor therapy.* J Control Release, 2016. **228**: p. 107-19.

137. Tredan, O., et al., *Drug resistance and the solid tumor microenvironment.* J Natl Cancer Inst, 2007. **99**(19): p. 1441-54.

138. Yao, Q., et al., *Improving Tumor Specificity and Anticancer Activity of Dasatinib by Dual-Targeted Polymeric Micelles.* ACS Appl Mater Interfaces, 2017. **9**(42): p. 36642-36654.

139. Horibe, T., et al., *Transfection efficiency of normal and cancer cell lines and monitoring of promoter activity by single-cell bioluminescence imaging.* Luminescence, 2014. **29**(1): p. 96-100.

140. Xu, W.H., et al., *Inhibitory effect of vascular endothelial growth factors-targeted small interfering RNA on proliferation of gastric cancer cells.* World J Gastroenterol, 2007. **13**(14): p. 2044-7.

141. Maeda, H., *Toward a full understanding of the EPR effect in primary and metastatic tumors as well as issues related to its heterogeneity.* Adv Drug Deliv Rev, 2015. **91**: p. 3-6.

142. Zuckerman, J.E., et al., *Polycation-siRNA nanoparticles can disassemble at the kidney glomerular basement membrane.* Proc Natl Acad Sci U S A, 2012. **109**(8): p. 3137-42.

143. Moghimi, S.M., et al., *A two-stage poly(ethylenimine)-mediated cytotoxicity: implications for gene transfer/therapy.* Mol Ther, 2005. **11**(6): p. 990-5.

144. Jere, D., et al., *Degradable polyethylenimines as DNA and small interfering RNA carriers.* Expert Opin Drug Deliv, 2009. **6**(8): p. 827-34.

145. Swierczewska, M., K.C. Lee, and S. Lee, *What is the future of PEGylated therapies?* Expert Opin Emerg Drugs, 2015. **20**(4): p. 531-6.

146. Zanoni, M., et al., *3D tumor spheroid models for in vitro therapeutic screening: a systematic approach to enhance the biological relevance of data obtained.* Sci Rep, 2016. **6**: p. 19103.

147. Desoize, B. and J. Jardillier, *Multicellular resistance: a paradigm for clinical resistance?* Crit Rev Oncol Hematol, 2000. **36**(2-3): p. 193-207.

148. Al-Abd, A.M., et al., *Penetration and efficacy of VEGF siRNA using polyelectrolyte complex micelles in a human solid tumor model in-vitro.* J Control Release, 2009. **137**(2): p. 130-5.

149. Kim, T.H., et al., *The delivery of doxorubicin to 3-D multicellular spheroids and tumors in a murine xenograft model using tumor-penetrating triblock polymeric micelles.* Biomaterials, 2010. **31**(28): p. 7386-97.

150. Waite, C.L. and C.M. Roth, *Nanoscale drug delivery systems for enhanced drug penetration into solid tumors: current progress and opportunities.* Crit Rev Biomed Eng, 2012. **40**(1): p. 21-41.

151. Bhise, N.S., et al., *The relationship between terminal functionalization and molecular weight of a gene delivery polymer and transfection efficacy in mammary epithelial 2-D cultures and 3-D organotypic cultures.* Biomaterials, 2010. **31**(31): p. 8088-96.

152. Bachelder, R.E., et al., *Vascular endothelial growth factor is an autocrine survival factor for neuropilin-expressing breast carcinoma cells.* Cancer Res, 2001. **61**(15): p. 5736-40.

153. Doan, C.C., et al., *Simultaneous silencing of VEGF and KSP by siRNA cocktail inhibits proliferation and induces apoptosis of hepatocellular carcinoma Hep3B cells.* Biol Res, 2014. **47**: p. 70.

154. Wang, L., et al., *Nanocomposite-siRNA approach for down-regulation of VEGF and its receptor in myeloid leukemia cells.* Int J Biol Macromol, 2014. **63**: p. 49-55.

155. Kim, S.H., et al., *Local and systemic delivery of VEGF siRNA using polyelectrolyte complex micelles for effective treatment of cancer.* J Control Release, 2008. **129**(2): p. 107-16.

156. Chen, Y., et al., *Highly effective antiangiogenesis via magnetic mesoporous silica-based siRNA vehicle targeting the VEGF gene for orthotopic ovarian cancer therapy.* Int J Nanomedicine, 2015. **10**: p. 2579-94.

157. Brabletz, T., et al., *Roadblocks to translational advances on metastasis research.* Nat Med, 2013. **19**(9): p. 1104-9.

158. Sun, B., et al., *Identification of metastasis-related proteins and their clinical relevance to triple-negative human breast cancer.* Clin Cancer Res, 2008. **14**(21): p. 7050-9.

159. Dent, R., et al., *Triple-negative breast cancer: clinical features and patterns of recurrence.* Clin Cancer Res, 2007. **13**(15 Pt 1): p. 4429-34.

160. Bachelder, R.E., M.A. Wendt, and A.M. Mercurio, *Vascular endothelial growth factor promotes breast carcinoma invasion in an autocrine manner by regulating the chemokine receptor CXCR4.* Cancer Res, 2002. **62**(24): p. 7203-6.

161. Wu, Y., W.L. Sun, and J.F. Feng, *Antiangiogenic therapy in the management of breast cancer.* Asia Pac J Clin Oncol, 2013. **9**(2): p. 110-6.

162. Deissler, H.L., H. Deissler, and G.E. Lang, *Actions of bevacizumab and ranibizumab on microvascular retinal endothelial cells: similarities and differences.* Br J Ophthalmol, 2012. **96**(7): p. 1023-8.

163. Rusovici, R., C.J. Patel, and K.V. Chalam, *Bevacizumab inhibits proliferation of choroidal endothelial cells by regulation of the cell cycle.* Clin Ophthalmol, 2013. **7**: p. 321-7.

164. Ferrara, N., H.P. Gerber, and J. LeCouter, *The biology of VEGF and its receptors.* Nat Med, 2003. **9**(6): p. 669-76.

165. Senapati, S., et al., *Controlled drug delivery vehicles for cancer treatment and their performance.* Signal Transduct Target Ther, 2018. **3**: p. 7.

166. Mattheolabakis, G., et al., *Hyaluronic acid targeting of CD44 for cancer therapy: from receptor biology to nanomedicine.* J Drug Target, 2015. **23**(7-8): p. 605-18.

167. Peach, R.J., et al., *Identification of hyaluronic acid binding sites in the extracellular domain of CD44.* J Cell Biol, 1993. **122**(1): p. 257-64.

168. Lv, Y., et al., *Nanoplatform Assembled from a CD44-Targeted Prodrug and Smart Liposomes for Dual Targeting of Tumor Microenvironment and Cancer Cells.* ACS Nano, 2018. **12**(2): p. 1519-1536.

169. Vogus, D.R., et al., *A hyaluronic acid conjugate engineered to synergistically and sequentially deliver gemcitabine and doxorubicin to treat triple negative breast cancer.* J Control Release, 2017. **267**: p. 191-202.

170. Liang, L., et al., *Novel cathepsin B-sensitive paclitaxel conjugate: Higher water solubility, better efficacy and lower toxicity.* J Control Release, 2012. **160**(3): p. 618-29.

171. Wei, X., et al., *Targeted nanogel conjugate for improved stability and cellular permeability of curcumin: synthesis, pharmacokinetics, and tumor growth inhibition.* Mol Pharm, 2014. **11**(9): p. 3112-22.

172. Cholkar, K., et al., *Optimization of dexamethasone mixed nanomicellar formulation.* AAPS PharmSciTech, 2014. **15**(6): p. 1454-67.

173. Hou, L., et al., *Pharmacokinetics of a paclitaxel-loaded low molecular weight heparin-all-trans-retinoid acid conjugate ternary nanoparticulate drug delivery system.* Biomaterials, 2012. **33**(21): p. 5431-40.

174. Yin, T., et al., *Co-delivery of hydrophobic paclitaxel and hydrophilic AURKA specific siRNA by redox-sensitive micelles for effective treatment of breast cancer.* Biomaterials, 2015. **61**: p. 10-25.

175. Azarenko, O., et al., *Antiproliferative mechanism of action of the novel taxane cabazitaxel as compared with the parent compound docetaxel in MCF7 breast cancer cells.* Mol Cancer Ther, 2014. **13**(8): p. 2092-103.

176. Khoeeniha, M.K., et al., *Targeted Delivery of Cabazitaxel by Conjugation to Albumin-PEG-folate Nanoparticles Using a Cysteine-acrylate Linker and Simple Synthesis Conditions.* Curr Drug Deliv, 2017. **14**(8): p. 1120-1129.

177. Jain, A., et al., *Comparison of Avidin, Neutravidin, and Streptavidin as Nanocarriers for Efficient siRNA Delivery.* Mol Pharm, 2017.

178. Barve, A., et al., *An enzyme-responsive conjugate improves the delivery of a PI3K inhibitor to prostate cancer.* Nanomedicine, 2016. **12**(8): p. 2373-2381.

179. Cheng, K., et al., *Biodistribution and hepatic uptake of triplex-forming oligonucleotides against type alpha1(I) collagen gene promoter in normal and fibrotic rats.* Mol Pharm, 2005. **2**(3): p. 206-17.

180. Mahato, R., B. Qin, and K. Cheng, *Blocking IKKalpha expression inhibits prostate cancer invasiveness.* Pharm Res, 2011. **28**(6): p. 1357-69.

181. Naha, P.C., et al., *Reactive oxygen species (ROS) induced cytokine production and cytotoxicity of PAMAM dendrimers in J774A.1 cells.* Toxicol Appl Pharmacol, 2010. **246**(1-2): p. 91-9.

182. Yang, C., et al., *Liver fibrosis: insights into migration of hepatic stellate cells in response to extracellular matrix and growth factors.* Gastroenterology, 2003. **124**(1): p. 147-59.

183. Benyon, R.C. and M.J. Arthur, *Mechanisms of hepatic fibrosis.* J Pediatr Gastroenterol Nutr, 1998. **27**(1): p. 75-85.

184. liu, H., et al., *Silencing of alphaCP2 reverses the alcohol- and cytokine-induced fibrogenesis in hepatic stellate cells* Liver Research, 2017: p. In Press.

185. Crespo Yanguas, S., et al., *Experimental models of liver fibrosis.* Arch Toxicol, 2016. **90**(5): p. 1025-48.

186. Harris, J.M. and R.B. Chess, *Effect of pegylation on pharmaceuticals.* Nat Rev Drug Discov, 2003. **2**(3): p. 214-21.

187. Moghimi, S.M. and J. Szebeni, *Stealth liposomes and long circulating nanoparticles: critical issues in pharmacokinetics, opsonization and protein-binding properties.* Prog Lipid Res, 2003. **42**(6): p. 463-78.

188. Tseng, Y.C., S. Mozumdar, and L. Huang, *Lipid-based systemic delivery of siRNA.* Adv Drug Deliv Rev, 2009. **61**(9): p. 721-31.

189. Bonora, G.M., et al., *Synthesis and characterization of high-molecular mass polyethylene glycol-conjugated oligonucleotides.* Bioconjug Chem, 1997. **8**(6): p. 793-7.

190. Townsend, R.W., A. Zutshi, and I. Bekersky, *Biodistribution of 4-[(14)C]cholesterol-AmBisome following a single intravenous administration to rats.* Drug Metab Dispos, 2001. **29**(5): p. 681-5.

191. Senoo, H., Y. Mezaki, and M. Fujiwara, *The stellate cell system (vitamin A-storing cell system).* Anat Sci Int, 2017.

192. Tabesh, M., et al., *Association of retinol-binding protein 4 with metabolic syndrome in first-degree relatives of type 2 diabetic patients.* J Res Med Sci, 2017. **22**: p. 28.

193. Domingos, M.A.M., et al., *Serum RBP4 and CKD: Association with insulin resistance and lipids.* J Diabetes Complications, 2017.

194. Yamaaki, N., et al., *Impact of serum retinol-binding protein 4 levels on regulation of remnant-like particles triglyceride in type 2 diabetes mellitus.* J Diabetes Res, 2013. **2013**: p. 143515.

195. Nagy, N.E., et al., *Storage of vitamin A in extrahepatic stellate cells in normal rats.* J Lipid Res, 1997. **38**(4): p. 645-58.

VITA

Zhen Zhao was born on Feb 11th, 1989 in Yangzhou, China. He received his Bachelor of Sciences degree in Pharmaceutics from China Pharmaceutical University in June 2011.

Before joining Dr. Kun Cheng's lab as a Graduate Teaching and Research Assistant in Division of Pharmaceutical Sciences, University of Missouri-Kansas City in August 2013, Zhen is working in Nanjing Yoko Biological Research Ltd., as a researcher in new drug design and research center from 2011 to 2013.

Zhen's project is mainly focusing on 1) Development of a polyethylenimine conjugated liner multiblock polymer to deliver VEGF siRNA for triple-negative breast cancer. 2) Development of a CD44 targeting, cabazitaxel loaded cholesterol modified IKBKE siRNA nanocomplex for triple-negative breast cancer. 3) Development of a IGF2R peptide modified PCBP2 siRNA nanocomplex for specific targeting hepatic stellate cells. He participated and published 6 different papers and received awards, including 2017 UMKC School of Graduate Studies Research Grant scholarship, 2017 American Association of Pharmaceutical Scientists (AAPS) Graduate Student Research Award in Biotechnology, UMKC School of Graduate Studies travel grant (2016, 2017), Outstanding Leadership Award of Pharmaceutical Sciences Graduate Student Association (PSGSA) (2015-2016, 2016-2017). He is a member of AAPS and The Rho Chi Society since 2016. He also served as president of the PSGSA (2016-2017) and logistics Co-chair of 2016 Pharmaceutics Graduate Student Research Meeting.

PUBLICATIONS

1. **Z. Zhao**, Y. Li, A. Jain, Z. Chen, H. Liu, W. Jin, K. Cheng. Development of a Peptide-Modified siRNA Nanocomplex for Hepatic Stellate cells. Nanomedicine.2018.14(1): p. 51-61
2. **Z. Zhao**, Y. Li, R. Shukla, H. Liu, A. Jain, A. Barve, K. Cheng. Development of a polyethylenimine conjugated linear multiblock polymer to deliver VEGF siRNA for triple negative breast cancer therapy, in progress.
3. **Z. Zhao**, Y. Li, H. Liu, A. Jain, A. Barve, K. Cheng. Silencing IKBKE gene with a peptide-based siRNA nanocomplex inhibits invasiveness and growth of triple negative breast cancer cells, in progress.
4. Y. Li, **Z. Zhao**, H. Liu, K. Cheng. Development of a multifunctional Nano-polyplex for Pancreatic Cancer therapy, in progress.
5. H. Liu, **Z. Zhao**, L. Zhang, Y. Li, A. Jain, A. Brave, K. Cheng. Discovery of Small Anti-PD-L1 Peptides for Cancer Immunotherapy, in progress.
6. H. Liu, **Z. Zhao**, L. Zhang, Y. Li, Z. Chen, A. Jain, A. Brave, K. Cheng. A Novel VHH Targeting PD-L1 for Cancer Immunotherapy, in progress.
7. R. Shukla, A. Jain, **Z. Zhao**, K. Cheng. Intracellular trafficking and exocytosis of a multi-component siRNA nanocomplex. Nanomedicine.2016.12(5): p.1323-34.
8. Z. Chen, W. Jin, H. Liu, **Z. Zhao**, K. Cheng. Discovery of Peptide Ligands for Hepatic Stellate Cells Using Phage Display. Molecular Pharmaceutics. 2015.12(6): p.2180-88.
9. A. Jain, A. Barve, **Z. Zhao**, W. Jin, and K. Cheng. Comparison of Avidin, Neutravidin, and Streptavidin as Nanocarriers for Efficient siRNA Delivery. Molecular Pharmaceutics. 2017. 14(5): p.1517-27

10. W. Jin, A. Jain, H. Liu, **Z. Zhao**, K. Cheng. Noncovalent Attachment of Chemical Moieties to siRNA Using Peptide Nucleic Acid As a Complementary Linker. ACS Applied Bio Materials. 2018